

On the neutron-capture elements across the Galactic thin disk using Cepheids ^{★, ★★}

R. da Silva^{1,2,3}, B. Lemasle⁴, G. Bono^{2,3}, K. Genovali², A. McWilliam⁵, S. Cristallo^{6,7}, M. Bergemann⁸, R. Buonanno^{2,6}, M. Fabrizio^{1,6}, I. Ferraro³, P. François^{9,10}, G. Iannicola³, L. Inno⁸, C.D. Laney^{11,12}, R.-P. Kudritzki^{13,14,15}, N. Matsunaga¹⁶, M. Nonino¹⁷, F. Primas¹⁸, N. Przybilla¹⁹, M. Romaniello^{18,20}, F. Thévenin²¹, and M.A. Urbaneja¹⁹

¹ ASI Science Data Center, Via del Politecnico snc, 00133 Rome, Italy

² Dipartimento di Fisica, Università di Roma Tor Vergata, via della Ricerca Scientifica 1, 00133 Rome, Italy

³ INAF–Osservatorio Astronomico di Roma, via Frascati 33, 00078 Monte Porzio Catone, Rome, Italy

⁴ Anton Pannekoek Institute for Astronomy, University of Amsterdam, Science Park 904, PO Box 94249, 1090 GE, Amsterdam, The Netherlands

⁵ The Observatories of the Carnegie Institute of Washington, 813 Santa Barbara Street, Pasadena, CA 91101, USA

⁶ INAF–Osservatorio Astronomico di Teramo, via Mentore Maggini s.n.c., 64100 Teramo, Italy

⁷ INFN Sezione Napoli, Napoli, Italy

⁸ Max-Planck-Institut für Astronomie, D-69117, Heidelberg, Germany

⁹ GEPI, Observatoire de Paris, CNRS, Université Paris Diderot, Place Jules Janssen, 92190 Meudon, France

¹⁰ UPJV, Université de Picardie Jules Verne, 33 rue St. Leu, 80080 Amiens, France

¹¹ Department of Physics and Astronomy, N283 ESC, Brigham Young University, Provo, UT 84601, USA

¹² South African Astronomical Observatory, PO Box 9, Observatory 7935, South Africa

¹³ Institute for Astronomy, University of Hawaii, 2680 Woodlawn Drive, Honolulu, HI 96822, USA

¹⁴ Max-Planck-Institute for Astrophysics, Karl-Schwarzschild-Str.1, D-85741 Garching, Germany

¹⁵ University Observatory Munich, Scheinerstr. 1, D-81679 Munich, Germany

¹⁶ Department of Astronomy, School of Science, The University of Tokyo, 7-3-1 Hongo, Bunkyo-ku, Tokyo 113-0033, Japan

¹⁷ INAF–Osservatorio Astronomico di Trieste, via G. B. Tiepolo 11, 34143, Trieste, Italy

¹⁸ European Southern Observatory, Karl-Schwarzschild-Str. 2, 85748 Garching bei München, Germany

¹⁹ Institute for Astro- and Particle Physics, University of Innsbruck, Technikerstr. 25/8, A-6020 Innsbruck, Austria

²⁰ Excellence Cluster Universe, Boltzmannstr. 2, 85748, Garching bei München, Germany

²¹ Laboratoire Lagrange, CNRS/UMR 7293, Observatoire de la Côte d’Azur, Bd de l’Observatoire, CS 34229, 06304 Nice, France

Received / accepted

ABSTRACT

We present new accurate abundances for five neutron-capture (Y, La, Ce, Nd, Eu) elements in 73 classical Cepheids located across the Galactic thin disk. Individual abundances are based on high spectral resolution ($R \sim 38\,000$) and high signal-to-noise ratio (S/N ~ 50 -300) spectra collected with UVES at ESO VLT for the DIONYSOS project. Taking account for similar Cepheid abundances provided either by our group (111 stars) or available in the literature, we end up with a sample of 435 Cepheids covering a broad range in iron abundances ($-1.6 < [\text{Fe}/\text{H}] < 0.6$). We found, using homogeneous individual distances and abundance scales, well defined gradients for the above elements. However, the slope of the light s-process element (Y) is at least a factor of two steeper than the slopes of heavy s- (La, Ce, Nd) and r- (Eu) process elements. The s to r abundance ratio ([La/Eu]) of Cepheids shows a well defined anticorrelation with both Eu and Fe. On the other hand, Galactic field stars attain an almost constant value and only when they approach solar iron abundance display a mild enhancement in La. The [Y/Eu] ratio shows a mild evidence of a correlation with Eu and, in particular, with iron abundance for field Galactic stars. We also investigated the s-process index – [hs/ls] – and we found a well defined anticorrelation, as expected, between [La/Y] and iron abundance. Moreover, we found a strong correlation between [La/Y] and [La/Fe] and, in particular, a clear separation between Galactic and Sagittarius red giants. Finally, the comparison between predictions for low-mass asymptotic giant branch stars and the observed [La/Y] ratio indicate a very good agreement over the entire metallicity range covered by Cepheids. However, the observed spread, at fixed iron content, is larger than predicted by current models.

Key words. stars: abundances - stars: variables: Cepheids - stars: oscillations - Galaxy: disk - open clusters and associations: general

1. Introduction

The use of classical Cepheids as solid distance indicators dates back to more than one century ago (Leavitt 1908; Leavitt & Pickering 1912). The evidence that individual distances could be estimated on the basis of the pulsation period and of the mean magnitude made Cepheids also very popular

* Based on spectra collected with the UVES spectrograph available at the ESO Very Large Telescope (VLT), Cerro Paranal, Chile (ESO Proposals: 081.D-0928(A), PI: S. Pedicelli; 082.D-0901(A), PI: S. Pedicelli; 089.D-0767(C), PI: K. Genovali).

** Tables ... are only available in electronic form at the CDS via anonymous ftp to cdsarc.u-strasbg.fr (130.79.128.5) or via <http://cdsweb.u-strasbg.fr/cgi-bin/qcat?J/A+A/>

stellar tracers. However, the use of classical Cepheids as tracers of young stellar populations is more recent and dates back to the seminal investigations by Kraft & Schmidt (1963). To constrain the geometry, the rotation, and the density distribution of the Galactic thin disk they used distances and radial velocities of a sample of 267 Cepheids. The above empirical evidences were soundly supplemented by pioneering evolutionary and pulsation investigations suggesting that the pulsation period of classical Cepheids is tightly anti-correlated with their age (Kippenhahn et al. 1969; Meyer-Hofmeister 1969).

During the last twenty years, classical Cepheids have been the cross road of several photometric and spectroscopic investigations. Thanks to the new optical – OGLE-IV (Udalski et al. 2015) – and NIR – IRIS (Miville-Deschénes & Lagache 2005), VVV (Minniti et al. 2010) – photometric surveys classical Cepheids have been identified and characterized in the thin disk and in the different components of the Galactic spheroid hosting young-stellar populations: *i*) inner disk (Matsunaga et al. 2013; Inno et al., in prep.); *ii*) nuclear bulge (Matsunaga et al. 2011); *iii*) beyond the nuclear bulge (Feast et al. 2014; Dékány et al. 2015); *iv*) outer disk (i.e., Metzger et al. 1992; Pont et al. 2001). Thus suggesting that they can provide solid constraints on the impact that environment has on the recent star formation episodes of the Galactic thin disk.

The use of high-resolution spectrographs revealed that classical Cepheids are also excellent tracers of the chemical enrichment of intermediate-mass stars across the thin disk (Kraft 1965; Conti & Wallerstein 1969). In spite of these indisputable advantages in using classical Cepheids as stellar tracers, the first detailed investigation of the thin disk iron gradient dates back to Harris (1981); Harris & Pilachowski (1984). More recent theoretical and empirical investigations revealed that classical Cepheids, being yellow and red giants (RGs) and supergiants, display in their spectra hundreds of iron lines (Andrievsky et al. 2002a,b,c, 2004; Yong et al. 2006; Luck et al. 2006; Lemasle et al. 2007, 2008; Pedicelli et al. 2010; Luck et al. 2011; Luck & Lambert 2011; Genovali et al. 2013, 2014), dozens of α -element (e.g., Andrievsky et al. 2004; Luck & Lambert 2011; Lemasle et al. 2013; Genovali et al. 2015), and iron peak lines (e.g., Andrievsky et al. 2004; Luck & Lambert 2011) together with a well defined continuum. They are also excellent laboratories to constrain the impact of non-LTE effects in the abundance of both CNO (Luck et al. 2011; Martin et al. 2015) and Na (Takeda et al. 2013; Genovali et al. 2015) in RGs. Cepheids have also been identified to constrain the abundance of lithium in young stellar populations (Kovtyukh et al. 2005; Luck & Lambert 2011).

The above investigations move along a well defined path concerning the elemental abundance analysis and the chemical enrichment history of the thin disk. In this context neutron capture elements play a crucial role, since they trace the yields of a broad range of stellar structures (see, e.g., Sneden et al. 2008). They are typically split in two different groups, the heavy elements formed either via slow neutron-capture (“s-process”) or rapid neutron capture (“r-process”), i.e., either slow or rapid compared to the β -decay time scale.

The “main s-process” is considered to occur in asymptotic giant branch (AGB) stars during recurrent thermal pulses (Gallino et al. 1998; Busso et al. 1999). On the other hand, the “weak s-process”, takes place in massive fast evolving primitive stars and produce elements with atomic mass number smaller than $A = 90$ (Raiteri et al. 1993; Pignatari et al. 2010). The astrophysical sites of the r-process elements are even more complex. Indeed, the recent literature on the nucle-

osynthesis of r elements is quite rich. It has been suggested that they can be produced by core-collapse supernovae (SNe) with a mass of the order of $20 M_{\odot}$ (Thielemann et al. 2011; Wanajo 2013; Tsujimoto & Nishimura 2015); by core-collapse SNe of very massive stars ($25 \leq M/M_{\odot} \leq 45$, Boyd et al. 2012); by electron capture SNe in intermediate-mass stars (8– $10 M_{\odot}$, Woosley & Heger 2015); and by more complex astrophysical mechanisms such as the neutrino driven wind ensuing to the merging of neutron stars (e.g., Wanajo & Janka 2012; Berger et al. 2013).

The abundance of s- and r-process elements in Galactic classical Cepheids have already been discussed in several recent papers (Andrievsky et al. 2004; Luck et al. 2011; Luck & Lambert 2011; Lemasle et al. 2013). However, we still lack a homogeneous and detailed analysis of weak and main s-process elements in the Galaxy and their dependence on the iron abundance – a detailed analysis of s and r elements of RGs in the Sagittarius dwarf galaxy has been performed by McWilliam et al. (2013, hereinafter M13). Moreover, and even more importantly, we still lack a quantitative analysis of the spatial abundance pattern of s- and r-process elements and, in particular, the possible occurrence of an age dependence.

In this investigation we focus our attention on the abundance of one light (Y) and three heavy (La, Ce, Nd) dominated s-process elements, and a single r-process dominated element (Eu). The abundances of 73 Galactic Cepheids of our sample were complemented with the abundances of 363 Cepheids available in the literature.

The structure of the paper is the following. In § 2 we discuss the spectra we collected together with the approach we adopted for data reduction and analysis. In this section we also mention the different samples of Cepheid abundances, based on high-resolution spectra, available in the literature and the approach we adopted to provide a homogeneous metallicity scale. In § 3 we discuss the radial gradients of [element/H] ratios for neutron-capture elements and their comparison with iron and α -element gradients. In this section we also discuss the radial gradients of [element/Fe] ratios and their age dependence. In § 4 we present s- and r-process element abundances and compare their distribution with dwarf and giant stars available in the literature. The differentiation between weak and main s-process elements and the comparison with the literature are also discussed in this section. The summary of the results of the current investigation are given in § 5 together with a brief outline of the future development of this project.

2. Observations, data reduction and analysis

2.1. Spectroscopic data

In this work we used the same high-resolution ($R \sim 38\,000$) and high signal-to-noise ratio (S/N) spectra reported in Genovali et al. (2014, hereinafter G14) in our determination of iron abundances and atmospheric parameters, and in Genovali et al. (2015, hereinafter G15) in our study of α -element abundances. A total of 122 spectra of 75 Galactic Cepheids were collected with the UVES spectrograph at the ESO VLT (Cerro Paranal, Chile) using two different instrument settings: *i*) with the former one we collected 80 spectra of 74 stars in the wavelength ranges of ~ 3760 – 4985 \AA , ~ 5684 – 7520 \AA , and ~ 7663 – 9458 \AA ; *ii*) with the latter one we collected 42 spectra of a control sample of 11 Cepheids in the wavelength ranges of ~ 4786 – 5750 \AA and ~ 5833 – 6806 \AA . For more details on the instrumental settings used we refer the reader to the G14 and G15 papers.

In the same way as done in the papers mentioned above, we used the 11 Cepheids (V340 Ara, AV Sgr, VY Sgr, UZ Sct, Z Sct, V367 Sct, WZ Sgr, XX Sgr, KQ Sco, RY Sco, V500 Sco) as a control sample. For these stars we have from four to six spectra each, collected with both the instrumental configurations (with the exception of V500 Sco, which has 4 spectra collected only with the second instrument setting). For the same reasons reported in G15, the stars BB Gem and GQ Ori (both observed using the first instrument setting) were not included in the current analysis, thus we are left with 73 stars. The S/N are typically better than ~ 100 per extracted pixel for all the échelle orders in the case of the first instrumental configuration (see examples in Fig. 1), and ranges from ~ 50 to roughly 300 for the second one. All the spectra were reduced using the ESO UVES pipeline Reflex v2.1 (Ballester et al. 2011).

2.2. Atmospheric parameters and abundances

We adopted the same iron abundances and atmospheric parameters derived by G14. The iron abundances are based on the equivalent width (EW) of about 100–200 Fe I and about 20–40 Fe II lines, the number of lines depending on the spectral range used. The number of lines also varies according to the metallicity and to the spectral type of the star (at the time of the observation). To determine the atmospheric parameters, we set a limit of $\text{EW} < 120 \text{ m}\AA$ to remain in the linear part of the curve of growth. For the objects where the number of weak lines was too small, we increased the limit to $180 \text{ m}\AA$. This slightly increases the uncertainties affecting the correlated atmospheric parameters, namely the effective temperature (T_{eff}) and the microturbulent velocity (v_t). For more details on the impact that typical uncertainties on T_{eff} , surface gravity ($\log g$), and v_t have on the iron abundances, see Table 2 of G14.

The T_{eff} of individual spectra was estimated using the line depth ratio (LDR) method and calibrations derived by Kovtyukh & Gorlova (2000). We adopted these calibrations because those provided by Kovtyukh (2007) are not publicly available. Note that the difference in the temperature scale between the two calibrations is quite modest (see Fig. 4 in Kovtyukh 2007). The latter calibrations have been criticized by Lyubimkov et al. (2010) and by Luck (2014), suggesting an overestimate for effective temperatures hotter than 6500–6800 K. In passing, we note that in our sample only a minor fraction, six out of 73 Cepheids, has an effective temperature hotter than 6300 K. We also note that the estimated values of T_{eff} were validated by verifying that the Fe I abundances do not depend on the excitation potential (χ_{ex}), i.e., the slope of $[\text{Fe I}/\text{H}]$ vs. χ_{ex} should be as close to zero.

The $\log g$ was derived through the ionization equilibrium between Fe I and Fe II lines, and v_t was derived by minimizing the slope in the $[\text{Fe I}]$ vs. EW plot. This means that the $\log g$ value is changed until the Fe I and Fe II lines provide the same abundance, while the v_t value is changed until the dependence of the derived abundances on the EWs is removed. Indeed, weak and strong lines are supposed to provide the same elemental abundances. In this context it is worth mentioning that we are dealing with radial variables and the quoted physical parameters (T_{eff} , $\log g$, v_t) undergo cyclic variation along the pulsation cycle. The internal consistency of the adopted values was validated by G14 using calibrating Cepheids, i.e., objects for which we have from four to six spectra.

Concerning the abundance of the neutron-capture elements Y, La, Ce, Nd, and Eu, we used the linelist provided by

Lemasle et al. (2013), with the same atomic parameters (χ_{ex} and $\log g_f$) listed in their Table A.1, but with small differences in the number of lines. We used six Y II lines (5119.12, 5289.81, 5402.77, 5509.91, 5728.89, and 7881.88 Å) instead of seven (the line at 6795.41 Å was not used because the abundances derived using this line are systematically smaller than those derived using the other six lines). We also used the six lines for La II (5114.56, 5290.82, 5805.77, 6262.29, 6390.48, and 6774.27 Å), three lines for Ce II (4562.37, 5518.49, and 6043.39 Å) instead of four (the abundance provided by the line at 4486.91 Å was very often discrepant to the values provided by the other lines, therefore we did not use it), the six Nd II lines (4959.12, 5092.79, 5130.59, 5181.17, 5431.52, and 6740.08 Å), and the two ones for Eu II (6437.64 and 6645.13 Å).

As previously done in G15 for the α elements, the EWs for these neutron-capture elements were measured using the *Automatic Routine for line Equivalent widths in stellar Spectra* (ARES, Sousa et al. 2007), and double-checked using the *splot* task of IRAF¹. Again, the internal dispersion is smaller than 6 mÅ and there is no evidence of systematics.

The abundances were derived with the *calrai* spectrum synthesis package, originally developed by Spite (1967) and regularly improved since then. The package allows us to compute synthetic spectra by interpolating over a large grid of hydrostatic, LTE, and plane-parallel or spherical stellar atmospheres models (MARCS, Gustafsson et al. 2008).

For all the elements studied here, we assumed the standard solar abundances provided by Grevesse et al. (1996), namely $A(\text{Fe})_{\odot} = 7.50$, $A(\text{Y})_{\odot} = 2.24$, $A(\text{La})_{\odot} = 1.17$, $A(\text{Ce})_{\odot} = 1.58$, $A(\text{Nd})_{\odot} = 1.50$, and $A(\text{Eu})_{\odot} = 0.51$. Note that recent spectroscopic estimates of solar abundances by Scott et al. (2015) and by Grevesse et al. (2015) indicate very similar abundances. Indeed, the difference in dex ranges from +0.01 for Eu to −0.03 for Fe and Y, to −0.06 for La, and to −0.08 for Nd, while the new Ce abundance is identical to the old one.

2.2.1. Hyperfine structure and isotopic splitting

Several lines used in our abundance analysis are affected by hyperfine structure (hereinafter HFS) and/or isotopic splitting in the line profile. We searched in the literature for atomic data required to compute the fine-structure components that form these lines. We found that several of them are already available and for those that are not available we adopted the same approach discussed in M13 to compute the HFS. The atomic data required to compute the HFS of La and Eu were taken from Lawler et al. (2001a) and Lawler et al. (2001b), respectively. For the La line at 6774.27 Å we adopted the HFS already computed by M13. The same outcome applies to Y: we adopted the HFS data given by M13, but they are only available for three (out of six) lines of this element ($\lambda = 5119.12, 5289.81, 5728.89 \text{ \AA}$).

No atomic data have been found in the literature for our lines of Ce and Nd. Only the odd isotopes ^{143}Nd and ^{145}Nd have HFS, but their effects can be safely ignored – in the solar system these isotopes constitute only 20.5% of the total Nd abundance, their lines are very narrow, and recent laboratory transition probabilities by Den Hartog et al. (2003) indicate no evident HFS structure for more than 700 lines of Nd II.

¹ *Image Reduction and Analysis Facility*, distributed by the National Optical Astronomy Observatories (NOAO), USA.

Table 1. Mean differences in the abundances derived before and after accounting for the HFS.

specie	λ [Å]	$[\text{X}/\text{H}]_{\text{HFS}} - [\text{X}/\text{H}]_{\text{no HFS}}$	correction (min, max)
Y II	5119.12	+0.013 ± 0.006	0.00, +0.03
Y II	5289.81	+0.008 ± 0.005	0.00, +0.02
Y II	5728.89	+0.008 ± 0.005	0.00, +0.02
La II	5114.56	-0.172 ± 0.128	-0.45, -0.01
La II	5290.82	-0.010 ± 0.013	-0.04, +0.01
La II	5805.77	-0.129 ± 0.098	-0.53, 0.00
La II	6262.29	-0.211 ± 0.178	-0.90, -0.01
La II	6390.48	-0.004 ± 0.009	-0.03, +0.01
La II	6774.27	+0.050 ± 0.050	-0.17, +0.11
Eu II	6437.64	-0.006 ± 0.008	-0.03, +0.01
Eu II	6645.13	-0.023 ± 0.021	-0.10, +0.01

Notes. The quoted errors in the third column represent the dispersion around the mean, and the forth column lists the minimum and maximum HFS corrections applied to the abundances.

2.2.2. Abundances corrected from HFS

We derived the abundances of the current sample of 73 Cepheids by accounting for the HFS of the elements and lines mentioned in the previous section. In order to quantify the effects of the HFS on the derived abundances and their dependence on other parameters, we performed a comparison between our abundance results before and after performing the HFS analysis. The mean differences in abundance are summarized in Table 1. Note that the differences are much larger for some of the La lines, but they are very close to zero for both Y and Eu lines. Concerning possible dependences on other parameters, we found that these differences and their dispersions become smaller with increasing T_{eff} (specially for $T_{\text{eff}} > 5500$ K), with increasing surface gravity (specially for $\log g > 0.5$), and with decreasing pulsation period ($\log P < 1.0$). No clear correlation with metallicity is observed.

Finally, we note that the lines selected to measure n-capture elements are typically weak (typically smaller than 180 mÅ) and unsaturated. This means that the derived abundances for La, Ce, Nd and Eu are marginally affected by HFS sub-structure, while for Y they are small (see Table 1).

Table 2 lists the abundances from individual spectra. Column 3 shows the iron abundances derived by G14, and column 4 the number of Fe I and Fe II lines used. The other columns show our results for the abundances of Y, La, Ce, Nd, and Eu, corrected for HFS when possible, together with the number of lines used. In Table 3 we list the mean abundances computed for the stars with multiple spectra. The HFS data that we adopted are listed in Table 4 for Y, La, and Eu lines.

2.3. Data available in the literature

We compared our abundance estimates, corrected for HFS, with the results provided by similar studies available in the literature: Lemasle et al. (2013, hereinafter LEM), Luck et al. (2011, LII), Luck & Lambert (2011, LIII), and Yong et al. (2006, YON). Note that none of the quoted investigations, but YON, take account of HFS corrections in their analysis of Cepheid spectra.

By comparing the stars in common among these different data sets, we evaluated the systematic difference among them. The mean differences between our measurements and those of

LEM, LII, LIII, and YON range, in modulus, from 0.02 dex for Eu up to 0.31 dex for Fe. The details on these comparisons are listed in Table 5, where we show the zero-point differences obtained by G14 for the iron abundances together with our determinations for the other elements. Each pair of data sets was chosen aiming to maximize the number of stars in common between them. To provide a homogeneous abundance scale for Galactic Cepheids, we applied these zero-point differences to the quoted data sets, putting them in the same scale of our current sample. The element abundances available in the literature and the rescaled values are listed in columns from 2 to 15 of Table 7.

The priority in using the abundances from the literature follows the same approach adopted by G14 and by G15: firstly, we adopt the abundances provided by our group, i.e., this study and the results from LEM, and finally those provided by the other studies, namely LIII, LII, and YON, in this order. We notice that the star HQ Car was also excluded from our analysis because it has been recently identified as a Type II Cepheid by Lemasle et al. (2015). The final sample has 435 Cepheids, with a homogeneous abundance scale for Fe, Y, La, Ce, Nd, and Eu.

3. Neutron-capture element gradients

3.1. Neutron-capture gradients from Cepheids

In this section we investigate the radial gradients of Y, La, Ce, Nd, and Eu across the Galactic disk using our sample of 73 classical Cepheids plus a sample of 363 Cepheids available in literature. Homogeneous iron abundances and Galactocentric distances for the entire sample were provided by G14 (see their Table 1 and Table 4). The key advantage of the current approach when compared with similar investigations are the following: *i*) the intrinsic parameters ($\log g$, T_{eff} , v_t) were estimated using the same approach; *ii*) elemental abundances are based on high-resolution and high signal-to-noise spectra and similar line lists; *iii*) individual Cepheid distances were estimated using near-infrared Period-Wesenheit relations that are reddening free and minimally affected by the metallicity (Inno et al. 2013).

In the following we discuss the radial gradients of four s-process (Y, La, Ce, Nd) elements and a single r-process element (Eu). We note that n-capture elements can be split according to solar system abundances in pure s-process, pure r-process, and mixed-parentage isotopes. Among the selected elements Eu is a pure r-process element, since the r-fraction abundance is 97% (Burris et al. 2000; Simmerer et al. 2004). On the other hand, the selected s-process elements have s-fraction abundances ranging from roughly 50% (Nd, 58%, Sneden et al. 2008) to more than 70% (Y, 72%; La, 75%; Ce, 81%). Note that the quoted s- and r-fraction abundances should be cautiously treated, since Bisterzo et al. (2011), using a different approach, found similar fractions for Eu (94%), Nd (52%), La (71%) and Ce (81%), but a significantly larger s-fraction for Y (92%).

Figure 2 shows the abundances scaled to hydrogen of Y, La, Ce, Nd, and Eu as a function of R_G for the final sample. Stars plotted in this figure include the current 73 Cepheids plus 38 from LEM, 263 from LIII and 61 from LII. Note that for the Cepheid XZ CMa the abundances of the above elements are not available, therefore, we ended up with a sample of 435 stars. The individual Cepheid Galactocentric distances were estimated by G14 and assume a solar Galactocentric distance of $7.94 \pm 0.37 \pm 0.26$ kpc (Groenewegen et al. 2008; Matsunaga et al. 2013). The individual R_G values are also listed in Table 3. The typical uncertainty on the individual distances is ~5% and is mainly due to the accuracy of the zero-point

in the adopted Period-Wesenheit relations (for more details see Inno et al. 2013).

The Cepheid abundances from the literature plotted in Fig. 2 were scaled adopting the zero-point differences listed in Table 5. A similar approach was adopted to scale both iron (G14) and α -element abundances (G15). This figure also shows the linear Least Squares fits to the current sample of 73 Cepheids (blue solid line) and to the entire sample (435, black dashed line). To avoid thorny problems in the estimate of both the zero-point and the slope due to possible outliers, we applied a *biweight* procedure (Beers et al. 1990). The slopes and the zero-points of the two radial gradients are labeled. The slopes and the zero-points of the fits based on the entire sample together with their uncertainties and standard deviations are also listed in columns from 2 to 4 of Table 6.

The empirical scenario emerging from the data plotted in this figures brings forward several interesting features.

i) – Radial gradients – The five investigated neutron-capture elements display well defined radial gradients. This evidence coupled with similar results concerning iron (see G14, and references therein), α (see G15, and references therein), and iron-group (LII, LIII) elements further indicates that young stellar tracers show radial gradients across the Galactic thin disk. A more quantitative discussion concerning the global behavior will be addressed in a forthcoming paper. Finally, we note that the occurrence of well defined radial gradients for light (Y) and heavy s-process elements (La, Ce, Nd) do not support the lack of a radial gradient for Ba as recently suggested by Andrievsky et al. (2014) and by Martin et al. (2015). The quoted authors used high-resolution spectra for a sizable sample of inner and outer disk classical Cepheids and take account of NLTE effects. However, Ba abundances in Classical Cepheids are affected by severe limits. In particular, Luck (2014) noted that strong Ba II lines are affected by line-formation effects, while Andrievsky et al. (2013) discussed in detail physical and atomic (isotopic shifts) effects. The reason for the lack of a Ba gradient remains still unclear.

ii) – Slopes – The slopes are quite similar and on average of the order of -0.025 ± 0.004 dex kpc $^{-1}$ for La, Ce, Nd, and Eu. The only exception is Y, for which the slope is more than a factor of two steeper (-0.053 ± 0.003 dex kpc $^{-1}$). The current slopes agree quite well, within the errors, with similar estimates available in the literature. We found that the slopes range from -0.053 ± 0.003 dex kpc $^{-1}$ for [Y/H] to -0.020 ± 0.003 for [La/H]. The slopes estimated by LII+LIII for the same elements range from -0.061 ± 0.003 to -0.019 ± 0.005 dex kpc $^{-1}$, while those estimated by LEM range from -0.062 ± 0.012 to -0.045 ± 0.012 dex kpc $^{-1}$. The latter is slightly steeper and the difference might be due to the limited range in Galactocentric distances covered by their Cepheid sample. The main difference in the comparison with similar estimates available in literature is for Nd. Indeed, LII found a flat distribution across the thin disk. We performed several tests using different cuts in Galactocentric distance and in sample size and we found that the slope is solid within the current uncertainties (see labeled error bars). Moreover, the standard deviation of the Nd gradient is the smallest among the investigated ones. The reader interested in more details on the slopes of the available data sets is referred to columns from 6 to 9 of Table 6.

iii) – Spread – The spread of the individual abundances attains similar values across the thin disk. The outermost disk regions are an exception, since the spread increases for R_G larger than 13 kpc. The neutron capture elements display the same trend of iron and α -element abundances. Among the investi-

gated elements, Y seems to be once again an exception, since the spread is homogeneous over the range of Galactocentric distances covered by the current sample.

iv) – Comparison with theory – Our results for La (-0.020 ± 0.003 dex kpc $^{-1}$) and for Eu (-0.030 ± 0.004 dex kpc $^{-1}$) agree quite well with theoretical predictions by Cescutti et al. (2007) for Galactocentric distances covering the entire thin disk ($4 \leq R_G \leq 22$ kpc). They found a slope of -0.021 dex kpc $^{-1}$ for La and of -0.030 dex kpc $^{-1}$ for Eu. The predicted slopes become steeper for Galactocentric distances shorter than 14 kpc and shallower for distances larger than 16 kpc (see their Table 5). Predictions for the other s-process elements are not available. In passing we note that the observed slope for Y (-0.053 ± 0.003 dex kpc $^{-1}$) is similar to the predicted slopes for iron and iron-group elements in the Galactocentric range between 4 and 14 kpc.

3.2. Comparisons with independent radial gradients

To further constrain the plausibility of the above radial gradients, Fig. 3 shows the comparison between Cepheid gradients and radial gradients of neutron-capture elements of Galactic field stars. The abundances of Y, Ce, Nd, and Eu for 181 F- and G-type dwarf stars provided by Reddy et al. (2003, hereinafter R03) are plotted. The La and Eu abundances for 159 dwarf and giant stars were provided by Simmerer et al. (2004, hereinafter S04). Their abundances were rescaled to the abundances of the solar mixture adopted in the current investigation (Grevesse et al. 1996). Moreover, to overcome possible differences between Cepheids and field stars concerning either the different diagnostics adopted to determine distances or the use of different spectral lines, in plotting their data we adopted the zero-points of our gradients at the solar Galactocentric distance. Note that in dealing with S04 data, we only selected the more metal-rich stars ($[Fe/H] > -1.0$) to be more consistent with the metallicity range of the current Cepheids. The figure shows that the radial gradient of the five neutron-capture elements based on Cepheids agree quite well with the abundances for field dwarf stars in the Galactic thin disk. The fact that the giants in the S04 sample covers only a limited range of Galactocentric distances across the solar circle does not allow us to constrain the radial gradient.

In Fig. 3 we also plot the Y abundances recently provided by Origlia et al. (2013, hereinafter O13) for three red supergiant (RSG) stars in the Scutum cluster. They used high-resolution ($R \sim 50\,000$) NIR (Y, J, H, K) spectra collected with GIANO at the Telescopio Nazionale Galileo (TNG). The comparison further supports previous results by Bono et al. (2015) and G15 concerning the underabundance of iron and α -elements in blue and red supergiants located either in the near end of the Galactic bar or in the Galactic center. The Y abundances display the same underabundance when compared with similar abundances of classical Cepheids located in the inner edge of the Galactic thin disk.

3.3. Age dependence of the [neutron-capture/H] ratios

The results concerning the abundance gradients discussed in the above sections use the Galactocentric distance as independent variable. However, classical Cepheids when compared with other stellar tracers have the key advantage that their pulsation period is tightly anti-correlated with their individual ages (Bono et al. 2005, G15). The typical pulsation age of short period ($P \sim 1.0\text{--}1.5$ days) Cepheids is indeed of the order of 200 Myr, while for long period ($P \sim 100$ days) ones is of the order of 10 Myr. The exact range in age does depend on the chemi-

cal composition and on the adopted evolutionary framework (see Table 4 and 5 in Bono et al. 2005, and Anderson et al. 2015). This provides the unique opportunity to constrain the chemical enrichment history of the thin disk during the last ~ 300 Myr (G14, G15).

To constrain the age dependence of the metallicity gradients, Fig. 4 shows the same elemental abundances plotted in Fig. 2, but as a function of the logarithmic period. Data plotted in this figure show that the investigated neutron-capture elements display well defined positive gradients as a function of the pulsation period. The α elements (Mg, Si, Ca) and the light elements (Na, Al) investigated by G15 show similar trends, but the current slopes are on average shallower. The slopes of three out of the four s-process elements (La, Ce, Nd) are equal or smaller than 0.10 dex per logarithmic day, however Y (s element) and Eu (r element) display steeper slopes (0.20 and 0.15 dex per logarithmic day, respectively).

The above empirical evidence indicates that the elements that are more typically associated with explosive nucleosynthesis (Si, Ca, Eu) display age gradients ranging from 0.09 (Ca) to 0.15 (Si, Eu) dex per logarithmic day. On the other hand, Y shows a slope (0.20 ± 0.03 dex per logarithmic day) that is at least a factor of two larger than the other s-process elements with similar s-fraction abundances (La, Ce). In this context it is worth mentioning that the 60–70% of Y is produced in the main s-process, while 5–10% comes from r-process and the remaining from the weak component. However, the significant difference in the Y slope when compared with the other s-process elements could suggest a larger contribution either from the r- and/or from the s-weak component.

To take account for the above empirical evidence we could also use plain stellar evolutionary arguments. We start from the evidence that Cepheid stellar masses range, according to chemical composition, from $3.0\text{--}3.5 M_{\odot}$ to $10\text{--}12 M_{\odot}$ (Bono et al. 2010). This means that a significant fraction of Cepheids evolve into the AGB phase. The difference in evolutionary time between the end of the so-called blue loop and the beginning of the AGB phase is negligible when compared with H and He burning phases. This means that Cepheids and AGB stars with stellar masses ranging from ~ 3 to $\sim 6 M_{\odot}$ evolve with similar evolutionary lifetimes. The current theoretical predictions indicate that intermediate-mass AGB stars in the quoted mass regime, mainly produce light s-process (ls) elements (such as Y), while the bulk of the heavy s-process (hs) elements (such as La) is mainly produced in low-mass ($M < 3 M_{\odot}$) AGB stars. To further constrain this effect, we mention that an AGB star of $6 M_{\odot}$ produces roughly 1/3 of the Y, but only 1/7 of the La produced by a $3 M_{\odot}$ (Cristallo et al. 2015a). This would imply that Y is for younger Cepheids a good tracer of the recent chemical enrichment of intermediate-mass AGB stars. The same outcome applies for the slope of Eu, since this element is mainly produced in stellar structures that are either coeval or even younger than Cepheids. It goes without saying that the quoted scenario is qualitative and more detailed calculations based on chemodynamical models are required to constrain the anti-correlation between s and r-process elements with age.

3.4. Radial gradient of [neutron-capture/Fe]

Figure 5 shows the radial gradients of the abundance ratios scaled to iron. Similar radial gradients for the α elements were recently investigated by G15. The test was motivated by the similarity in the slope of [Fe/H] and [α /H] ratios. Indeed, they found that the slopes of [α /Fe] ratios as a function of the Galactocen-

tric distance are typically smaller than 0.018 ± 0.002 dex kpc $^{-1}$. The conclusion for the quoted elements was that they show, on average, quite flat distribution across the entire thin disk.

Data plotted in Fig. 5 display a different empirical scenario for neutron-capture elements. The s- (La, Ce, Nd) and the r- (Eu) process elements display slopes that are on average a factor of two larger when compared with [α /Fe] ratios. The only element to show a flat distribution over the entire disk is Y. The above evidence is suggesting that the steady enhancement in four out of the five neutron-capture elements investigated is mainly caused by the slopes of La, Ce, Nd, and Eu radial gradients: they are at least a factor of two smaller than the iron slope (-0.060 ± 0.002 dex kpc $^{-1}$). The [Y/Fe] ratio is flat because the slope of Y gradient (-0.053 ± 0.003 dex kpc $^{-1}$) is quite similar to the iron one.

The above findings indicate that the chemical enrichment history of La, Ce, Nd, and Eu across the Galactic thin disk is quite different when compared with α elements and iron. Although Y is considered mainly a s-process element, its abundance ratios appear to be more similar to iron and to α elements than to the other neutron-capture elements. It is worth mentioning that the spread in [element/Fe] of the five investigated elements appears to be quite constant when moving from the inner to the outer disk (see Fig. 5). There is also a mild evidence of a flattening in the above ratios towards the outer disk. Indeed, the radial gradients based on the current sample are steeper than the slopes based on the entire sample. The difference is mainly due to the limited Galactocentric distance covered by our sample. However, the number of Cepheids with Galactocentric distance larger than 13 kpc is limited, and new identifications of classical Cepheids in the outer disk are required to further constrain the quoted trends (see also G15). In this context, it is worth mentioning that Gaia is going to play a crucial role, since detailed calculations indicate that the number of Galactic Cepheids will increase at least one order of magnitude (Bono 2003; Windmark et al. 2011).

3.5. Comparisons with independent radial gradients

To validate the new slopes of the [neutron-capture/Fe] radial gradients, Fig. 6 shows the comparison with similar data available in the literature. The colored symbols denote the same field dwarf and giant stars plotted in Fig. 3. Note that the abundances ratios plotted in this figure were scaled both in iron and in neutron-capture element abundances. The flatness of the [neutron-capture/Fe] ratios for Y and the increasing trends for La, Ce, Nd, and Eu are quite similar to the results based on the entire Cepheid sample.

This evidence further supports our working hypothesis that neutron-capture elements – but Y – experienced during the last 300 Myr a different chemical enrichment history from iron and α elements. The current predictions concerning the chemical enrichment of AGB stars indicate that ls elements (such as Y) are mainly synthesized in the more metal-rich ([Fe/H] > -0.6) regime, while the hs elements (such as La) are more favored in the metal-intermediate regime (see also § 4). The quoted theoretical framework supports the mild enhancement in hs elements when moving from the inner (more metal-rich) to the outer (more metal-poor) Galactic thin disk. On the other hand, the lack of a clear trend in the [Y/Fe] abundance ratio indicates a substantial balance across the entire disk. However, the most metal-rich ([Fe/H] $\sim 0.4\text{--}0.5$) Cepheids in our sample that are located in the inner disk ($5 \leq R_G \leq 7$ kpc) show a downturn in [Y/Fe], suggesting an underabundance of Y at super-solar iron abundance. This

finding further supports a similar trend in [Y/Fe] abundances provided by Feltzing & Gustafsson (1998, hereinafter FG98) using high-resolution spectra for 47 dwarf stars with super-solar iron abundance (see their Fig. 22 and § 6.13). However, the presence of a mild enhancement of Eu in the outer disk is even more compelling, since this is considered a solid r-process element mainly produced by the same stellar masses producing α elements.

In passing we also note that the reduced spread of the above elements, at fixed R_G distance, is also suggesting a quite homogeneous spatial enrichment across the four Galactic quadrants. This is also an interesting evidence worth being investigated in more detail, since AGB stars can have both intermediate-age (1–9 Gyr) and old (~ 10 Gyr) progenitors.

3.6. Age dependence of the [neutron-capture/Fe] ratios

To constrain the age dependence of the [neutron-capture/Fe] abundance ratios, Fig. 7 shows the same elemental abundances plotted in Fig. 5, but as a function of the logarithmic period. A glance at the data plotted in this figure shows that the ratios are approximately constant over the entire period range. The only exception is Ce, showing a mild negative gradient (-0.09 ± 0.02 dex per logarithmic day). Similar trends are also showed by light and α elements. Indeed, Ca showed (see Fig. 5 in G15) a negative gradient (-0.11 ± 0.02 dex per logarithmic day), while the others either a mild gradient (Al, Si) or a flat distribution (Na, Mg). The flattening of the s-process elements is once again an interesting finding, since it is suggesting that s elements and iron enrichment across the Galactic thin disk have been quite homogenous over a broad range in age. The zero-point, the slope, their uncertainties, and the standard deviation of the Ce gradient are listed in the bottom line of Table 6.

4. Neutron-capture element relative abundances

4.1. Metallicity dependence of the [neutron-capture/Fe] ratios

The comparison with abundances of neutron-capture elements available in the literature discussed in the above sections were limited to the data sets for which were also available individual Galactocentric distances. In this section we perform the comparison only using elemental abundances. In particular, we selected: *i*) Y, Ce, Nd, and Eu abundances of F- and G-type field dwarf stars provided by R03 (181 objects); *ii*) Y and Eu abundances of F- and G-type field dwarf stars estimated by Bensby et al. (2005, hereinafter B05, 102 objects) including both thin and thick disk stars; *iii*) La and Eu abundances of field dwarf and giant stars provided by S04 (159 objects); *iv*) Y abundances of field dwarfs analyzed by Edvardsson et al. (1993, hereinafter E93, 157 objects); *v*) Y, La, Nd, and Eu abundances of 47 super-metal-rich field dwarfs by FG98; and *vi*) Y abundances of three RSG stars in the Scutum cluster measured by O13.

Figure 8 shows the comparison between Cepheid [neutron-capture/Fe] abundance ratios with the quoted data sets. Note that we applied a shift in the abundances by FG98, R03, and B05 in order to put them in the same scale of our data at solar metallicity. Data plotted in this figure show that the agreement between Cepheids and both field dwarfs and field giants in the Galactic disk is quite good over the entire metallicity range covered by the above samples. The trends are flat across solar iron abundances and display a modest abundance dispersion. Moreover, there is a clear decrease in the [element/Fe] ratios in the super metal-rich

regime ([Fe/H] > 0.2). Thus suggesting a significant contribution in this iron regime from SNe type Ia ejecta.

The [Y/Fe] ratios has, once again, a different trend: it is underabundant and almost constant over the entire metallicity range (see the top panel of Fig. 8). This trend is supported by field dwarfs available in the literature, though for the super-metal-rich stars provided by FG98 the trend seems to be slightly steeper. The three RSGs observed by O13 also appear, within the errors, similar to the other field disk stars.

The [La/Fe] abundance ratio shows a steady enhancement when moving from the metal-rich into the metal-poor regime. M13 suggested that this trend is mainly caused by the metallicity dependence in the production of the neutron-capture s-process elements (see also Gallino et al. 1998; Busso et al. 1999). The above ratio approaches solar values for [Fe/H] ~ -0.2 and attains a constant value in the more metal-poor regime, thus suggesting no dependence on iron in this metallicity range. The trend in the metal-rich regime ([Fe/H] ≥ 0) is similar to those for Ce and Nd, i.e., it is roughly 0.5 dex underabundant for [Fe/H] ~ 0.5 . The quoted trend is quite evident for La, Ce, and Nd as well as for Eu. The Y in the metal-rich regime shows a similar trend, but the underabundance is milder when compared with the above elements.

The [Eu/Fe] abundance ratio shows a different trend. The enhancement is steady over the entire metallicity range covered by Cepheids and by S04 sample. This evidence suggests a strong anticorrelation with iron concerning the Eu production. It is worth mentioning that data plotted in the bottom panel of this figure further support the contribution of SNe type Ia to the iron abundance. Indeed, the steady decrease in [Eu/Fe] abundance ratio can be explained as a steady increase in iron abundance and a marginal, if any, production of Eu. This trend fully supports early results from FG98 for field super-metal-rich dwarfs.

Finally, we also note that the spread in s-elements and in Eu is constant over the metallicity range covered by the current samples. There is solid empirical evidence that the spread in Eu increases in the most metal-poor regime, for [Fe/H] $\lesssim -2.0$ (Cescutti et al. 2006), but we still lack a detailed quantitative explanation of the observed trend.

4.2. The [La/Eu] and [Y/Eu] abundance ratios

The left panel of Fig. 9 shows the s to r abundance ratio [La/Eu] vs. the [Eu/H] abundance. Note that the abundances derived by S04, McWilliam & Smecker-Hane (2005, hereinafter MS05), and M13 were only rescaled to take account of the solar mixture adopted in the current investigation (Grevesse et al. 1996). Note also that we are plotting the [La/Eu] ratio versus the [Eu/H] abundance to separate the role played by pure explosive nucleosynthesis of iron in SNe type Ia and type II from the neutron capture enrichments. The Cepheids in this plane show a well defined anticorrelation. The [La/Eu] ratio, when moving from the most Eu-rich to the most Eu-poor stars, increases by almost one dex. The Cepheid abundance ratio becomes even more compelling in the comparison with field giant and dwarf stars provided by S04. The latter sample shows an almost constant ratio over a broad range in Eu abundances and a mild increase in the approach to solar Eu abundances. The [La/Eu] abundance ratios provided by M13 and by MS05 for Sagittarius RGs show a similar distribution, but three stars display large Eu abundances. Two out of the three display a solar ratio, while the third one is 0.4 dex enhanced in La.

Data plotted in the middle panel of Fig. 9 shows the same abundance ratios, but versus the [La/Fe] ratio. The empirical

scenario becomes more clear, and indeed we found that RGs in Sagittarius are systematically more enhanced in La when compared with Galactic thin disk stellar population. Indeed, only a few Sagittarius stars are located in the same region covered by thin disk stars. In passing we note that a similar enhancement in La has also been found in several dwarf spheroidal galaxies (Shetrone et al. 2003; Geisler et al. 2005; Pompeia et al. 2008; Letarte et al. 2010; Lemasle et al. 2014). Thus suggesting that the above plane is a good diagnostic to identify relic stars of dwarf galaxies that have been accreted by the Milky Way.

The right panel of Fig. 9 shows the same abundance ratio, but versus the iron abundance. The trend is quite similar to the left panel of the same figure. However, Cepheids and field stars display, at fixed [La/Eu], a larger spread in iron. The RGs in Sagittarius (MS05, M13) display a trend similar to the Galactic stars, and for $[Fe/H] > -0.3$ it is also similar to Galactic Cepheids. The above evidence indicates that s- and r-process elements in the Galactic thin disk have similar enrichment histories in the metal-poor regime ($[Fe/H] \leq -0.3$). The same ratio shows, in the more metal-rich regime, a well defined anticorrelation with iron and with Eu abundances.

To further constrain the ratio between s- and r- process elements we also investigate the abundance ratio between a light s-element (Y) and Eu. The left panel of Fig. 10 shows $[Y/Eu]$ versus $[Eu/H]$ plane. The distribution of Cepheids in this plane is quite different than in the $[La/Eu]$ versus $[Eu/H]$ plane. Indeed, Cepheids show a larger dispersion over the entire metallicity range they cover, and there is no clear evidence of an anticorrelation with the europium content. On the other hand, field stars show a mild evidence of a correlation with Eu abundance when moving from the Eu-intermediate into the more Eu-rich regime.

Data plotted in the middle panel of Fig. 10 shows a well defined correlation between $[Y/Eu]$ and $[Y/Fe]$. This finding together with the constant value of the $[Y/Fe]$ as a function of both Cepheid ages and iron abundance, is suggesting a different enrichment history between Y and Eu, but also a difference between light (Y) and heavy (La) s-process elements. Note that the three Sagittarius RGs attain in this plane the lowest values, thus suggesting that they are quite Y poor when compared with field Galactic stars.

The right panel of Fig. 10 shows the same data, but in the $[Y/Eu]$ versus iron abundance. The bulk of the data seems to suggest a correlation between the s to r abundance ratio and iron content. In this context it is worth mentioning that for iron abundances more metal-poor than the sun there is a mild evidence of a possible dichotomous distribution. In particular, field dwarf stars associated with the Galactic thick disk provided by B05 display, at fixed iron content, lower $[Y/Eu]$ abundance ratios. The difference with similar abundances provided by E93 plus S04 and by R03 is slightly larger than one sigma and needs to be further investigated with larger homogeneous sample.

4.3. The $[La/Y]$ abundance ratio

Figure 11 shows the ratio between a heavy (La) and a light (Y) neutron-capture element. Such a ratio is a good diagnostic for the s-process index $[hs/ls]$, i.e., the ratio between the heavy s-process elements and the light ones. The quoted ratio and its dependence on the metallicity are solid tracers of the role played by AGB stars in the chemical enrichment (Gallino et al. 1998; Busso et al. 1999, 2001; Cristallo et al. 2009). The production of hs elements (such as La) is favored in the metal- intermediate regime ($[Fe/H] \sim -0.6$), while in the more metal-rich regime ls elements (such as Y) are mostly synthesized. Therefore, the ratio

$[hs/ls]$ is expected to be under-abundant in the metal-rich regime and enhanced in the more metal-poor regime. Our Cepheid data in the left panel of this figure display, in agreement with theoretical predictions (Cristallo et al. 2009, 2011, 2015b), a well defined anticorrelation between the $[La/Y]$ ratio and the Y abundance. The Galactic field stars measured by E93 and S04 display a large spread, at fixed Y abundance, but the trend is similar. Interestingly enough, we found that Sagittarius RGs – provided by MS05, M13, and Sbordone et al. (2007, hereinafter S07) – display two distinctive features: *i*) a strong enhancement in La, with a marginal overlap with Galactic stars; and *ii*) the spread in $[La/Y]$ abundance ratio is significantly larger than Galactic stars. Thus suggesting that the enrichment of neutron-capture elements in Sagittarius is more complex than in the thin disk.

The trend of the data plotted in the left panel of Fig. 11 becomes even more clear in the $[La/Y]$ versus $[La/Fe]$ plane (middle panel). Galactic stars and Sagittarius RGs display, at fixed $[La/Fe]$ abundance, a smaller spread in $[La/Y]$ abundances. Moreover, the separation between Sagittarius and Galactic stars becomes even more solid. Indeed, only the three most metal-poor objects in the Sagittarius sample overlap with Galactic thin disk stars. This finding indicates a strong correlation between Y and Fe over the entire metallicity range.

The right panel of Fig. 11 shows the same data, but they are plotted as a function of the iron abundance. The distribution in this plane is quite similar to the left panel, but with a larger spread in iron abundances. In passing, we note that the separation between Galactic and Sagittarius stars might be even more compelling than suggested by current data. The 17 Cepheids with $[La/Y] > 0.3$ come from the LIII sample. The authors did not take account of the hyperfine structure, moreover, 15 out of the 17 are located in the 1st quadrant and at Galactocentric distance larger than 9 kpc. Cepheids in the outer disk will play a crucial role to further constrain the use of the quoted chemical diagnostics to separate Galactic and dwarf galaxy stars.

In this context it is worth mentioning that the star Sgr 247 from the M13 sample lies off the main trend in the left and in the right panel of Fig. 11. The peculiar position of this object shows also up in the left and in the right panel of Fig. 10. The current findings further support the results by M13 suggesting that this object was polluted by more metal-poor ($[Fe/H]$ ranging from about -0.5 to about -1.0 dex) AGB ejecta. The AGB yields in this object were polluted but less than similar Sagittarius stars. This hypothesis is further supported by the evidence that the same object follow the main trend in the $[hs/ls]$ and in the $[s/r]$ abundance ratios (middle panels of Fig. 10 and Fig 11).

4.4. Comparison between predicted and observed $[hs/ls]$ s-process index

To further constrain the difference between the s-process index $[hs/ls]$ in Cepheids with field Galactic stars and in nearby dwarf galaxies, Fig. 12 shows the comparison between theoretical and observed $[La/Y]$ as a function of iron content. The black lines display predicted final surface abundances for four low-mass (see labeled values) AGB models available on the FRUITY database² Cristallo et al. (2011, 2015b). The symbols and error bars for the data are the same as in the right panel of Fig. 11. The comparison brings forward several interesting new findings:

i) The agreement between theory and observations is quite good over the entire metallicity range covered by Cepheids. In this context it is worth mentioning that Cepheids offer a new

² fruity.ox-teramo.inaf.it

opportunity to validate the [hs/ls] s-process index. Theoretical predictions are validated using a broad range of s-enhanced stars – O-rich and C-rich AGB stars, post-AGB stars, Ba-rich stars and CH-rich stars – for which the evolutionary status is not well established. The advantage in using Cepheids is that they do belong to the first stellar generation formed after the recent enrichment of the interstellar medium. The current comparison between theory and observations should be cautiously treated because we are not accounting for dilution effects and for detailed chemical evolution models.

However, it is worth mentioning that the above comparison was performed overplotting predicted abundances on top of the observed values. This means that once corrected for the adopted solar abundances, we did not apply any shift in the predicted abundances. Data plotted in this figure suggest that predicted [La/Y] abundances display, in the metal-rich regime a spread that is systematically smaller than observed. The reader interested in a detailed discussion concerning the theoretical parameters affecting the spread of the above s-process index is referred to Cristallo et al. (2015a) (see also Piersanti et al. 2013). In this context we would like to stress the similarity in the slope when moving from the metal-rich to the metal-poor regime of Galactic Cepheids. The current empirical uncertainties do not allow us to constrain whether field dwarf stars provided by E93 and S04 do show a shallower slope when compared with Cepheids.

ii) Theory and observation display a steady increase in [La/Y] when moving from the metal-rich into the metal-intermediate regime, i.e., $[Fe/H] \sim -0.4/-0.7$. The [La/Y] abundances, as expected, decrease in the metal-poor regime (Cristallo et al. 2009). There is a group of Sagittarius stars showing [La/Y] abundances larger – s-process enhanced – than predicted by AGB models and they have already been discussed by M13. A similar discrepancy has also been found in CEMP stars at very low metallicities, which attain values of s-process index of the order of +1.3 dex (Spite & Spite 2014; Beers et al. 2005). The lack of a sizable sample of Cepheids in the metal-intermediate regime do not allow us to provide independent constraints on the possible mismatch between predicted and observed [hs/ls] abundance ratios. In passing we note that Mishenina et al. (2015), in a recent investigation of more than two dozen of giant stars in five Galactic open clusters, found solid evidence of [Ba/Fe] and [Ba/La] enhancement. They suggested that the quoted empirical evidence might be explained assuming a significant contribution from non standard s-process, i.e., the intermediate neutron-capture process suggested by Cowan & Rose (1977).

To further validate the plausibility of the adopted theoretical framework for the production of s-process elements from AGB stars, we performed a plain test to constrain the slope of $[Y/H]$ versus the Galactocentric distance. We performed a linear fit of the Cepheids plotted in Fig. 12 (i.e. [La/Y] vs. $[Fe/H]$). To overcome the increase in the spread in the more metal-poor and in the more metal-rich regime we selected the objects with iron abundances included between -0.3 and $+0.3$ dex. The current fit was combined with the analytical fits for $[Fe/H]$ and $[La/H]$ as a function of Galactocentric distance. We found that the expected slope for $[Y/H]$ as a function of Galactocentric distance is quite similar to the observed slope (-0.052 vs. -0.053 dex kpc $^{-1}$, respectively). This evidence indicates that s-process elements predicted by AGB models take account for the observed slopes among the investigated elements.

5. Summary and final remarks

This is the 10th of a series of papers focussed on the metallicity distribution of the Galactic thin disk using classical Cepheids as stellar tracers. The project (Disk Optical Near-infrared Young Stellar Object Spectroscopy, DIONYSOS) is aimed at providing homogeneous and accurate elemental abundances and distances for a significant fraction of the known Galactic Cepheids.

In this investigation we present accurate and homogeneous measurements of five neutron capture elements (Y, La, Ce, Nd, Eu) for 73 Galactic classical Cepheids. The current abundances are based on high-spectral resolution ($R \sim 38\,000$) and high signal-to-noise ratio ($S/N \sim 50\text{--}300$) spectra collected with UVES at ESO VLT. They were derived by accounting for the HFS of some lines of Y, La, and Eu, for which atomic data are available in the literature. The iron, α plus Na and Al abundances of the same Cepheids have already been discussed in Genovali et al. (2013, 2014, 2015). Our Cepheids are representative of the Galactic sample, and indeed they cover a broad range in pulsation periods ($0.36 \leq \log P \leq \sim 1.54$) and in Galactocentric distances ($4.6 \leq R_G \leq 14.3$ kpc).

We also selected similar abundances for Galactic Cepheids available in the literature and we ended up with homogenous measurements for 435 Galactic Cepheids. Roughly one third of the entire sample have measurements provided by our group (current plus LEM), while the others come from LII, LIII, and YON. The different samples have from one to 4 dozen of Cepheids in common, which allowed us to provide homogeneous abundance scales for the quoted five elements plus iron and α elements (G14, G15).

The individual distances for the entire Cepheid sample are based on homogeneous NIR photometry, transformed into the 2MASS photometric system, and on the Period-Wesenheit relations provided by Inno et al. (2013). The main findings of the current analysis are the following:

i) $[element/H]$ radial gradients: The investigated neutron capture elements display well defined radial gradients. The slopes for four (La, Ce, Nd, Eu) out of the five elements are quite average (-0.025 ± 0.004 dex kpc $^{-1}$). The Y slope is more than a factor of two steeper and more similar to the slopes of iron and α elements. The current estimates agree quite well with similar radial gradients available in the literature. However, we provide firm constraints concerning the Nd gradient for which it was suggested a flat distribution when moving from the inner to the outer disk. Moreover, the difference in the slope between Y and the other three s-process elements (La, Ce, Nd) brings forward a more complex enrichment history for this element.

ii) Comparison with theory: The comparison with radial gradients predicted by chemical evolution models provided by Cescutti et al. (2006, 2007), indicates a very good agreement for the slopes of both La and Eu.

iii) Comparison with observations: The comparison with similar abundances for field thin and thick dwarf and giant stars provided by E93, FG98, R03, S04, B05, and O13 indicates a very good agreement over the Galactocentric distances covered by the quoted samples.

iv) Age dependence: We took advantage of the tight anti-correlation between pulsation period and age to constrain the age dependence of the investigated elements. We found that the slopes are positive, i.e., they are more abundant in young (a few tens of Myrs) than in old (~ 300 Myr) Cepheids. However, the slopes of La, Ce, and Nd are shallower than for iron, α elements, and light elements, while for Y and Eu are more similar.

v) [element/Fe] radial gradients: We found that three s-process dominated elements (La, Ce, Nd) and one r-process dominated element (Eu) display slopes that are on average a factor of two larger than similar slopes of the α and light elements investigated by G15. The slope of Y is once again an exception, and indeed this element shows a flat distribution across the entire disk. The quoted trends are the consequence of the difference/similarity with the iron radial gradient.

vi) [element/Fe] abundance ratios in the super-metal-rich regime: We found that s- and r-process abundance ratios display a steady decrease for iron abundances larger than solar. The change in the slope indicates a clear contribution from SNe type Ia ejects. The trend in the [Eu/Fe] abundance ratio as a function of iron abundance further supports the above hypothesis with a steady decrease in the slope when moving from [Fe/H] ~ -1.2 to [Fe/H] ~ -0.5 . The current findings support previous results for super-metal-rich field dwarfs by FG98.

vii) Spatial and temporal homogeneity: The reduced scatter in the above radial gradients at fixed Galactocentric distance and the lack of well defined slopes for [element/Fe] as a function of the pulsation period (but Ce) is indicating that the chemical enrichment across the Galactic thin disk is characterized by firm spatial and temporal homogeneity.

viii) s to r abundance ratio: We found that Cepheid [La/Eu] abundance ratios show a well defined anticorrelation when plotted as a function of Eu and Fe abundances. Field stars display a different trend. Indeed, they attain an almost constant ratio in the metal-poor regime and only for [Eu/H] and [Fe/H] larger than ~ -0.5 dex show a mild enhancement in La. The light s-to r-process element abundance ratio ([Y/Eu]) shows a different trend. The Cepheids do not show a clear anticorrelation with [Y/H] and with [Y/Fe]. On the other hand, field stars display a correlation with both Y and iron. Moreover, [Y/Eu] shows a well defined correlation with iron abundance. This trend appears as the consequence of the strong correlation between Y and iron abundances.

ix) Heavy to light s element abundance ratio: We found that Cepheid [La/Y] abundance ratios show a strong anticorrelation when plotted as a function of Y and Fe abundances. Field Galactic stars display the same trend, thus supporting the metallicity dependence of heavy (La, Ce, Nd) and light (Y) s-process elements on the metal content (Cristallo et al. 2009, 2011, 2015b). Moreover, we also found that the dispersion in [La/Y] as a function of [La/Fe] is small among Galactic and Sagittarius stars, further supporting similarity in the origin of Fe and Y. Interestingly enough, we also found that in the quoted planes, in particular, in the [La/Y] vs. [La/Fe] one, the Sagittarius RGs are well separated by Galactic stars, due to their La enhancement. Thus suggesting that they can be adopted as solid diagnostics to identify relic stars of dwarf galaxies accreted by our galaxies.

x) Comparison between predicted and observed s-process index: We performed a detailed comparison between predicted and observed s-process index [La/Y]. We found that final surface abundances of low-mass ($1.5 \leq M/M_{\odot} \leq 3.0$) AGB stars agree quite well over the entire metallicity range covered by the current sample of classical Cepheids.

Acknowledgements. This work was partially supported by PRIN-MIUR (2010LY5N2T) “Chemical and dynamical evolution of the Milky Way and Local Group galaxies” (P.I.: F. Matteucci) and PRIN-MIUR (20128PCN59) “Nucleosynthesis in AGB stars: an integrated approach” project (P.I.: L. Gialanella). We also acknowledge an anonymous referee for the positive opinions concerning this experiment and for the very pertinent suggestions that improved the content and the readability of the paper.

References

- Anderson, R.I., Ekström, S., Georgy, C., et al. 2015, IAU Symposium, 307, 206
 Andrievsky, S.M., Kovtyukh, V.V., Luck, R.E., et al. 2002a, A&A, 381, 32
 Andrievsky, S.M., Bersier, D., Kovtyukh, V.V., et al. 2002b, A&A, 384, 140
 Andrievsky, S.M., Kovtyukh, V.V., Luck, R.E., et al. 2002c, A&A, 392, 491
 Andrievsky, S.M., Luck, R.E., Martin, P., & Lépine, J.R.D. 2004, A&A, 413, 159
 Andrievsky, S.M., Lépine, J.R.D., & Korotin, S.A. 2013, MNRAS, 428, 3252
 Andrievsky, S.M., Luck, R.E., & Korotin, S.A. 2014, MNRAS, 437, 2106
 Ballester, P., Bramich, D., Forchi, V., et al. 2011, Astronomical Data Analysis Software and Systems XX, 442, 261
 Beers, T.C., Flynn, K., & Gebhardt, K. 1990, AJ, 43, 531
 Beers, T.C., & Christlieb, N. 2005, A&A Rev., 100, 32
 Bensby, T., Feltzing, S., & Lundström, I. 2003, A&A, 410, 527 (B05)
 Berger, E., Fong, W., & Chornock, R. 2013, ApJ, 774, L23
 Bisterzo, S., Gallino, R., Straniero, O., Cristallo, S., Käppeler, F. 2011, MNRAS, 418, 284
 Bono, G. 2003, ASP Conf. Ser. 291, 45
 Bono, G., Marconi, M., Cassini, S., et al. 2005, ApJ, 621, 966
 Bono, G., Caputo, F., Marconi, M., & Musella, I. 2010, ApJ, 715, 277
 Bono, G., Genovali, K., Lemasle, B., et al. 2015, ASP Conf. Ser., 491, 148
 Boyd, R.N., Famiano, M.A., Meyer, B.S., et al. 2012, ApJ, 744, 14
 Burris, D.L., Pilachowski, C.A., Armandroff, T.E., et al. 2000, ApJ, 544, 302
 Busso, M., Gallino, R., & Wasserburg, G.J. 1999, ARA&A, 37, 239
 Busso, M., Gallino, R., Lambert, D.L., Travaglio, C., & Smith, V.V. 2001, ApJ, 557, 802
 Cescutti, G., Françoise, P., Matteucci, F., Cayrel, R., & Spite, M. 2006, A&A, 448, 557
 Cescutti, G., Matteucci, F., Françoise, P., & Chiappini, C. 2007, A&A, 462, 943
 Clayton, D.D., & Rassbach, M.E. 1967, ApJ, 148, 69
 Conti, P.S., & Wallerstein, G. 1969, ApJ, 155, 11
 Cowan, J.J., & Rose, W.K. 1977, ApJ, 212, 149
 Cristallo, S., Straniero, O., Gallino, R., et al. 2009, ApJ, 696, 797
 Cristallo, S., Piersanti, L., Straniero, O., et al. 2011, ApJS, 197, 17
 Cristallo, S., Abia, C., Straniero, O., & Piersanti, L. 2015a, ApJ, 801, 53
 Cristallo, S., Straniero, O., Piersanti, L., & Gobrecht, D. 2015b, ApJS, 219, 40
 Dékány, I., Minniti, D., Hajdu, G., et al. 2015, ApJ, 799, 11
 Den Hartog, E.A., Lawler, J.E., Sneden, C., & Cowan, J.J. 2003, ApJS, 148, 543
 Edvardsson, B., Andersen, J., Gustafsson, B., et al. 1993, A&A, 275, 101 (E93)
 Feast, M.W., Menzies, J.W., Matsunaga, N., & Whitelock, P.A. 2014, Nature, 509, 342
 Feltzing, S., & Gustafsson, B. 1998, A&AS, 129, 237 (FG98)
 Gallino, R., Arlandini, C., Busso, M., et al. 1998, ApJ, 497, 388
 Geisler, D., Smith, V.V., Wallerstein, G., Gonzalez, G., Charbonnel, C. 2005, AJ, 129, 1428
 Genovali, K., Lemasle, B., Bono, G., et al. 2013, A&A, 554, A132
 Genovali, K., Lemasle, B., Bono, G., et al. 2014, A&A, 566, A37 (G14)
 Genovali, K., Lemasle, B., da Silva, R., et al. 2015, A&A, accepted (G15)
 Grevesse, N., Noels, A., & Sauval, A.J. 1996, Cosmic Abundances, 99, 117
 Grevesse, N., Scott, P., Asplund, M., & Sauval, J. 2015, A&A, 573, 27
 Groenewegen, M.A.T., Udalski, A., & Bono, G. 2008, A&A, 481, 441
 Gustafsson, B., Edvardsson, B., Eriksson, K., et al. 2008, A&A, 486, 951
 Harris, H.C. 1981, AJ, 86, 707
 Harris, H.C., & Pilachowski, C.A. 1984, ApJ, 282, 655
 Inno, L., Matsunaga, N., Bono, G. 2013, ApJ, 764, 84
 Kippenhahn, R., & Smith, L. 1969, A&A, 1, 142
 Kovtyukh, V.V., & Gorlova, N.I. 2000, A&A, 358, 587
 Kovtyukh, V.V., Wallerstein, G., & Andrievsky, S.M. 2005, PASP, 117, 1182
 Kovtyukh, V.V. 2007, MNRAS, 378, 617
 Kraft, R.P., Galactic structure. Edited by Adriaan Blaauw and Maarten Schmidt. Published by the University of Chicago Press, Chicago, ILL USA, 1965, p.157
 Kraft, R.P., & Schmidt, M. 1963, ApJ, 137, 249
 Lawler, J.E., Bonvallet, G., & Sneden, C. 2001a, ApJ, 556, 452
 Lawler, J.E., Wickliffe, M.E., Den Hartog, E.A., & Sneden, C. 2001b, ApJ, 563, 1075
 Leavitt, H.S. 1908, AnHar, 60, 87
 Leavitt, H.S., & Pickering, E.C. 1912, Harvard College Observatory Circular, vol. 173, pp.1-3
 Lemasle, B., Françoise, P., Bono, G., et al. 2007, A&A, 467, 283
 Lemasle, B., Françoise, P., Piersimoni, A., et al. 2008, A&A, 490, 613
 Lemasle, B., Françoise, P., Genovali, K., et al. 2013, A&A, 558, A31 (LEM)
 Lemasle, B., de Boer, T.J.L., Hill, V., et al. 2014, A&A, 572, 88
 Lemasle, B., Kovtyukh, V.V., Bono, G., et al. 2015, A&A, accepted
 Letarte, B., Hill, V., Tolstoy, E., et al. 2010, A&A, 523, 17
 Luck, R.E. 2014, AJ, 147, 137
 Luck, R.E., Kovtyukh, V.V., & Andrievsky, S.M. 2006, AJ, 132, 902
 Luck, R.E., Andrievsky, S.M., Kovtyukh, V.V., Gieren, W., & Graczyk, D. 2011, AJ, 142, 51 (LII)
 Luck, R.E., & Lambert, D.L. 2011, AJ, 142, 136 (LIII)

- Lyubimkov, L.S., Lambert, D.L., Rostopchin, S.I., Rachkovskaya, T.M., & Poklad, D.B. 2010, MNRAS, 402, 1369
- Matsunaga, N., Kawadu, T., Nishiyama, S., et al. 2011, Nature, 477, 188
- Matsunaga, N., Feast, M.W., Kawadu, T., et al. 2013, MNRAS, 429, 385
- Martin, R.P., Andrievsky, S.M., Kovtyukh, V.V., et al. 2015, MNRAS, 449, 4071
- McWilliam, A., Wallerstein, G., & Mottini, M. 2013, ApJ, 778, 149 (M13)
- McWilliam, A., & Smecker-Hane, T.A. 2005, ASP Conf. Ser. 336, 221 (MS05)
- Metzger, M.R., Caldwell, J.A.R., & Schechter, P.L. 1992, AJ, 103, 529
- Meyer-Hofmeister, E. 1969, A&A, 2, 143
- Minniti, D., Lucas, P.W., Emerson, J.P., et al. 2010, NewA, 15, 433
- Mishenina, T., Pignatari, M., Carraro, G., et al. 2015, MNRAS, 446, 3651
- Miville-Deschénes, M.-A., & Lagache, G. 2005, ApJS, 157, 302
- Origlia, L., Oliva, E., Maiolino, R., et al. 2013, A&A, 560, A46 (O13)
- Pedicelli, S., Lemasle, B., Groenewegen, M., et al. 2010, A&A, 518, 11
- Piersanti, L., Cristallo, S., & Straniero, O. 2013, ApJ, 774, 98
- Pignatari, M., Gallino, R., Heil, M., et al. 2010, ApJ, 710, 1557
- Pompéia, L., Hill, V., Spite, M., et al. 2008, A&A, 480, 379
- Pont, F., Kienzle, F., Gieren, W., & Fouqué, P. 2001, A&A, 376, 892
- Raiteri, C.M., Gallino, R., Busso, M., Neuberger, D., & Kaeppler, F. 1993, ApJ, 419, 207
- Reddy, B.E., Tomkin, J., Lambert, D.L., & Prieto, C.A. 2003, MNRAS, 340, 304 (R03)
- Sbordone, L., Bonifacio, P., Buonanno, R., et al. 2007, A&A, 465, 815 (S07)
- Scott, P., Asplund, M., Grevesse, N., Bergemann, M., & Sauval, J. 2015, A&A, 573, 26
- Shetrone, M., Venn, K.A., Tolstoy, E., et al. 2003, AJ, 125, 684
- Simmerer, J., Sneden, C., Cowan, J.J., et al. 2004, ApJ, 617, 1091 (S04)
- Sneden, C., Cowan, J.J., & Gallino, R. 2008, A&A Rev., 46, 241
- Sousa, S.G., Santos, N.C., Israelian, G., Mayor, M., & Monteiro, J.P.F.G. 2007, A&A, 469, 783
- Spite, M. 1967, Annales d'Astrophysique, 30, 211
- Spite, M., & Spite, F. 2014, Astron. Nachr., 335, 65
- Takeda, Y., Kang, D.-I., Han, I., Lee, B.-C., & Kim, K.-M. 2013, MNRAS, 432, 769
- Thielemann, F.-K., Arcones, A., Käppeli, R., et al. 2011, PrPNP, 66, 346
- Travaglio, C., Gallino, R., Arnone, E., et al. 2004, ApJ, 601, 864
- Tsujimoto, T., & Nishimura, N. 2015, arXiv:1509.00004v1
- Udalski, A., Szymański, M.K., & Szymański, G. 2015, AcA, 65, 1
- Wanajo, S. 2013, ApJ, 770, 22
- Wanajo, S., & Janka, H.-T. 2012, ApJ, 746, 180
- Windmark, F., Lindegren, L., & Hobbs, D. 2011, A&A, 530, 76
- Woosley, S.E., & Heger, A. 2015, ApJ, 810, 34
- Yong, D., Carney, B.W., Teixera de Almeida, M.L., & Pohl, B.L. 2006, AJ, 131, 2256 (YON)

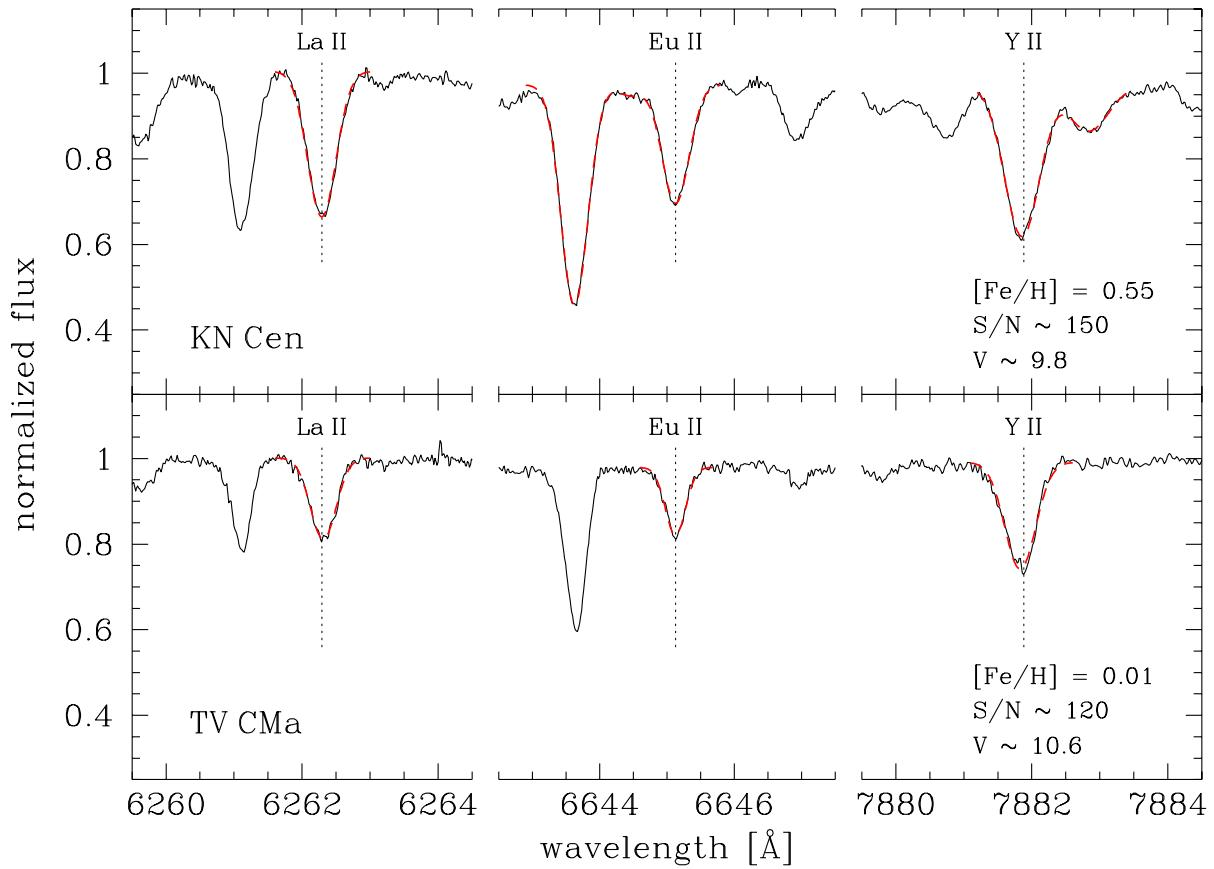


Fig. 1. High-resolution ($R \sim 38\,000$) UVES spectrum of KN Cen and TV CMa. The apparent visual magnitude and the S/N in the spectral range $\lambda \sim 5650 - 7500 \text{ \AA}$ are also labeled. The vertical dashed lines display some of the spectral lines (La II 6262.29, Eu II 6645.13, Y II 7881.88 \AA) adopted to estimate the abundances.

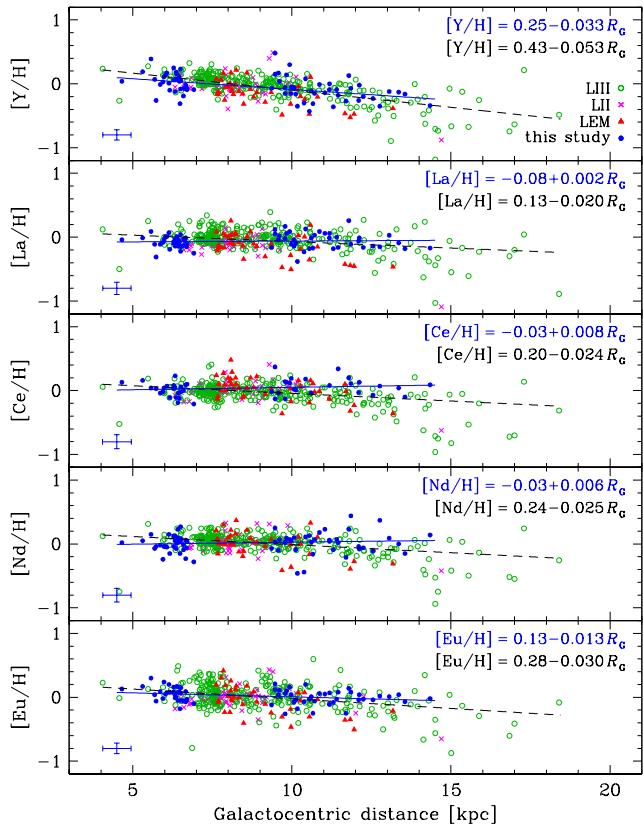


Fig. 2. Abundances of neutron-capture elements as a function of R_G . Our results (filled blue circles) are compared with those of Luck et al. (2011, LII, magenta crosses), Luck & Lambert (2011, LIII open green circles), and Lemasle et al. (2013, LEM, red triangles). The blue solid line shows the linear regression of our Cepheid sample, while the black dashed line the linear regression of the entire Cepheid sample. The blue error bars display the mean spectroscopic error of the current sample. The abundances available in the literature have similar errors.

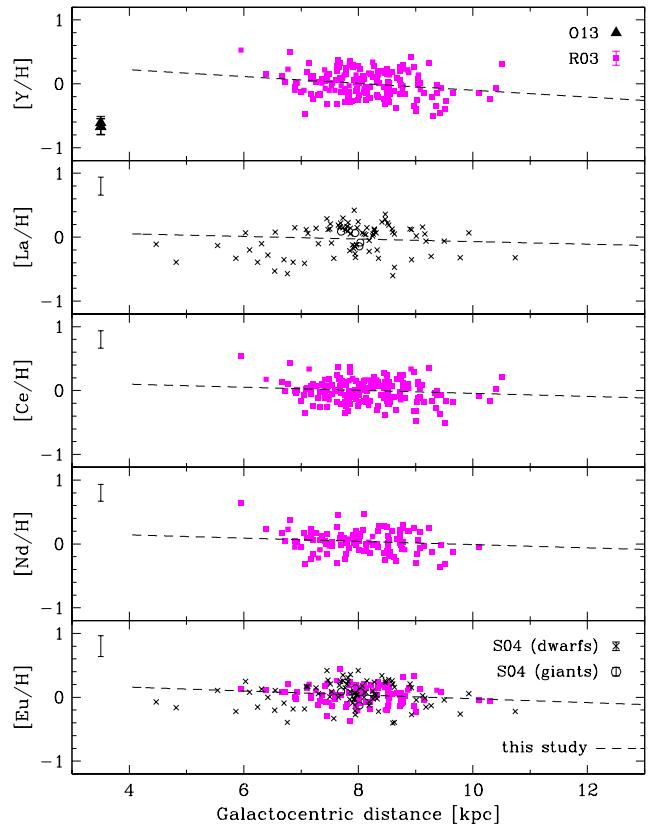


Fig. 3. Abundances of neutron-capture elements as a function of R_G . The radial gradients we derived for Cepheid stars (dashed line) are compared with field dwarfs analyzed by Reddy et al. (2003, R03, magenta squares) and with field dwarfs (crosses) and giants (open circles) analyzed by Simmerer et al. (2004, S04). From the latter only stars with $[Fe/H] > -1.0$ are plotted. RSGs in the Scutum cluster analyzed by Origlia et al. (2013, O13, triangles) are also shown.

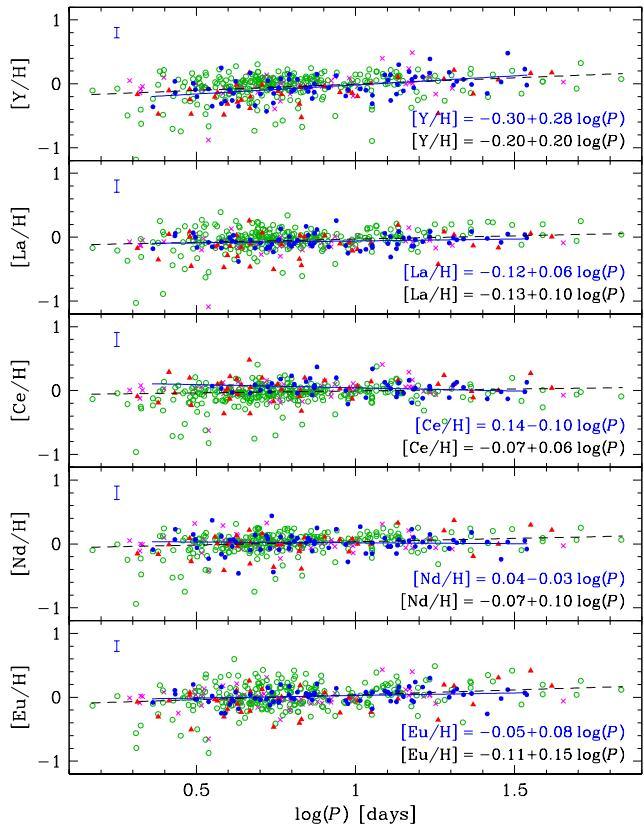


Fig. 4. Abundances of neutron-capture elements as a function of the logarithmic pulsation period. Symbols and colors are the same as in Fig. 2.

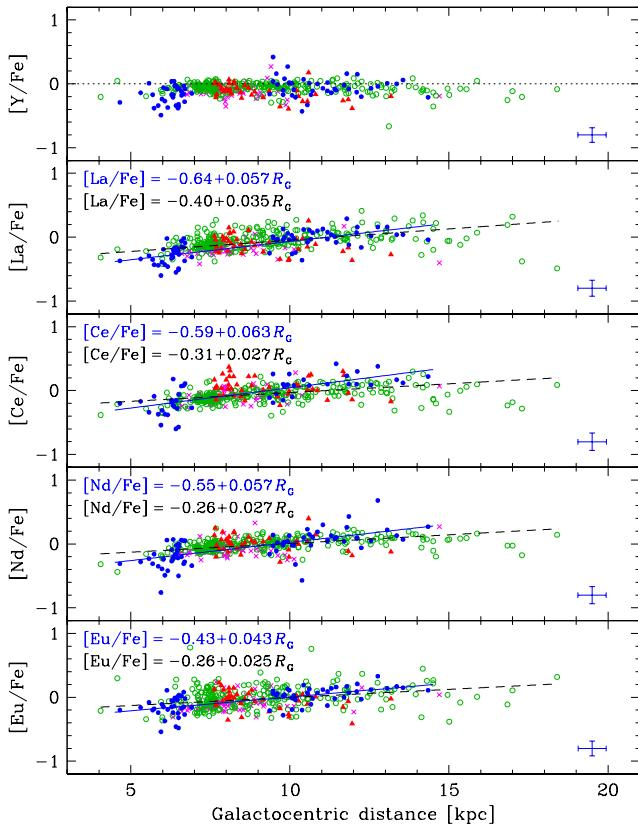


Fig. 5. The same as Fig. 2 but the abundances are scaled to iron. The dotted line displays the positions of solar abundance ratios.

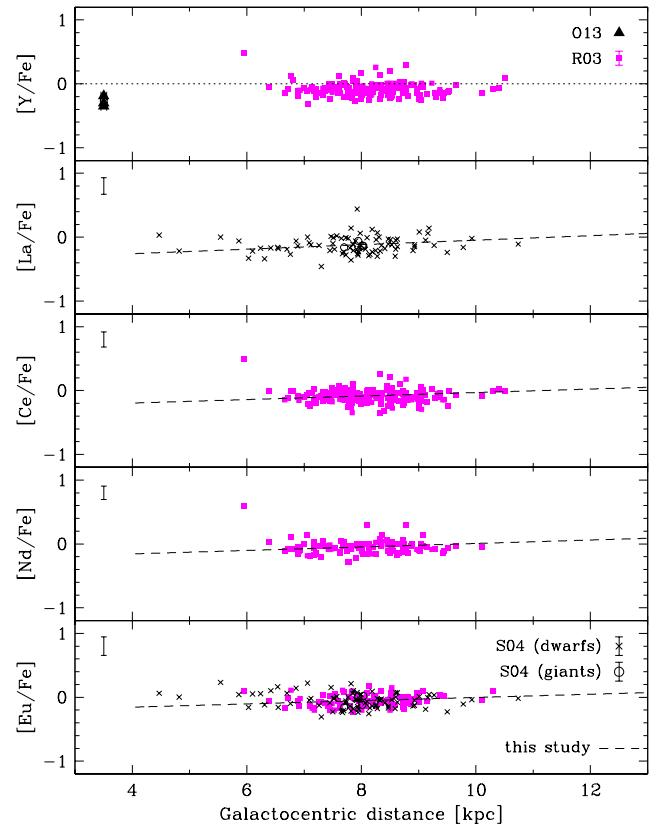


Fig. 6. The same as Fig. 3, but the abundances are scaled to iron. The dotted line displays the positions of solar abundance ratios.

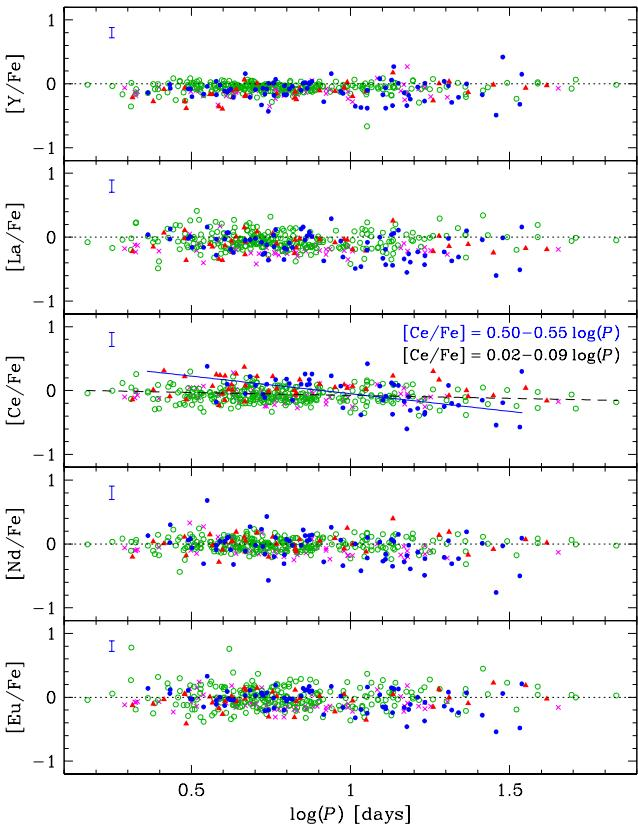


Fig. 7. The same as Fig. 4 but the abundances are scaled to iron. The dotted lines display the positions of solar abundance ratios. Symbols and colors are the same as in Fig. 2

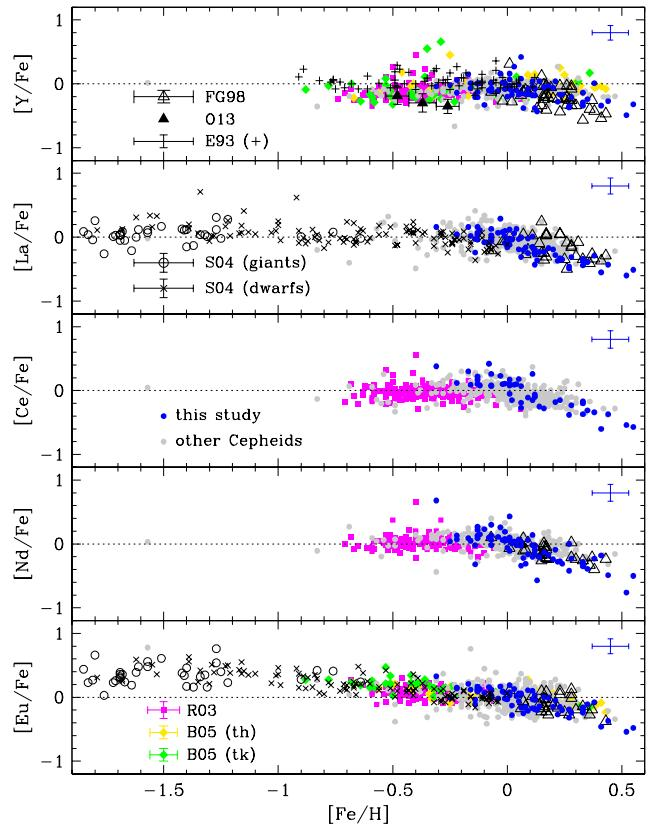


Fig. 8. Abundances of neutron-capture elements as a function of the metallicity. Cepheid stars (filled circles) are compared with field dwarfs from the thin disk by R03 (magenta squares), from the thin (yellow diamonds) and thick (green diamonds) disks analyzed by Bensby et al. (2005, B05), with field dwarfs (crosses) and giants (open circles) by S04, and with field dwarfs analyzed by Edvardsson et al. (1993, E93, pluses) and by Feltzing & Gustafsson (1998, FG98, open triangles). RSG in the Scutum cluster by O13 (filled triangles) are also shown. The dotted lines display the positions of solar abundance ratios.

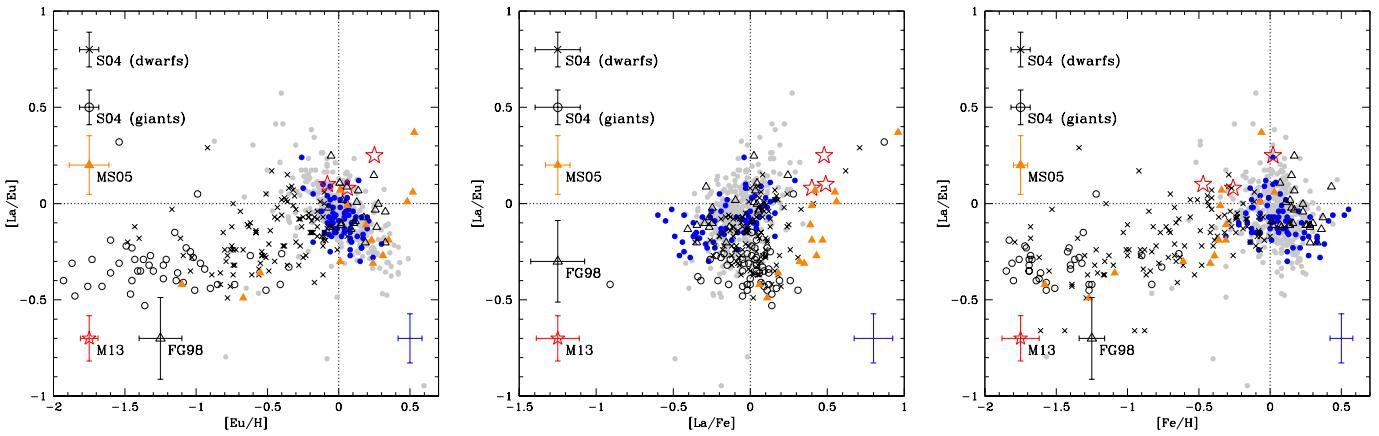


Fig. 9. Abundance ratios between La and Eu as a function of $[Eu/H]$ (left panel), $[La/Fe]$ (middle panel), and $[Fe/H]$ (right panel). Cepheid stars (filled circles) are compared with Galactic field dwarfs (crosses) and giants (open circles) by S04, with field dwarfs by FG98 (open triangles) and with Sgr field stars studied by McWilliam & Smecker-Hane (2005, MS05, filled triangles) and by McWilliam et al. (2013, M13, red stars).

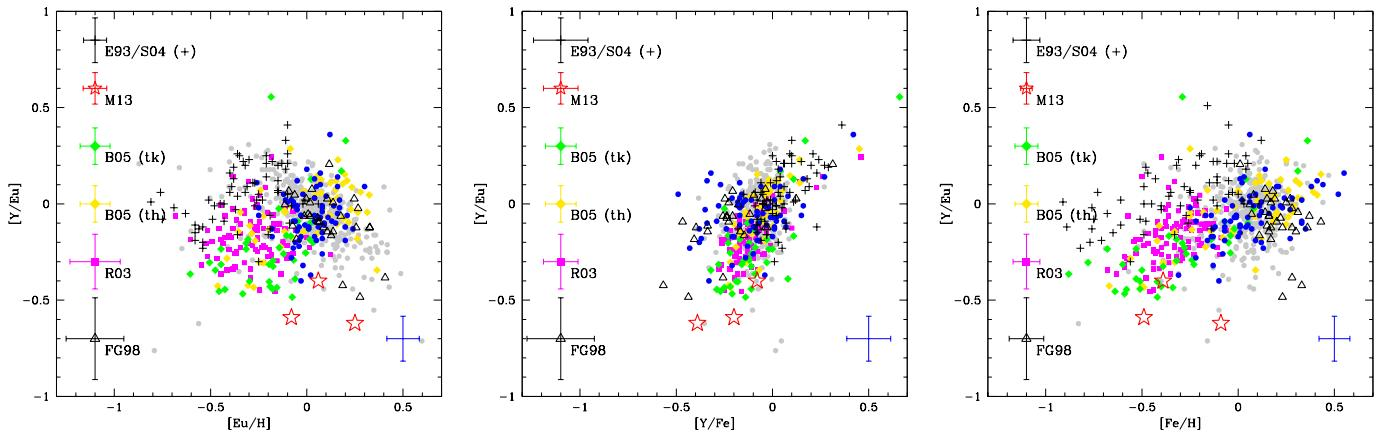


Fig. 10. The same as in Fig. 9, but for Y and Eu ratios. Galactic field dwarfs by E93/S04 (pluses), field dwarfs from the thin disk by R03 (magenta squares), and field dwarfs from the thin (yellow diamonds) and thick (green diamonds) disks by B05 are also shown.

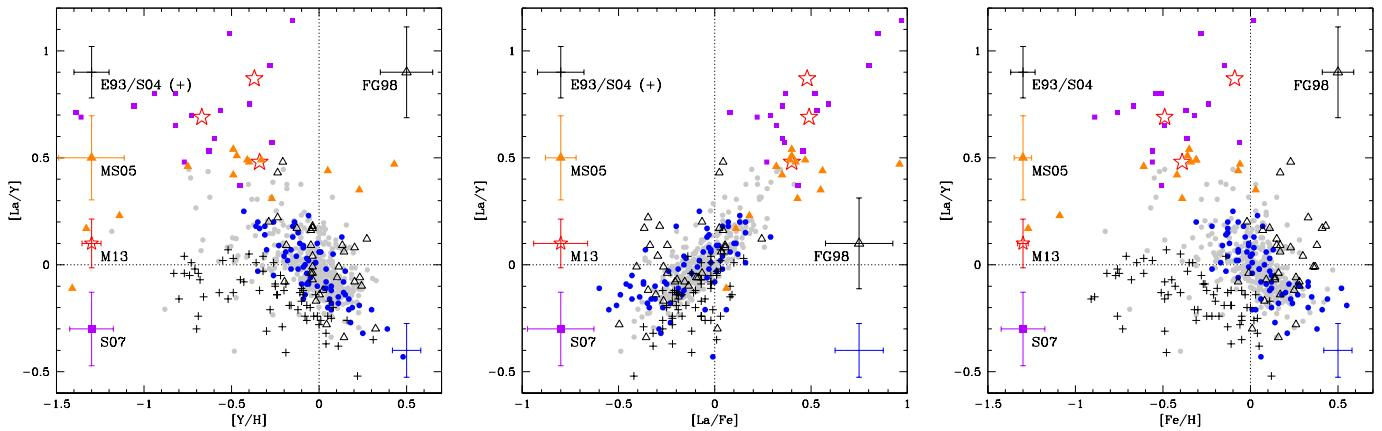


Fig. 11. The same as in Fig. 9, but for La and Y ratios. Sgr stars studied by Sbordone et al. (2007, S07, violet squares) are also plotted.

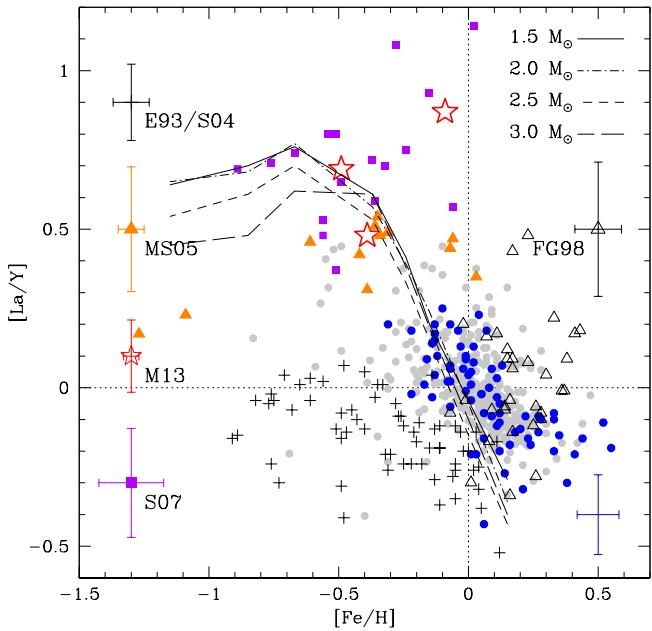


Fig. 12. The same as in the *left panel* of Fig. 11, but comparing the observational data with theoretical models available on the FRUITY database (Cristallo et al. 2011, 2015b).

Table 2. Abundances of heavy elements for our sample of classical Cepheids derived based on individual spectra.

Name	MJD	[Fe/H]	N_L (Fe I, Fe II)	[Y/H]	N_L	[La/H]	N_L	[Ce/H]	N_L	[Nd/H]	N_L	[Eu/H]	N_L
V340 Ara	56137.137	0.27 ± 0.10	(23, 2)	-0.24 ± 0.16	5	-0.19 ± 0.07	5	-0.09 ± 0.16	2	-0.25 ± 0.16	5	-0.01 ± 0.10	2
V340 Ara	54708.065	0.53 ± 0.09	(53, 4)	-0.02 ± 0.13	3	-0.07 ± 0.11	4	0.06 ± 0.18	2	-0.15 ± 0.15	2	0.00 ± 0.03	2
V340 Ara	54709.079	0.53 ± 0.16	(26, 3)	-0.05 ± 0.10	3	0.01 ± 0.11	4	0.05 ± 0.02	2	-0.04 ± 0.19	2	0.17 ± 0.03	2
V340 Ara	56138.094	0.32 ± 0.09	(41, 2)	-0.08 ± 0.16	5	-0.08 ± 0.04	5	-0.06 ± 0.15	2	-0.02 ± 0.15	5	0.04 ± 0.01	2
V340 Ara	56139.185	0.22 ± 0.01	(51, 2)	-0.17 ± 0.10	6	-0.11 ± 0.06	4	-0.23 ± 0.14	2	-0.15 ± 0.19	4	0.05 ± 0.04	2
V340 Ara	56152.054	0.24 ± 0.18	(15, 2)	0.04 ± 0.12	3	0.18 ± 0.07	4	0.52 ± 0.15	2	-0.04 ± 0.12	2	0.27 ± 0.04	2
AS Aur	54845.136	0.00 ± 0.08	(74, 8)	-0.20 ± 0.13	2	-0.16 ± 0.19	3	-0.06 ± 0.10	2	-0.03 ± 0.02	2
KN Cen	54862.355	0.55 ± 0.12	(14, 3)	0.23 ± 0.08	1	0.04 ± 0.15	4	-0.02 ± 0.11	1	0.05 ± 0.21	2	0.07 ± 0.16	2
MZ Cen	54584.280	0.27 ± 0.10	(45, 4)	-0.08 ± 0.14	2	-0.22 ± 0.15	4	0.27 ± 0.11	1	-0.05 ± 0.08	2
OO Cen	54585.060	0.20 ± 0.06	(30, 4)	0.14 ± 0.07	2	0.01 ± 0.11	3	-0.04 ± 0.05	2	0.05 ± 0.07	2
TX Cen	54862.363	0.44 ± 0.12	(78, 7)	0.17 ± 0.06	2	0.01 ± 0.01	2	0.07 ± 0.11	1	-0.05 ± 0.48	2	0.07 ± 0.09	2
V339 Cen	54584.304	0.06 ± 0.03	(39, 3)	-0.09 ± 0.03	2	-0.25 ± 0.13	4	-0.21 ± 0.11	1	-0.28 ± 0.37	2	-0.10 ± 0.03	2
VW Cen	54862.359	0.41 ± 0.08	(43, 2)	0.07 ± 0.08	1	-0.14 ± 0.07	4	-0.19 ± 0.11	1	0.23 ± 0.11	1	-0.05 ± 0.08	2
AO CMa	54839.053	0.01 ± 0.06	(75, 5)	0.08 ± 0.10	2	0.13 ± 0.08	4	0.18 ± 0.11	1	0.11 ± 0.08	2	0.20 ± 0.08	2
RW CMa	54839.138	-0.07 ± 0.08	(83, 5)	-0.06 ± 0.01	2	-0.04 ± 0.05	4	-0.08 ± 0.08	1
SS CMa	54839.066	0.06 ± 0.04	(57, 5)	0.14 ± 0.13	2	0.06 ± 0.08	4	0.13 ± 0.11	1	0.09 ± 0.15	2	0.10 ± 0.01	2
TV CMa	54847.246	0.01 ± 0.07	(89, 6)	0.17 ± 0.14	2	-0.04 ± 0.03	4	-0.04 ± 0.11	1	-0.10 ± 0.19	2	0.04 ± 0.04	2
TW CMa	54839.077	0.04 ± 0.09	(38, 4)	-0.06 ± 0.27	2	0.17 ± 0.29	3	0.14 ± 0.11	1	0.02 ± 0.11	1	0.06 ± 0.08	1
AA Gem	54846.149	-0.08 ± 0.05	(74, 5)	-0.18 ± 0.06	2	-0.16 ± 0.08	4	0.34 ± 0.45	2	0.02 ± 0.21	2	0.08 ± 0.03	2
AD Gem	54846.221	-0.14 ± 0.06	(70, 7)	-0.31 ± 0.11	2	-0.17 ± 0.17	2	-0.16 ± 0.11	1	-0.25 ± 0.08	1
BW Gem	54845.122	-0.22 ± 0.09	(99, 6)	-0.36 ± 0.06	2	-0.18 ± 0.03	4	-0.09 ± 0.11	1	-0.08 ± 0.13	2
DX Gem	54846.196	-0.01 ± 0.09	(72, 6)	-0.09 ± 0.01	2	0.00 ± 0.09	3	0.07 ± 0.11	1	-0.03 ± 0.08	1
RZ Gem	54845.094	-0.16 ± 0.03	(44, 5)	-0.15 ± 0.08	1
BE Mon	54846.201	0.05 ± 0.09	(78, 5)	0.04 ± 0.04	2	0.02 ± 0.05	4	0.07 ± 0.10	2	0.11 ± 0.04	2
CV Mon	54846.182	0.09 ± 0.09	(52, 2)	-0.07 ± 0.16	2	-0.16 ± 0.10	4	-0.02 ± 0.11	1	-0.07 ± 0.49	2	-0.12 ± 0.06	2
FT Mon	54845.104	-0.13 ± 0.08	(61, 8)	-0.34 ± 0.13	2	-0.17 ± 0.08	4	0.09 ± 0.11	1	0.14 ± 0.21	2	-0.02 ± 0.05	2
SV Mon	54845.119	0.12 ± 0.08	(54, 8)	-0.06 ± 0.01	2	-0.14 ± 0.16	4	0.02 ± 0.11	1	0.10 ± 0.24	2	-0.07 ± 0.05	2
TW Mon	54796.347	-0.13 ± 0.07	(75, 6)	-0.12 ± 0.02	2	0.03 ± 0.06	4	0.09 ± 0.04	2	0.01 ± 0.04	2
TX Mon	54798.345	-0.03 ± 0.05	(76, 4)	0.13 ± 0.03	2	0.26 ± 0.19	4	0.20 ± 0.11	1	0.23 ± 0.16	2	0.14 ± 0.09	2
TY Mon	54846.139	0.02 ± 0.08	(85, 6)	-0.09 ± 0.03	2	-0.01 ± 0.07	2	0.06 ± 0.11	1	-0.11 ± 0.08	1
TZ Mon	54847.237	-0.02 ± 0.07	(94, 6)	0.00 ± 0.04	2	0.06 ± 0.07	4	0.08 ± 0.11	1	0.04 ± 0.02	2	0.07 ± 0.01	2
V465 Mon	54847.241	-0.07 ± 0.07	(107, 6)	-0.14 ± 0.15	2	0.06 ± 0.10	4	0.23 ± 0.11	1	0.05 ± 0.08	1
V495 Mon	54846.167	-0.13 ± 0.07	(73, 4)	-0.26 ± 0.04	2	-0.06 ± 0.07	3	-0.03 ± 0.11	1	-0.04 ± 0.09	2	-0.04 ± 0.01	2
V508 Mon	54847.232	-0.04 ± 0.10	(118, 7)	-0.15 ± 0.01	2	0.03 ± 0.08	4	0.07 ± 0.11	1	-0.06 ± 0.08	1
V510 Mon	54846.153	-0.16 ± 0.06	(80, 3)	-0.23 ± 0.08	2	-0.14 ± 0.10	4	-0.07 ± 0.11	1	-0.11 ± 0.06	2	-0.04 ± 0.05	2
XX Mon	54798.335	0.01 ± 0.08	(55, 2)	-0.07 ± 0.04	2	-0.11 ± 0.18	4	0.11 ± 0.11	1	0.44 ± 0.20	2	0.08 ± 0.01	2
GU Nor	54667.205	0.08 ± 0.06	(80, 7)	-0.08 ± 0.04	2	-0.08 ± 0.19	2	-0.23 ± 0.11	1	-0.07 ± 0.08	1
IQ Nor	54584.299	0.22 ± 0.07	(63, 7)	-0.06 ± 0.15	2	-0.15 ± 0.09	3	-0.06 ± 0.11	1	-0.05 ± 0.06	2
QZ Nor	54863.366	0.18 ± 0.08	(81, 3)	-0.08 ± 0.11	2	0.00 ± 0.02	4	0.09 ± 0.13	3	-0.19 ± 0.03	2	0.15 ± 0.06	2
QZ Nor	54923.345	0.23 ± 0.07	(86, 2)	-0.08 ± 0.10	2	-0.07 ± 0.02	4	0.03 ± 0.06	3	0.21 ± 0.11	1	0.15 ± 0.04	2
RS Nor	54863.361	0.18 ± 0.08	(82, 5)	0.15 ± 0.09	2	0.01 ± 0.04	3	0.01 ± 0.11	1	0.17 ± 0.02	2
SY Nor	54708.061	0.27 ± 0.10	(46, 5)	-0.06 ± 0.05	3	-9.99 ± 0.10	0	0.14 ± 0.03	3	-0.39 ± 0.27	2	0.02 ± 0.08	2
SY Nor	54709.075	0.20 ± 0.09	(58, 4)	-0.04 ± 0.15	3	-0.03 ± 0.04	3	0.01 ± 0.10	3	-0.16 ± 0.10	2	0.09 ± 0.02	2
TW Nor	54666.127	0.27 ± 0.10	(69, 7)	-0.10 ± 0.18	2	-0.19 ± 0.15	4	-0.11 ± 0.11	1	-0.15 ± 0.50	2	0.08 ± 0.08	2
V340 Nor	54873.376	0.07 ± 0.07	(47, 4)	-0.31 ± 0.04	2	-0.13 ± 0.26	4	-0.15 ± 0.11	1	-0.18 ± 0.02	2
CS Ori	54845.085	-0.25 ± 0.06	(68, 6)	-0.27 ± 0.09	2	-0.21 ± 0.11	1	-0.25 ± 0.08	1
RS Ori	54845.100	0.11 ± 0.09	(71, 5)	0.15 ± 0.01	2	0.12 ± 0.11	3	0.37 ± 0.01	2	0.25 ± 0.11	1	0.21 ± 0.08	2
AQ Pup	54839.075	0.06 ± 0.05	(14, 2)	0.48 ± 0.08	1	0.05 ± 0.14	3	-0.13 ± 0.11	1	0.03 ± 0.11	1	0.12 ± 0.15	2
BC Pup	54839.147	-0.31 ± 0.07	(57, 3)	-0.35 ± 0.16	2	-0.15 ± 0.10	4	0.07 ± 0.11	1	0.37 ± 0.11	1	0.02 ± 0.10	2
BM Pup	54839.086	-0.07 ± 0.08	(61, 7)	-0.05 ± 0.01	2	-0.11 ± 0.16	4	0.19 ± 0.11	1	0.06 ± 0.23	2	0.04 ± 0.08	2
BN Pup	54839.109	0.03 ± 0.05	(69, 4)	0.30 ± 0.18	2	0.09 ± 0.14	4	0.12 ± 0.11	1	0.07 ± 0.13	2	0.16 ± 0.16	2
CK Pup	54839.113	-0.15 ± 0.08	(72, 4)	-0.15 ± 0.12	3	0.01 ± 0.04	3	0.22 ± 0.11	3	-0.16 ± 0.11	2	0.08 ± 0.11	2
CK Pup	54839.173	-0.12 ± 0.08	(78, 11)	-0.26 ± 0.02	2	-0.11 ± 0.04	4	0.11 ± 0.09	3	-0.17 ± 0.02	2	-0.01 ± 0.12	2
HW Pup	54792.249	-0.22 ± 0.09	(70, 3)	-0.16 ± 0.07	2	-0.18 ± 0.12	4	-0.10 ± 0.11	1	-0.15 ± 0.16	2	-0.07 ± 0.06	2
LS Pup	54839.081	-0.12 ± 0.11	(18, 1)	-0.11 ± 0.06	2	-0.01 ± 0.13	4	-0.04 ± 0.11	1	0.03 ± 0.33	2	0.01 ± 0.01	2
VW Pup	54832.331	-0.14 ± 0.06	(50, 4)	-0.35 ± 0.16	2	-0.38 ± 0.05	4	-0.46 ± 0.11	1	-0.18 ± 0.08	2
VZ Pup	54839.096	-0.01 ± 0.04	(27, 2)	-0.01 ± 0.05	2	0.09 ± 0.11	4	0.18 ± 0.11	1	0.06 ± 0.08	1
WW Pup	54839.091	0.13 ± 0.16	(18, 1)	-0.30 ± 0.06	2	-0.23 ± 0.09	4	-0.44 ± 0.11	1	-0.07 ± 0.07	2
WY Pup	54839.100	-0.10 ± 0.08	(49, 6)	-0.43 ± 0.08	1	-0.18 ± 0.04	3	0.13 ± 0.03	2	-0.03 ± 0.08	1
WZ Pup	54839.104	-0.07 ± 0.06	(72, 7)	-0.16 ± 0.08	2	-0.09 ± 0.05	3	0.01 ± 0.11	1	-0.09 ± 0.30	2	-0.04 ± 0.02	2

continued on next page

Notes. Column 3 lists the weighted mean and standard deviation of the Fe I and Fe II abundances derived by Genovali et al. (2014). Column 4 lists the respective number (N_L) of iron lines used. The other N_L values indicate the number of lines used for the other elements to derive their abundances. For these elements, the quoted errors represent either the dispersion around the mean if two or more lines were measured, or the mean dispersion computed for the eleven calibrating stars if only one line was available.

Table 2. continued.

Name	MJD	[Fe/H]	N_L (Fe I, Fe II)	[Y/H]	N_L	[La/H]	N_L	[Ce/H]	N_L	[Nd/H]	N_L	[Eu/H]	N_L
X Pup	54839.070	0.02 ± 0.08	(15, 2)	-0.15 ± 0.02	2	-0.02 ± 0.10	3	-0.13 ± 0.11	1	0.03 ± 0.11	1	-0.26 ± 0.01	2
KQ Sco	56139.021	0.26 ± 0.15	(32, 0)	-0.22 ± 0.16	5	-0.24 ± 0.18	5	-0.21 ± 0.24	2	-0.24 ± 0.09	5	-0.12 ± 0.04	2
KQ Sco	54873.379	0.52 ± 0.08	(51, 4)	-0.14 ± 0.37	2	-0.01 ± 0.02	4	0.03 ± 0.27	2	-0.75 ± 0.11	1	-0.13 ± 0.08	2
KQ Sco	56152.097	0.30 ± 0.21	(16, 1)	0.07 ± 0.15	5	0.04 ± 0.12	3	0.27 ± 0.23	2	-0.13 ± 0.08	4	0.06 ± 0.08	2
KQ Sco	56163.004	0.22 ± 0.27	(20, 1)	0.00 ± 0.19	3	-0.15 ± 0.09	4	-0.29 ± 0.28	2	-0.21 ± 0.08	4	-0.09 ± 0.02	2
KQ Sco	56166.004	0.21 ± 0.28	(15, 1)	-0.12 ± 0.08	2	-0.18 ± 0.09	5	0.02 ± 0.15	2	-0.15 ± 0.04	3	-0.06 ± 0.01	2
RY Sco	56140.187	0.06 ± 0.01	(74, 2)	0.04 ± 0.12	5	0.07 ± 0.09	5	0.12 ± 0.11	2	0.08 ± 0.18	6	0.10 ± 0.02	2
RY Sco	54599.412	0.06 ± 0.02	(34, 5)	-0.07 ± 0.02	3	0.01 ± 0.10	4	0.03 ± 0.04	2	-0.22 ± 0.02	2	0.07 ± 0.02	2
RY Sco	56152.143	0.01 ± 0.03	(75, 3)	-0.16 ± 0.07	6	-0.06 ± 0.09	5	0.01 ± 0.08	2	-0.08 ± 0.18	6	-0.01 ± 0.01	2
RY Sco	56162.170	-0.03 ± 0.05	(66, 2)	-0.13 ± 0.12	6	-0.03 ± 0.08	5	0.05 ± 0.12	2	-0.02 ± 0.20	6	0.02 ± 0.02	2
RY Sco	56167.085	-0.04 ± 0.08	(45, 2)	-0.01 ± 0.01	4	0.01 ± 0.13	5	0.09 ± 0.09	2	-0.11 ± 0.18	6	0.10 ± 0.01	2
V470 Sco	54708.073	0.16 ± 0.06	(66, 4)	0.11 ± 0.09	2	-0.07 ± 0.09	4	-0.12 ± 0.11	1	0.03 ± 0.11	1	0.16 ± 0.10	2
V500 Sco	56140.191	-0.01 ± 0.05	(86, 3)	-0.17 ± 0.07	6	0.01 ± 0.07	5	0.08 ± 0.07	2	0.10 ± 0.15	5	0.05 ± 0.04	2
V500 Sco	56152.092	0.00 ± 0.10	(67, 3)	-0.18 ± 0.17	6	-0.11 ± 0.07	5	-0.01 ± 0.09	2	-0.18 ± 0.18	6	-0.07 ± 0.02	2
V500 Sco	56162.998	-0.03 ± 0.12	(53, 3)	-0.32 ± 0.05	4	-0.26 ± 0.08	5	-0.12 ± 0.08	2	-0.25 ± 0.18	5	-0.19 ± 0.02	2
V500 Sco	56167.077	-0.11 ± 0.07	(97, 5)	-0.19 ± 0.07	6	-0.03 ± 0.07	5	0.03 ± 0.04	2	-0.08 ± 0.20	6	0.00 ± 0.04	2
EV Sct	54708.086	0.09 ± 0.07	(57, 3)	0.01 ± 0.04	2	0.07 ± 0.09	3	0.15 ± 0.11	2	0.20 ± 0.09	2
RU Set	54906.414	0.16 ± 0.05	(95, 7)	-0.03 ± 0.16	3	-0.13 ± 0.09	4	-0.05 ± 0.21	2	-0.25 ± 0.21	2	-0.03 ± 0.04	2
RU Set	54923.375	0.09 ± 0.07	(45, 5)	0.06 ± 0.15	3	-0.06 ± 0.08	4	0.13 ± 0.40	2	-0.19 ± 0.17	2	-0.05 ± 0.10	2
UZ Set	56137.160	0.28 ± 0.12	(17, 4)	0.15 ± 0.08	4	-0.08 ± 0.11	4	0.23 ± 0.24	2	-0.36 ± 0.17	4	0.29 ± 0.02	2
UZ Set	54906.400	0.36 ± 0.10	(34, 5)	0.19 ± 0.05	2	0.00 ± 0.08	4	0.03 ± 0.02	2	-0.05 ± 0.17	2	0.03 ± 0.09	2
UZ Set	54923.366	0.45 ± 0.07	(63, 7)	0.09 ± 0.02	2	-0.08 ± 0.14	4	-0.16 ± 0.06	2	-0.22 ± 0.13	2	0.09 ± 0.04	2
UZ Set	56152.064	0.25 ± 0.28	(8, 0)	0.11 ± 0.13	4	0.00 ± 0.11	4	0.45 ± 0.04	2	-0.23 ± 0.08	2	0.32 ± 0.10	2
UZ Set	56160.167	0.36 ± 0.10	(47, 2)	0.18 ± 0.13	4	0.01 ± 0.08	5	0.08 ± 0.08	2	0.03 ± 0.17	5	0.00 ± 0.03	2
UZ Set	56175.049	0.31 ± 0.21	(36, 2)	-0.01 ± 0.17	5	-0.06 ± 0.08	5	0.04 ± 0.15	2	-0.05 ± 0.18	4	-0.05 ± 0.19	2
V367 Set	56137.147	0.13 ± 0.07	(72, 3)	-0.13 ± 0.09	6	-0.08 ± 0.07	5	0.02 ± 0.20	2	-0.03 ± 0.17	5	0.03 ± 0.09	2
V367 Set	54709.128	-0.04 ± 0.04	(56, 4)	-0.05 ± 0.05	2	-0.08 ± 0.11	4	-0.09 ± 0.06	3	-0.28 ± 0.31	2	0.07 ± 0.04	2
V367 Set	56175.105	0.14 ± 0.06	(50, 3)	-0.13 ± 0.07	5	-0.08 ± 0.09	5	-0.02 ± 0.12	2	0.14 ± 0.21	3	0.04 ± 0.09	2
V367 Set	56184.000	0.03 ± 0.07	(84, 4)	-0.32 ± 0.07	6	-0.22 ± 0.13	5	-0.17 ± 0.04	2	-0.15 ± 0.19	4	-0.14 ± 0.05	2
X Sct	54709.122	0.12 ± 0.09	(72, 9)	0.04 ± 0.16	2	-0.07 ± 0.10	4	0.03 ± 0.11	2	0.08 ± 0.07	2
Z Sct	56137.123	0.10 ± 0.16	(20, 0)	-0.40 ± 0.09	3	-0.38 ± 0.05	3	-0.43 ± 0.03	2	-0.51 ± 0.17	4	-0.27 ± 0.08	1
Z Sct	54678.090	0.18 ± 0.09	(41, 3)	-0.43 ± 0.11	3	-0.36 ± 0.08	4	-0.57 ± 0.37	2	-0.60 ± 0.48	2	-0.21 ± 0.07	2
Z Sct	56152.073	0.11 ± 0.02	(49, 2)	-0.22 ± 0.05	4	-0.18 ± 0.13	5	-0.22 ± 0.13	2	-0.38 ± 0.18	4	0.04 ± 0.08	2
Z Sct	56159.186	0.26 ± 0.08	(45, 2)	-0.17 ± 0.12	5	-0.19 ± 0.06	5	-0.08 ± 0.13	2	-0.17 ± 0.15	3	0.01 ± 0.01	2
Z Sct	56175.038	0.00 ± 0.30	(25, 0)	-0.42 ± 0.18	5	-0.42 ± 0.16	5	-0.31 ± 0.07	2	-0.36 ± 0.09	5	-0.03 ± 0.11	2
AA Ser	54708.040	0.38 ± 0.20	(24, 1)	0.39 ± 0.06	2	0.09 ± 0.15	4	0.04 ± 0.11	1	0.15 ± 0.71	2	0.30 ± 0.18	2
CR Ser	54709.116	0.12 ± 0.08	(53, 5)	0.05 ± 0.04	2	-0.15 ± 0.16	4	0.06 ± 0.11	1	0.08 ± 0.49	2	0.15 ± 0.18	2
AV Sgr	56136.169	0.40 ± 0.15	(29, 2)	0.09 ± 0.09	4	0.03 ± 0.12	4	0.11 ± 0.19	2	-0.23 ± 0.10	4	0.26 ± 0.08	2
AV Sgr	56136.192	0.44 ± 0.15	(31, 2)	-0.01 ± 0.05	4	-0.06 ± 0.08	5	0.01 ± 0.17	2	-0.22 ± 0.09	4	0.24 ± 0.04	2
AV Sgr	54923.348	0.53 ± 0.17	(16, 2)	0.06 ± 0.09	2	-0.06 ± 0.06	3	-0.18 ± 0.27	2	-0.61 ± 0.40	2	0.03 ± 0.05	2
AV Sgr	56152.082	0.42 ± 0.17	(24, 2)	-0.07 ± 0.04	3	0.07 ± 0.03	4	0.06 ± 0.21	2	-0.32 ± 0.19	4	0.18 ± 0.01	2
AV Sgr	56168.049	0.30 ± 0.22	(19, 1)	0.08 ± 0.16	4	0.06 ± 0.10	4	0.15 ± 0.29	2	-0.33 ± 0.17	4	0.27 ± 0.07	2
AY Sgr	54599.398	0.11 ± 0.06	(58, 5)	0.07 ± 0.16	2	-0.05 ± 0.04	4	-0.04 ± 0.11	1	0.09 ± 0.11	1	0.08 ± 0.08	2
V1954 Sgr	54599.389	0.24 ± 0.10	(61, 4)	0.07 ± 0.08	2	-0.11 ± 0.12	4	-0.07 ± 0.11	1	0.04 ± 0.06	2
V773 Sgr	54669.207	0.11 ± 0.06	(58, 8)	-0.07 ± 0.03	2	-0.04 ± 0.09	4	-0.09 ± 0.11	1	-0.06 ± 0.18	2
VY Sgr	56160.179	0.27 ± 0.25	(14, 1)	-0.01 ± 0.02	2	-0.17 ± 0.12	5	0.00 ± 0.14	2	-0.44 ± 0.18	4	0.05 ± 0.02	2
VY Sgr	54923.356	0.42 ± 0.14	(30, 6)	0.05 ± 0.04	2	0.04 ± 0.15	4	0.13 ± 0.31	2	-0.08 ± 0.25	2	0.06 ± 0.05	2
VY Sgr	56162.162	0.32 ± 0.27	(17, 1)	-0.24 ± 0.15	4	-0.32 ± 0.07	5	-0.32 ± 0.06	2	-0.34 ± 0.16	5	-0.13 ± 0.05	2
VY Sgr	56168.062	0.31 ± 0.05	(51, 2)	-0.02 ± 0.18	4	0.00 ± 0.07	5	0.09 ± 0.19	2	0.10 ± 0.19	5	0.17 ± 0.13	2
WZ Sgr	56132.190	0.18 ± 0.08	(56, 2)	-0.08 ± 0.09	4	0.04 ± 0.12	5	-0.02 ± 0.07	2	-0.02 ± 0.15	6	0.17 ± 0.02	2
WZ Sgr	54599.395	0.35 ± 0.08	(42, 2)	0.17 ± 0.06	2	-0.15 ± 0.14	4	-0.21 ± 0.07	2	-0.99 ± 0.11	0	-0.01 ± 0.05	2
WZ Sgr	56136.213	0.24 ± 0.01	(48, 2)	-0.02 ± 0.18	5	0.05 ± 0.10	5	0.17 ± 0.11	2	0.06 ± 0.14	5	0.09 ± 0.14	2
WZ Sgr	56152.044	0.28 ± 0.12	(28, 2)	-0.23 ± 0.16	5	-0.14 ± 0.08	5	-0.09 ± 0.12	2	-0.30 ± 0.16	5	-0.07 ± 0.12	2
WZ Sgr	56159.125	0.37 ± 0.06	(44, 2)	0.08 ± 0.14	5	0.04 ± 0.09	5	0.19 ± 0.12	2	0.21 ± 0.19	4	-0.10 ± 0.07	2
XX Sgr	56054.234	-0.01 ± 0.10	(100, 5)	-0.14 ± 0.08	5	0.03 ± 0.09	5	0.12 ± 0.05	2	-0.02 ± 0.17	6	0.06 ± 0.03	2
XX Sgr	54599.404	-0.07 ± 0.07	(59, 4)	-0.13 ± 0.11	2	-0.04 ± 0.05	3	0.08 ± 0.12	3	-0.19 ± 0.20	2	-0.01 ± 0.07	2
XX Sgr	56136.223	-0.05 ± 0.05	(101, 6)	-0.27 ± 0.07	5	-0.09 ± 0.10	5	-0.06 ± 0.08	2	-0.15 ± 0.15	5	-0.10 ± 0.09	2
XX Sgr	56152.047	0.05 ± 0.03	(43, 3)	-0.15 ± 0.04	4	-0.12 ± 0.12	5	-0.02 ± 0.06	2	-0.07 ± 0.19	6	-0.06 ± 0.03	2
XX Sgr	56159.128	-0.02 ± 0.12	(64, 4)	-0.14 ± 0.12	5	-0.12 ± 0.15	5	0.07 ± 0.06	2	-0.12 ± 0.18	5	-0.04 ± 0.03	2
EZ Vel	54759.348	-0.17 ± 0.15	(23, 1)	-0.02 ± 0.08	2	-0.01 ± 0.23	3	0.13 ± 0.11	1	-0.08 ± 0.11	1	0.04 ± 0.10	2

Table 3. Mean abundances of heavy elements for our sample of classical Cepheids.

Name	$\log P$ [days]	R_G [pc]	[Fe/H]	[Y/H]	[La/H]	[Ce/H]	[Nd/H]	[Eu/H]	N_S
V340 Ara	1.3183	4657 ± 427	0.33 ± 0.09	0.04 ± 0.14	-0.04 ± 0.09	0.13 ± 0.13	0.02 ± 0.25	0.13 ± 0.07	6
QZ Nor	0.5782	6283 ± 447	0.21 ± 0.06	0.25 ± 0.32	-0.07 ± 0.02	0.03 ± 0.11	0.12 ± 0.01	0.16 ± 0.07	2
SY Nor	1.1019	6286 ± 446	0.23 ± 0.07	0.06 ± 0.01	-0.10 ± 0.08	0.08 ± 0.11	-0.04 ± 0.06	0.08 ± 0.01	2
CK Pup	0.8703	13357 ± 423	-0.13 ± 0.06	-0.13 ± 0.04	-0.09 ± 0.04	0.04 ± 0.11	0.00 ± 0.11	0.04 ± 0.16	2
KQ Sco	1.4577	5948 ± 451	0.52 ± 0.08	0.03 ± 0.15	-0.08 ± 0.12	-0.02 ± 0.25	-0.24 ± 0.25	-0.02 ± 0.07	5
RY Sco	1.3078	6663 ± 453	0.01 ± 0.06	-0.02 ± 0.08	-0.01 ± 0.11	0.09 ± 0.11	0.06 ± 0.16	0.09 ± 0.02	5
V500 Sco	0.9693	6590 ± 453	-0.07 ± 0.08	-0.19 ± 0.10	-0.13 ± 0.09	0.00 ± 0.12	-0.01 ± 0.20	-0.05 ± 0.04	4
RU Sct	1.2945	6361 ± 449	0.14 ± 0.04	0.18 ± 0.21	-0.09 ± 0.10	-0.11 ± 0.11	-0.07 ± 0.29	0.00 ± 0.13	2
UZ Sct	1.1686	5309 ± 448	0.33 ± 0.08	0.19 ± 0.09	-0.01 ± 0.12	0.16 ± 0.12	0.05 ± 0.32	0.17 ± 0.12	6
V367 Sct	0.7989	6332 ± 451	0.05 ± 0.08	-0.12 ± 0.10	-0.14 ± 0.10	0.23 ± 0.11	0.12 ± 0.21	-0.01 ± 0.08	4
Z Sct	1.1106	5733 ± 445	0.12 ± 0.09	-0.26 ± 0.12	-0.31 ± 0.11	0.03 ± 0.12	-0.04 ± 0.25	-0.06 ± 0.08	5
AV Sgr	1.1879	5980 ± 455	0.35 ± 0.17	0.11 ± 0.15	-0.04 ± 0.20	0.04 ± 0.25	-0.04 ± 0.26	0.24 ± 0.10	5
VY Sgr	1.1322	5862 ± 453	0.33 ± 0.12	-0.01 ± 0.08	-0.11 ± 0.12	-0.04 ± 0.13	-0.02 ± 0.28	0.09 ± 0.08	4
WZ Sgr	1.3394	6326 ± 453	0.28 ± 0.08	0.07 ± 0.08	-0.03 ± 0.11	0.05 ± 0.12	0.05 ± 0.23	0.04 ± 0.11	5
XX Sgr	0.8078	6706 ± 453	-0.01 ± 0.06	-0.09 ± 0.06	-0.10 ± 0.12	0.10 ± 0.07	0.04 ± 0.15	-0.03 ± 0.02	5
AS Aur	0.5017	12244 ± 469	0.00 ± 0.08	-0.20 ± 0.13	-0.16 ± 0.19	...	-0.06 ± 0.10	-0.03 ± 0.02	1
KN Cen	1.5321	6498 ± 417	0.55 ± 0.12	0.23 ± 0.08	0.04 ± 0.15	-0.02 ± 0.11	0.05 ± 0.21	0.07 ± 0.16	1
MZ Cen	1.0151	6501 ± 391	0.27 ± 0.10	-0.08 ± 0.14	-0.22 ± 0.15	...	0.27 ± 0.11	-0.05 ± 0.08	1
OO Cen	1.1099	6025 ± 389	0.20 ± 0.06	0.14 ± 0.07	0.01 ± 0.11	...	-0.04 ± 0.05	0.05 ± 0.07	1
TX Cen	1.2328	6070 ± 419	0.44 ± 0.12	0.17 ± 0.06	0.01 ± 0.01	0.07 ± 0.11	-0.05 ± 0.48	0.07 ± 0.09	1
V339 Cen	0.9762	6917 ± 446	0.06 ± 0.03	-0.09 ± 0.03	-0.25 ± 0.13	-0.21 ± 0.11	-0.28 ± 0.37	-0.10 ± 0.03	1
VW Cen	1.1771	6417 ± 405	0.41 ± 0.08	0.07 ± 0.08	-0.14 ± 0.07	-0.19 ± 0.11	0.23 ± 0.11	-0.05 ± 0.08	1
AO CMa	0.7646	10430 ± 433	0.01 ± 0.06	0.08 ± 0.10	0.13 ± 0.08	0.18 ± 0.11	0.11 ± 0.08	0.20 ± 0.08	1
RW CMa	0.7581	10057 ± 445	-0.07 ± 0.08	-0.06 ± 0.01	-0.04 ± 0.05	-0.08 ± 0.08	1
SS CMa	1.0921	9829 ± 439	0.06 ± 0.04	0.14 ± 0.13	0.06 ± 0.08	0.13 ± 0.11	0.09 ± 0.15	0.10 ± 0.01	1
TV CMa	0.6693	9575 ± 447	0.01 ± 0.07	0.17 ± 0.14	-0.04 ± 0.03	-0.04 ± 0.11	-0.10 ± 0.19	0.04 ± 0.04	1
TW CMa	0.8448	9788 ± 445	0.04 ± 0.09	-0.06 ± 0.27	0.17 ± 0.29	0.14 ± 0.11	0.02 ± 0.11	0.06 ± 0.08	1
AA Gem	1.0532	11454 ± 459	-0.08 ± 0.05	-0.18 ± 0.06	-0.16 ± 0.08	0.34 ± 0.45	0.02 ± 0.21	0.08 ± 0.03	1
AD Gem	0.5784	10662 ± 455	-0.14 ± 0.06	-0.31 ± 0.11	-0.17 ± 0.17	...	-0.16 ± 0.11	-0.25 ± 0.08	1
BW Gem	0.3633	11302 ± 463	-0.22 ± 0.09	-0.36 ± 0.06	-0.18 ± 0.03	...	-0.09 ± 0.11	-0.08 ± 0.13	1
DX Gem	0.4966	11407 ± 473	-0.01 ± 0.09	-0.09 ± 0.01	0.00 ± 0.09	...	0.07 ± 0.11	-0.03 ± 0.08	1
RZ Gem	0.7427	9973 ± 454	-0.16 ± 0.03	-0.15 ± 0.08	1
BE Mon	0.4322	9609 ± 452	0.05 ± 0.09	0.04 ± 0.04	0.02 ± 0.05	...	0.07 ± 0.10	0.11 ± 0.04	1
CV Mon	0.7307	9362 ± 452	0.09 ± 0.09	-0.07 ± 0.16	-0.16 ± 0.10	-0.02 ± 0.11	-0.07 ± 0.49	-0.12 ± 0.06	1
FT Mon	0.6843	14344 ± 468	-0.13 ± 0.08	-0.34 ± 0.13	-0.17 ± 0.08	0.09 ± 0.11	0.14 ± 0.21	-0.02 ± 0.05	1
SV Mon	1.1828	10070 ± 453	0.12 ± 0.08	-0.06 ± 0.01	-0.14 ± 0.16	0.02 ± 0.11	0.10 ± 0.24	-0.07 ± 0.05	1
TW Mon	0.8511	13059 ± 457	-0.13 ± 0.07	-0.12 ± 0.02	0.03 ± 0.06	...	0.09 ± 0.04	0.01 ± 0.04	1
TX Mon	0.9396	11790 ± 452	-0.03 ± 0.05	0.13 ± 0.03	0.26 ± 0.19	0.20 ± 0.11	0.23 ± 0.16	0.14 ± 0.09	1
TY Mon	0.6045	11180 ± 451	0.02 ± 0.08	-0.09 ± 0.03	-0.01 ± 0.07	...	0.06 ± 0.11	-0.11 ± 0.08	1
TZ Mon	0.8709	11183 ± 451	-0.02 ± 0.07	0.00 ± 0.04	0.06 ± 0.07	0.08 ± 0.11	0.04 ± 0.02	0.07 ± 0.01	1
V465 Mon	0.4335	11037 ± 450	-0.07 ± 0.07	-0.14 ± 0.15	0.06 ± 0.10	...	0.23 ± 0.11	0.05 ± 0.08	1
V495 Mon	0.6124	12098 ± 453	-0.13 ± 0.07	-0.26 ± 0.04	-0.06 ± 0.07	-0.03 ± 0.11	-0.04 ± 0.09	-0.04 ± 0.01	1
V508 Mon	0.6163	10714 ± 452	-0.04 ± 0.10	-0.15 ± 0.01	0.03 ± 0.08	...	0.07 ± 0.11	-0.06 ± 0.08	1
V510 Mon	0.8637	12550 ± 456	-0.16 ± 0.06	-0.23 ± 0.08	-0.14 ± 0.10	-0.07 ± 0.11	-0.11 ± 0.06	-0.04 ± 0.05	1
XX Mon	0.7369	11854 ± 451	0.01 ± 0.08	-0.07 ± 0.04	-0.11 ± 0.18	0.11 ± 0.11	0.44 ± 0.20	0.08 ± 0.01	1
GU Nor	0.5382	6663 ± 450	0.08 ± 0.06	-0.08 ± 0.04	-0.08 ± 0.19	...	-0.23 ± 0.11	-0.07 ± 0.08	1
IQ Nor	0.9159	6691 ± 448	0.22 ± 0.07	-0.06 ± 0.15	-0.15 ± 0.09	...	-0.06 ± 0.11	-0.05 ± 0.06	1
RS Nor	0.7923	6385 ± 449	0.18 ± 0.08	0.15 ± 0.09	0.01 ± 0.04	...	0.01 ± 0.11	0.17 ± 0.02	1
TW Nor	1.0329	6160 ± 447	0.27 ± 0.10	-0.10 ± 0.18	-0.19 ± 0.15	-0.11 ± 0.11	-0.15 ± 0.50	0.08 ± 0.08	1
V340 Nor	1.0526	6483 ± 449	0.07 ± 0.07	-0.31 ± 0.04	-0.13 ± 0.26	...	-0.15 ± 0.11	-0.18 ± 0.02	1
CS Ori	0.5899	11701 ± 458	-0.25 ± 0.06	-0.27 ± 0.09	-0.21 ± 0.11	-0.25 ± 0.08	1
RS Ori	0.8789	9470 ± 453	0.11 ± 0.09	0.15 ± 0.01	0.12 ± 0.11	0.37 ± 0.01	0.25 ± 0.11	0.21 ± 0.08	1
AQ Pup	1.4786	9472 ± 436	0.06 ± 0.05	0.48 ± 0.08	0.05 ± 0.14	-0.13 ± 0.11	0.03 ± 0.11	0.12 ± 0.15	1
BC Pup	0.5495	12763 ± 426	-0.31 ± 0.07	-0.35 ± 0.16	-0.15 ± 0.10	0.07 ± 0.11	0.37 ± 0.11	0.02 ± 0.10	1
BM Pup	0.8572	9981 ± 435	-0.07 ± 0.08	-0.05 ± 0.01	-0.11 ± 0.16	0.19 ± 0.11	0.06 ± 0.23	0.04 ± 0.08	1
BN Pup	1.1359	9930 ± 428	0.03 ± 0.05	0.30 ± 0.18	0.09 ± 0.14	0.12 ± 0.11	0.07 ± 0.13	0.16 ± 0.16	1
HW Pup	1.1289	13554 ± 436	-0.22 ± 0.09	-0.16 ± 0.07	-0.18 ± 0.12	-0.10 ± 0.11	-0.15 ± 0.16	-0.07 ± 0.06	1
LS Pup	1.1506	10610 ± 423	-0.12 ± 0.11	-0.11 ± 0.06	-0.01 ± 0.13	-0.04 ± 0.11	0.03 ± 0.33	0.01 ± 0.01	1
VW Pup	0.6320	10175 ± 443	-0.14 ± 0.06	-0.35 ± 0.16	-0.38 ± 0.05	...	-0.46 ± 0.11	-0.18 ± 0.08	1
VZ Pup	1.3649	10867 ± 425	-0.01 ± 0.04	-0.01 ± 0.05	0.09 ± 0.11	...	0.18 ± 0.11	0.06 ± 0.08	1
WW Pup	0.7417	10382 ± 436	0.13 ± 0.16	-0.30 ± 0.06	-0.23 ± 0.09	...	-0.44 ± 0.11	-0.07 ± 0.07	1
WY Pup	0.7202	10549 ± 430	-0.10 ± 0.08	-0.43 ± 0.08	-0.18 ± 0.04	...	0.13 ± 0.03	-0.03 ± 0.08	1
WZ Pup	0.7013	10123 ± 437	-0.07 ± 0.06	-0.16 ± 0.08	-0.09 ± 0.05	0.01 ± 0.11	-0.09 ± 0.30	-0.04 ± 0.02	1
X Pup	1.4143	9788 ± 441	0.02 ± 0.08	-0.15 ± 0.02	-0.02 ± 0.10	-0.13 ± 0.11	0.03 ± 0.11	-0.26 ± 0.01	1
V470 Sco	1.2112	6461 ± 454	0.16 ± 0.06	0.11 ± 0.09	-0.07 ± 0.09	-0.12 ± 0.11	0.03 ± 0.11	0.16 ± 0.10	1
EV Sct	0.4901	6135 ± 449	0.09 ± 0.07	0.01 ± 0.04	0.07 ± 0.09	...	0.15 ± 0.11	0.20 ± 0.09	1
X Sct	0.6230	6464 ± 452	0.12 ± 0.09	0.04 ± 0.16	-0.07 ± 0.10	...	0.03 ± 0.11	0.08 ± 0.07	1
AA Ser	1.2340	5572 ± 437	0.38 ± 0.20	0.39 ± 0.06	0.09 ± 0.15	0.04 ± 0.11	0.15 ± 0.71	0.30 ± 0.18	1
CR Ser	0.7244	6510 ± 452	0.12 ± 0.08	0.05 ± 0.04	-0.15 ± 0.16	0.06 ± 0.11	0.08 ± 0.49	0.15 ± 0.18	1
AY Sgr	0.8175	6429 ± 452	0.11 ± 0.06	0.07 ± 0.16	-0.05 ± 0.04	-0.04 ± 0.11	0.09 ± 0.11	0.08 ± 0.08	1
V1954 Sgr	0.7909	5687 ± 456	0.24 ± 0.10	0.07 ± 0.08	-0.11 ± 0.12	...	-0.07 ± 0.11	0.04 ± 0.06	1
V773 Sgr	0.7596	6595 ± 454	0.11 ± 0.06	-0.07 ± 0.03	-0.04 ± 0.09	...	-0.09 ± 0.11	-0.06 ± 0.18	1
EZ Vel	1.5383	12119 ± 358	-0.17 ± 0.15	-0.02 ± 0.08	-0.01 ± 0.23	0.13 ± 0.11	-0.08 ± 0.11	0.04 ± 0.10	1

Notes. The weighted (in the case of iron) or the arithmetic (for the other elements) mean abundances of the stars with multiple spectra (Table 2) are listed first. Columns 2 and 3 shows the logarithmic of the pulsation period and the Galactocentric distance (R_G), respectively. The N_S values indicate the number of spectra available for each star.

Table 4. Hyperfine structure list for some of the lines in our linelist.

specie	λ [Å]	$\log gf$	specie	λ [Å]	$\log gf$	specie	λ [Å]	$\log gf$
Y II	5119.113	-1.758	La II	6262.166	-2.471	Eu II	6437.630	-2.281
Y II	5119.109	-2.904	La II	6262.169	-2.596	Eu II	6437.634	-2.281
Y II	5119.111	-1.603	La II	6262.171	-3.269	Eu II	6437.637	-1.391
Y II	5289.814	-2.248	La II	6262.211	-2.286	Eu II	6437.637	-1.463
Y II	5289.816	-3.394	La II	6262.215	-2.535	Eu II	6437.640	-2.238
Y II	5289.815	-2.093	La II	6262.218	-3.290	Eu II	6437.640	-2.238
Y II	5728.889	-1.564	La II	6262.269	-2.130	Eu II	6437.642	-2.292
Y II	5728.891	-2.518	La II	6262.274	-2.531	Eu II	6437.642	-2.489
Y II	5728.888	-2.518	La II	6262.277	-3.400	Eu II	6437.642	-1.569
Y II	5728.890	-1.372	La II	6262.340	-1.994	Eu II	6437.643	-2.319
La II	5114.512	-1.624	La II	6262.346	-2.597	Eu II	6437.644	-1.711
La II	5114.529	-1.820	La II	6262.350	-3.612	Eu II	6437.644	-1.659
La II	5114.556	-1.820	La II	6262.425	-1.873	Eu II	6437.644	-2.292
La II	5114.573	-3.005	La II	6262.431	-2.802	Eu II	6437.645	-2.489
La II	5114.586	-1.824	La II	6262.437	-4.015	Eu II	6437.650	-2.319
La II	5114.608	-1.824	La II	6390.460	-2.012	Eu II	6437.656	-1.502
La II	5114.621	-2.079	La II	6390.472	-2.753	Eu II	6437.662	-2.276
La II	5290.787	-3.048	La II	6390.472	-2.183	Eu II	6437.667	-2.276
La II	5290.788	-2.872	La II	6390.482	-3.753	Eu II	6437.672	-1.607
La II	5290.796	-2.872	La II	6390.482	-2.570	Eu II	6437.677	-2.330
La II	5290.797	-4.796	La II	6390.483	-2.390	Eu II	6437.679	-2.330
La II	5290.796	-2.699	La II	6390.491	-3.335	Eu II	6437.684	-1.697
La II	5290.808	-2.699	La II	6390.491	-2.536	Eu II	6437.687	-2.527
La II	5290.809	-3.370	La II	6390.492	-2.661	Eu II	6437.689	-2.527
La II	5290.810	-2.688	La II	6390.498	-3.101	Eu II	6437.692	-1.749
La II	5290.825	-2.688	La II	6390.499	-2.595	Eu II	6645.098	-0.837
La II	5290.826	-2.674	La II	6390.499	-3.079	Eu II	6645.099	-2.106
La II	5290.827	-2.846	La II	6390.503	-2.955	Eu II	6645.100	-0.799
La II	5290.846	-2.846	La II	6390.504	-2.778	Eu II	6645.101	-3.749
La II	5290.847	-2.276	La II	6390.507	-2.858	Eu II	6645.104	-2.144
La II	5805.620	-3.387	La II	6774.157	-3.869	Eu II	6645.112	-3.787
La II	5805.621	-3.241	La II	6774.168	-3.392	Eu II	6645.114	-0.875
La II	5805.636	-3.045	La II	6774.159	-3.392	Eu II	6645.116	-1.911
La II	5805.638	-3.058	La II	6774.187	-3.170	Eu II	6645.121	-3.432
La II	5805.639	-3.718	La II	6774.173	-3.170	Eu II	6645.123	-0.954
La II	5805.663	-2.811	La II	6774.190	-4.015	Eu II	6645.124	-0.913
La II	5805.666	-2.936	La II	6774.214	-3.071	Eu II	6645.128	-1.866
La II	5805.668	-3.609	La II	6774.196	-3.071	Eu II	6645.131	-1.037
La II	5805.702	-2.626	La II	6774.219	-3.385	Eu II	6645.131	-1.949
La II	5805.705	-2.875	La II	6774.250	-3.045	Eu II	6645.134	-3.359
La II	5805.708	-3.630	La II	6774.226	-3.045	Eu II	6645.136	-1.121
La II	5805.752	-2.470	La II	6774.256	-2.999	Eu II	6645.137	-1.917
La II	5805.756	-2.871	La II	6774.293	-3.098	Eu II	6645.139	-3.470
La II	5805.759	-3.740	La II	6774.265	-3.098	Eu II	6645.140	-1.204
La II	5805.813	-2.334	La II	6774.301	-2.713	Eu II	6645.142	-2.112
La II	5805.818	-2.937	La II	6774.343	-3.293	Eu II	6645.143	-3.527
La II	5805.822	-3.952	La II	6774.311	-3.293	Eu II	6645.145	-0.993
La II	5805.886	-2.213	La II	6774.353	-2.485	Eu II	6645.153	-1.904
La II	5805.891	-3.142	Eu II	6437.610	-1.243	Eu II	6645.160	-3.397
La II	5805.896	-4.355	Eu II	6437.611	-1.281	Eu II	6645.164	-1.075
La II	6262.116	-3.047	Eu II	6437.613	-2.473	Eu II	6645.171	-1.956
La II	6262.117	-2.901	Eu II	6437.619	-2.511	Eu II	6645.177	-3.565
La II	6262.134	-2.705	Eu II	6437.624	-2.473	Eu II	6645.179	-1.159
La II	6262.136	-2.718	Eu II	6437.627	-1.353	Eu II	6645.185	-2.150
La II	6262.138	-3.378	Eu II	6437.629	-2.511	Eu II	6645.190	-1.242

Notes. The second column displays the wavelength of each component that forms the line profile.

Table 5. Abundance difference of stars in common among the current sample and other data sets.

Abundance ratio	Data sets ¹	Zero-point difference	N_{Common}
[Fe/H]	LII–G14	-0.05 ± 0.11	45
[Fe/H]	LIII–G14	0.03 ± 0.08	33
[Fe/H]	LII–LEM	0.08 ± 0.12	51
[Fe/H]	LIII–YON	0.34 ± 0.20	20
[Y/H]	LII–TS	0.21 ± 0.20	37
[Y/H]	LIII–TS	0.15 ± 0.18	34
[Y/H]	LII–LEM	0.09 ± 0.15	46
[La/H]	LII–TS	0.29 ± 0.18	40
[La/H]	LIII–TS	0.31 ± 0.16	34
[La/H]	LII–LEM	0.06 ± 0.20	47
[La/H]	LIII–YON	0.27 ± 0.33	16
[Ce/H]	LII–TS	-0.06 ± 0.16	24
[Ce/H]	LIII–TS	0.17 ± 0.17	19
[Ce/H]	LII–LEM	-0.21 ± 0.21	50
[Nd/H]	LII–TS	0.09 ± 0.24	42
[Nd/H]	LIII–TS	0.15 ± 0.18	33
[Nd/H]	LII–LEM	-0.08 ± 0.29	50
[Eu/H]	LII–TS	0.10 ± 0.17	41
[Eu/H]	LIII–TS	0.11 ± 0.21	34
[Eu/H]	LII–LEM	-0.09 ± 0.20	53
[Eu/H]	LIII–YON	0.12 ± 0.25	15

Notes. ⁽¹⁾ G14: Genovali et al. (2014); TS: this study; LII: Luck et al. (2011); LIII: Luck & Lambert (2011); LEM: Lemasle et al. (2013); YON: Yong et al. (2006). For Y, La, and Eu, the differences were computed after accounting for the HFS affecting some lines of these elements in the current sample. The quoted errors represent the dispersion around the mean.

Table 6. Slopes and zero-points of the abundance gradients as a function of the Galactocentric distance and of the pulsation period.

Abundance ratio	Slope ^a	Zero-point [dex]	σ [dex]	N	Slope ^a (TS)	Slope ^a (LEM)	Slope ^a (LII)	Slope ^a (LIII)
as a function of R_G								
[Y/H]	-0.053 ± 0.003	0.43 ± 0.03	0.14	429	-0.033 ± 0.007	-0.062 ± 0.012	-0.044 ± 0.004	-0.061 ± 0.003
[La/H]	-0.020 ± 0.003	0.13 ± 0.03	0.14	424	0.002 ± 0.005	-0.045 ± 0.012	-0.019 ± 0.005	-0.031 ± 0.004
[Ce/H]	-0.024 ± 0.003	0.20 ± 0.03	0.14	421	0.008 ± 0.007	-0.043 ± 0.012	-0.021 ± 0.004	-0.034 ± 0.003
[Nd/H]	-0.025 ± 0.003	0.24 ± 0.03	0.13	430	0.006 ± 0.006	-0.046 ± 0.013	-0.006 ± 0.004	-0.037 ± 0.003
[Eu/H]	-0.030 ± 0.004	0.28 ± 0.03	0.16	420	-0.013 ± 0.005	-0.066 ± 0.013	-0.021 ± 0.004	-0.042 ± 0.005
[La/Fe]	0.035 ± 0.003	-0.40 ± 0.03	0.13	425	0.057 ± 0.006	0.011 ± 0.011	0.043 ± 0.004	0.029 ± 0.003
[Ce/Fe]	0.027 ± 0.003	-0.31 ± 0.02	0.12	419	0.063 ± 0.008	0.009 ± 0.012	0.033 ± 0.004	0.027 ± 0.002
[Nd/Fe]	0.027 ± 0.002	-0.26 ± 0.02	0.10	427	0.057 ± 0.006	-0.023 ± 0.011	0.045 ± 0.004	0.023 ± 0.002
[Eu/Fe]	0.025 ± 0.003	-0.26 ± 0.03	0.14	420	0.043 ± 0.006	-0.007 ± 0.010	0.030 ± 0.003	0.015 ± 0.004
as a function of $\log P$								
[Y/H]	0.20 ± 0.03	-0.20 ± 0.03	0.17	430	0.28 ± 0.06	0.27 ± 0.07	0.12 ± 0.03	0.13 ± 0.03
[La/H]	0.10 ± 0.02	-0.13 ± 0.02	0.14	424	0.06 ± 0.04	0.16 ± 0.07	0.04 ± 0.03	0.11 ± 0.03
[Ce/H]	0.06 ± 0.02	-0.07 ± 0.02	0.13	417	-0.10 ± 0.07	0.10 ± 0.07	0.00 ± 0.03	0.04 ± 0.03
[Nd/H]	0.10 ± 0.02	-0.07 ± 0.02	0.14	430	-0.03 ± 0.05	0.13 ± 0.07	0.04 ± 0.03	0.12 ± 0.02
[Eu/H]	0.15 ± 0.03	-0.11 ± 0.03	0.17	418	0.08 ± 0.04	0.26 ± 0.08	0.09 ± 0.03	0.15 ± 0.04
[Ce/Fe]	-0.09 ± 0.02	0.02 ± 0.02	0.13	423	-0.55 ± 0.10	-0.04 ± 0.07	-0.08 ± 0.03	-0.09 ± 0.02

Notes. ^(a) In units of dex kpc⁻¹ if in function of R_G , and dex per logarithmic day if in function of $\log P$. Columns from 2 to 5 shows the results for all the different samples fitted together. We also list the standard deviation (σ) of the residuals and the number of data points (N) used in the fit. The slopes using only the stars of our sample (TS: this study) and of previous studies (LEM, LII, and LIII) are shown for comparison.

Table 7. Galactic Cepheids for which the abundances heavy elements was available in the literature.

Name	[Y/H] _{lit}	[Y/H]	Ref.	[La/H] _{lit}	[La/H]	Ref.	[Ce/H] _{lit}	[Ce/H]	Ref.	[Nd/H] _{lit}	[Nd/H]	Ref.	[Eu/H] _{lit}	[Eu/H]	Ref.
T Ant	-0.06	-0.21	LIII	0.19	-0.12	LIII	0.02	-0.15	LIII	0.04	-0.11	LIII	0.08	-0.03	LIII
BC Aql	-0.11	-0.26	LIII	-0.19	-0.50	LIII	-0.35	-0.52	LIII	-0.60	-0.75	LIII	0.10	-0.01	LIII
EV Aql	0.19	0.04	LIII	0.34	0.03	LIII	0.18	0.01	LIII	0.19	0.04	LIII	0.31	0.20	LIII
FF Aql	0.27	0.06	LII	0.23	-0.06	LII	-0.14	-0.08	LII	0.12	0.03	LII	0.14	0.04	LII
FM Aql	0.31	0.16	LIII	0.65	0.34	LIII	0.29	0.12	LIII	0.39	0.24	LIII	0.22	0.11	LIII
FN Aql	0.05	-0.10	LIII	0.13	-0.18	LIII	0.02	-0.15	LIII	0.07	-0.08	LIII	0.05	-0.06	LIII
KL Aql	0.38	0.23	LIII	0.39	0.08	LIII	0.35	0.18	LIII	0.36	0.21	LIII	0.34	0.23	LIII
SZ Aql	0.37	0.16	LII	0.27	-0.02	LII	-0.09	-0.03	LII	0.15	0.06	LII	0.14	0.04	LII
TT Aql	0.28	0.13	LIII	0.33	0.02	LIII	0.32	0.15	LIII	0.25	0.10	LIII	0.17	0.06	LIII
U Aql	0.24	0.09	LIII	0.36	0.05	LIII	0.21	0.04	LIII	0.26	0.11	LIII	0.16	0.05	LIII
V1162 Aql	0.21	-0.00	LII	0.09	-0.20	LII	-0.24	-0.18	LII	0.02	-0.07	LII	-0.06	-0.16	LII
V1344 Aql	0.16	0.01	LIII	0.28	-0.03	LIII	0.13	-0.04	LIII	0.17	0.02	LIII	0.03	-0.08	LIII
V1359 Aql	0.38	0.23	LIII	0.24	-0.07	LIII	0.25	0.08	LIII	0.28	0.13	LIII	0.12	0.01	LIII
V336 Aql	0.27	0.12	LIII	0.30	-0.01	LIII	0.15	-0.02	LIII	0.24	0.09	LIII	0.21	0.10	LIII
V493 Aql	0.02	-0.13	LIII	0.25	-0.06	LIII	-0.02	-0.19	LIII	0.05	-0.10	LIII	-0.01	-0.12	LIII
V496 Aql	0.14	-0.07	LII	0.09	-0.20	LII	-0.23	-0.17	LII	0.02	-0.07	LII	-0.01	-0.11	LII
V526 Aql	0.43	0.28	LIII	0.56	0.25	LIII	0.36	0.19	LIII	0.46	0.31	LIII	0.24	0.13	LIII
V600 Aql	0.16	-0.05	LII	0.15	-0.14	LII	-0.05	0.01	LII	0.03	-0.06	LII	0.00	-0.10	LII
V733 Aql	0.16	-0.05	LII	0.21	-0.08	LII	-0.13	-0.07	LII	0.02	-0.07	LII	-0.08	-0.18	LII
V916 Aql	0.34	0.19	LIII	0.32	0.01	LIII	0.36	0.19	LIII	0.27	0.12	LIII	0.19	0.08	LIII
η Aql	0.27	0.06	LII	0.24	-0.05	LII	-0.07	-0.01	LII	0.16	0.07	LII	0.09	-0.01	LII
V340 Ara	0.04	0.04	TS	-0.04	-0.04	TS	0.13	0.13	TS	0.02	0.02	TS	0.13	0.13	TS
AN Aur	0.09	-0.06	LIII	0.27	-0.04	LIII	0.18	0.01	LIII	0.20	0.05	LIII	-0.04	-0.15	LIII
AO Aur	-0.40	-0.52	LEM	-0.21	-0.44	LEM	-0.17	-0.32	LEM	-0.22	-0.39	LEM	-0.15	-0.34	LEM
AS Aur	-0.20	-0.20	TS	-0.16	-0.16	TS	-0.05	-0.22	LIII	-0.06	-0.06	TS	-0.03	-0.03	TS
AX Aur	-0.35	-0.47	LEM	-0.22	-0.45	LEM	-0.08	-0.23	LEM	-0.10	-0.27	LEM	-0.31	-0.50	LEM
BK Aur	0.08	-0.04	LEM	0.26	0.03	LEM	0.31	0.16	LEM	0.28	0.11	LEM	0.27	0.08	LEM
CO Aur	0.08	-0.07	LIII	0.10	-0.21	LIII	0.13	-0.04	LIII	0.14	-0.01	LIII	0.13	0.02	LIII
CY Aur	0.02	-0.13	LIII	0.36	0.05	LIII	0.13	-0.04	LIII	0.15	0.00	LIII	0.19	0.08	LIII
ER Aur	-0.10	-0.25	LIII	0.08	-0.23	LIII	-0.03	-0.20	LIII	0.01	-0.14	LIII	-0.18	-0.29	LIII
EW Aur	-0.55	-0.70	LIII	-0.13	-0.44	LIII	-0.54	-0.71	LIII	-0.38	-0.53	LIII	-0.24	-0.35	LIII
FF Aur	-0.47	-0.62	LIII	0.00	-0.31	LIII	-0.11	-0.28	LIII	-0.33	-0.48	LIII
GT Aur	0.03	-0.12	LIII	0.14	-0.17	LIII	0.12	-0.05	LIII	0.18	0.03	LIII	-0.02	-0.13	LIII
GV Aur	-0.21	-0.36	LIII	0.08	-0.23	LIII	-0.04	-0.21	LIII	-0.05	-0.20	LIII	-0.07	-0.18	LIII
IN Aur	-0.26	-0.41	LIII	-0.07	-0.38	LIII	-0.05	-0.22	LIII	-0.09	-0.24	LIII	0.06	-0.05	LIII
RT Aur	0.26	0.11	LIII	0.29	-0.02	LIII	0.16	-0.01	LIII	0.17	0.02	LIII	0.19	0.08	LIII
RX Aur	0.21	0.06	LIII	0.49	0.18	LIII	0.17	-0.00	LIII	0.33	0.18	LIII	0.24	0.13	LIII
SY Aur	-0.07	-0.19	LEM	0.04	-0.19	LEM	0.22	0.07	LEM	0.17	-0.00	LEM	0.14	-0.05	LEM
V335 Aur	-0.21	-0.36	LIII	-0.20	-0.37	LIII	-0.04	-0.19	LIII
V637 Aur	-0.09	-0.24	LIII	0.09	-0.22	LIII	0.07	-0.10	LIII	0.11	-0.04	LIII	-0.03	-0.14	LIII
Y Aur	-0.36	-0.48	LEM	-0.24	-0.47	LEM	-0.21	-0.36	LEM	-0.24	-0.41	LEM	-0.11	-0.30	LEM
YZ Aur	-0.34	-0.46	LEM	-0.19	-0.42	LEM	0.25	0.10	LEM	-0.17	-0.32	LIII	-0.16	-0.35	LEM
AO CMa	0.08	0.08	TS	0.13	0.13	TS	0.18	0.18	TS	0.11	0.11	TS	0.20	0.20	TS
RW CMa	-0.06	-0.06	TS	-0.04	-0.04	TS	-0.08	-0.08	TS
RY CMa	-0.08	-0.20	LEM	0.13	-0.10	LEM	0.20	0.05	LEM	0.19	0.02	LEM	0.28	0.09	LEM
RZ CMa	-0.16	-0.28	LEM	-0.07	-0.30	LEM	0.09	-0.06	LEM	0.14	-0.03	LEM	0.09	-0.10	LEM
SS CMa	0.14	0.14	TS	0.06	0.06	TS	0.13	0.13	TS	0.09	0.09	TS	0.10	0.10	TS
TV CMa	0.17	0.17	TS	-0.04	-0.04	TS	-0.04	-0.04	TS	-0.10	-0.10	TS	0.04	0.04	TS
TW CMa	-0.06	-0.06	TS	0.17	0.17	TS	0.14	0.14	TS	0.02	0.02	TS	0.06	0.06	TS
VZ CMa	0.33	0.04	LII	-0.02	0.04	LII	0.41	0.32	LII	0.22	0.12	LII
XZ CMa
AB Cam	0.05	-0.10	LIII	0.22	-0.09	LIII	0.14	-0.03	LIII	0.21	0.06	LIII	-0.03	-0.14	LIII
AC Cam	0.04	-0.11	LIII	-0.04	-0.35	LIII	-0.08	-0.25	LIII	0.03	-0.12	LIII	0.71	0.60	LIII
AD Cam	-0.25	-0.40	LIII	0.08	-0.23	LIII	0.05	-0.12	LIII	-0.07	-0.22	LIII	-0.16	-0.27	LIII
AM Cam	-0.01	-0.16	LIII	0.21	-0.10	LIII	0.15	-0.02	LIII	0.01	-0.14	LIII	0.08	-0.03	LIII
CK Cam	0.12	-0.03	LIII	0.19	-0.12	LIII	0.11	-0.06	LIII	0.13	-0.02	LIII	0.12	0.01	LIII
LO Cam	0.16	0.01	LIII	0.30	-0.01	LIII	0.20	0.03	LIII	0.22	0.07	LIII	0.30	0.19	LIII
MN Cam	0.10	-0.05	LIII	0.24	-0.07	LIII	0.13	-0.04	LIII	0.23	0.08	LIII	0.06	-0.05	LIII
MQ Cam	-0.11	-0.26	LIII	0.19	-0.12	LIII	0.01	-0.16	LIII	0.10	-0.05	LIII	-0.12	-0.23	LIII
OX Cam	0.10	-0.05	LIII	0.31	0.00	LIII	0.25	0.08	LIII	0.29	0.14	LIII	0.04	-0.07	LIII
PV Cam	-0.08	-0.23	LIII	0.13	-0.18	LIII	0.03	-0.14	LIII	0.00	-0.15	LIII	-0.02	-0.13	LIII
QS Cam	0.15	-0.00	LIII	0.43	0.12	LIII	0.15	-0.02	LIII	0.22	0.07	LIII	0.54	0.43	LIII
RW Cam	-0.06	-0.21	LIII	0.38	0.07	LIII	-0.14	-0.31	LIII	0.05	-0.10	LIII	0.15	0.04	LIII
RX Cam	0.16	0.01	LIII	0.34	0.03	LIII	0.17	-0.00	LIII	0.22	0.07	LIII	0.12	0.01	LIII
TV Cam	0.14	-0.01	LIII	0.29	-0.02	LIII	0.24	0.07	LIII	0.29	0.14	LIII	-0.08	-0.19	LIII
V359 Cam	-0.23	-0.38	LIII	0.23	-0.08	LIII	-0.05	-0.22	LIII	-0.06	-0.21	LIII	-0.11	-0.22	LIII
AQ Car	-0.02	-0.14	LEM	0.02	-0.21	LEM	0.02	-0.13	LEM	0.25	0.08	LEM	0.18	0.07	LIII
CN Car	0.34	0.19	LIII	0.45	0.14	LIII	0.24	0.07	LIII	0.28	0.13	LIII	0.43	0.32	LIII
CY Car	0.18	0.03	LIII	0.25	-0.06	LIII	0.09	-0.08	LIII	0.17	0.02	LIII	0.07	-0.04	LIII
DY Car	0.18	0.03	LIII	0.21	-0.10	LIII	0.01	-0.16	LIII	0.25	0.10	LIII	0.01	-0.09	LII
ER Car	0.17	0.02	LIII	0.30	-0.01	LIII	0.18	0.01	LIII	0.20	0.05	LIII	0.14	0.03	LIII
FI Car	0.25	0.10	LIII	0.52	0.21	LIII	0.35	0.18	LIII	0.44	0.29	LIII	0.44	0.33	LIII
FR Car	0.20	0.05	LIII	0.30	-0.01	LIII	0.17	-0.00	LIII	0.21	0.06	LIII	0.34	0.23	LIII
GH Car	0.35	0.20	LIII	0.41	0.10	LIII	0.26	0.09	LIII	0.30	0.15	LIII	0.47	0.36	LIII
GX Car	0.23	0.08	LIII	0.30	-0.01	LIII	0.16	-0.01	LIII	0.26	0.11	LIII	0.04	-0.07	LIII

continued on next page

Notes. The columns first give the original abundance estimate available in the literature and then the abundances rescaled according to the zero-point differences listed in Table 5. The priority was given in the following order: we first adopt the abundances provided by our group, this study (TS) and LEM, and then those provided by the other studies, LIII, LII, and YON.

Table 7. continued.

Name	[Y/H] _{lit}	[Y/H]	Ref.	[La/H] _{lit}	[La/H]	Ref.	[Ce/H] _{lit}	[Ce/H]	Ref.	[Nd/H] _{lit}	[Nd/H]	Ref.	[Eu/H] _{lit}	[Eu/H]	Ref.
HW Car	0.15	-0.00	LIII	0.21	-0.10	LIII	0.11	-0.06	LIII	0.17	0.02	LIII	0.04	-0.07	LIII
IO Car	0.28	0.13	LIII	0.36	0.05	LIII	0.18	0.01	LIII	0.25	0.10	LIII	0.21	0.10	LIII
IT Car	0.17	0.02	LIII	0.26	-0.05	LIII	0.17	-0.00	LIII	0.22	0.07	LIII	0.13	0.02	LIII
L Car	0.29	0.17	LEM	0.29	0.06	LEM	0.42	0.27	LEM	0.47	0.30	LEM	0.61	0.42	LEM
SX Car	0.22	0.07	LIII	0.39	0.08	LIII	0.06	-0.11	LIII	0.19	0.04	LIII	0.03	-0.08	LIII
U Car	0.19	0.04	LIII	0.51	0.20	LIII	-0.09	-0.26	LIII	0.24	0.09	LIII	0.16	0.05	LIII
UW Car	0.17	0.02	LIII	0.27	-0.04	LIII	0.10	-0.07	LIII	0.07	-0.08	LIII	0.22	0.11	LIII
UX Car	-0.01	-0.13	LEM	0.11	-0.12	LEM	0.25	0.10	LEM	0.18	0.01	LEM	0.14	-0.05	LEM
UY Car	0.23	0.08	LIII	0.33	0.02	LIII	0.10	-0.07	LIII	0.13	-0.02	LIII	0.13	0.03	LII
UZ Car	0.16	0.01	LIII	0.42	0.11	LIII	0.08	-0.09	LIII	0.16	0.01	LIII	0.03	-0.08	LIII
V Car	0.07	-0.05	LEM	0.26	0.03	LEM	0.15	-0.00	LEM	0.16	-0.01	LEM	0.38	0.19	LEM
V397 Car	-0.04	-0.16	LEM	0.06	-0.17	LEM	0.06	-0.09	LEM	0.02	-0.15	LEM	0.12	-0.07	LEM
VY Car	0.20	0.08	LEM	0.32	0.09	LEM	0.39	0.24	LEM	0.38	0.21	LEM	0.39	0.20	LEM
WW Car	0.05	-0.10	LIII	0.14	-0.17	LIII	0.01	-0.16	LIII	0.03	-0.12	LIII	0.01	-0.10	LIII
WZ Car	0.01	-0.14	LIII	0.37	0.06	LIII	0.03	-0.14	LIII	0.05	-0.10	LIII	0.26	0.15	LIII
XX Car	0.38	0.23	LIII	0.42	0.11	LIII	0.25	0.08	LIII	0.40	0.25	LIII	0.26	0.15	LIII
XY Car	0.15	-0.00	LIII	0.26	-0.05	LIII	0.14	-0.03	LIII	0.15	0.00	LIII	0.32	0.21	LIII
XZ Car	0.23	0.08	LIII	0.32	0.01	LIII	0.17	-0.00	LIII	0.19	0.04	LIII	0.38	0.27	LIII
YZ Car	0.20	0.05	LIII	0.30	-0.01	LIII	0.16	-0.01	LIII	0.17	0.02	LIII	0.05	-0.06	LIII
AP Cas	0.03	-0.12	LIII	0.18	-0.13	LIII	0.10	-0.07	LIII	0.12	-0.03	LIII	0.04	-0.07	LIII
AS Cas	-0.12	-0.27	LIII	0.35	0.04	LIII	0.07	-0.10	LIII	0.07	-0.08	LIII
AW Cas	0.11	-0.04	LIII	0.23	-0.08	LIII	0.13	-0.04	LIII	0.15	0.00	LIII	0.08	-0.03	LIII
AY Cas	0.11	-0.04	LIII	0.23	-0.08	LIII	0.13	-0.04	LIII	0.20	0.05	LIII	0.10	-0.01	LIII
BF Cas	0.10	-0.05	LIII	0.14	-0.17	LIII	0.01	-0.16	LIII	0.05	-0.10	LIII
BP Cas	0.18	0.03	LIII	0.26	-0.05	LIII	0.27	0.10	LIII	0.27	0.12	LIII	0.19	0.08	LIII
BV Cas	0.14	-0.01	LIII	0.22	-0.09	LIII	0.09	-0.08	LIII	0.16	0.01	LIII	0.09	-0.02	LIII
BY Cas	0.25	0.10	LIII	0.22	-0.09	LIII	0.29	0.12	LIII	0.23	0.08	LIII	0.21	0.10	LIII
CD Cas	0.21	0.06	LIII	0.17	-0.14	LIII	0.14	-0.03	LIII	0.24	0.09	LIII	0.45	0.34	LIII
CFCas	0.12	-0.03	LIII	0.20	-0.11	LIII	0.18	0.01	LIII	0.16	0.01	LIII	0.10	-0.01	LIII
CG Cas	0.18	0.03	LIII	0.33	0.02	LIII	0.14	-0.03	LIII	0.16	0.01	LIII	0.03	-0.08	LIII
CH Cas	0.70	0.49	LII	LII	0.11	0.17	LII	0.20	0.11	LII	0.50	0.40	LII
CT Cas	-0.02	-0.17	LIII	0.31	0.00	LIII	0.02	-0.15	LIII	0.07	-0.08	LIII	0.03	-0.08	LIII
CY Cas	0.21	-0.00	LII	0.23	-0.06	LII	0.00	0.06	LII	0.03	-0.06	LII	0.22	0.12	LII
CZ Cas	0.14	-0.01	LIII	0.24	-0.07	LIII	0.08	-0.09	LIII	0.15	0.00	LIII	0.18	0.07	LIII
DD Cas	0.24	0.03	LII	0.09	-0.20	LII	-0.02	0.04	LII	0.06	-0.03	LII	0.09	-0.01	LII
DF Cas	0.06	-0.15	LII	LII	0.07	0.13	LII	0.38	0.29	LII	0.28	0.18	LII
DL Cas	0.21	-0.00	LII	0.12	-0.17	LII	0.09	0.15	LII	0.12	0.03	LII	0.11	0.01	LII
DW Cas	0.15	-0.00	LIII	0.31	0.00	LIII	0.14	-0.03	LIII	0.15	0.00	LIII	0.09	-0.02	LIII
EX Cas	-0.03	-0.18	LIII	0.48	0.17	LIII	0.19	0.02	LIII	0.12	-0.03	LIII	-0.29	-0.40	LIII
FM Cas	-0.06	-0.27	LII	-0.01	-0.30	LII	-0.25	-0.19	LII	-0.14	-0.23	LII	-0.25	-0.35	LII
FO Cas	-0.52	-0.67	LIII	-0.30	-0.61	LIII	-0.36	-0.53	LIII	-0.35	-0.50	LIII
FW Cas	-0.10	-0.25	LIII	0.22	-0.09	LIII	0.11	-0.06	LIII	0.06	-0.09	LIII	-0.10	-0.21	LIII
GL Cas	0.00	-0.15	LIII	0.29	-0.02	LIII	0.14	-0.03	LIII	0.02	-0.13	LIII	0.11	-0.00	LIII
GM Cas	-0.03	-0.18	LIII	0.26	-0.05	LIII	0.04	-0.13	LIII	0.05	-0.10	LIII	0.26	0.15	LIII
GO Cas	0.17	0.02	LIII	0.37	0.06	LIII	0.12	-0.05	LIII	0.16	0.01	LIII	0.01	-0.10	LIII
HK Cas	0.37	0.22	LIII	0.35	0.04	LIII	0.31	0.14	LIII	0.39	0.24	LIII
IO Cas	-0.48	-0.63	LIII	0.11	-0.20	LIII	-0.53	-0.70	LIII	-0.40	-0.55	LIII	-0.30	-0.41	LIII
KK Cas	0.21	0.06	LIII	0.33	0.02	LIII	0.24	0.07	LIII	0.33	0.18	LIII	-0.10	-0.21	LIII
LT Cas	-0.42	-0.57	LIII	-0.25	-0.56	LIII	-0.25	-0.42	LIII	-0.19	-0.34	LIII	-0.17	-0.28	LIII
NP Cas	0.05	-0.10	LIII	0.39	0.08	LIII	0.05	-0.12	LIII	0.17	0.02	LIII	0.28	0.17	LIII
NY Cas	-0.59	-0.74	LIII	0.01	-0.30	LIII	-0.55	-0.72	LIII	-0.37	-0.52	LIII	-0.49	-0.60	LIII
OP Cas	0.15	-0.00	LII	0.14	-0.17	LII	0.10	-0.07	LII	0.19	0.04	LII	0.03	-0.08	LII
OZ Cas	-0.03	-0.18	LIII	0.50	0.19	LIII	0.21	0.04	LIII	0.09	-0.06	LIII	-0.08	-0.19	LIII
PW Cas	0.11	-0.04	LIII	0.28	-0.03	LIII	0.22	0.05	LIII	0.20	0.05	LIII	0.01	-0.10	LIII
RS Cas	0.26	0.11	LIII	0.24	-0.07	LIII	0.36	0.19	LIII	0.34	0.19	LIII	0.26	0.15	LIII
RW Cas	0.23	0.02	LII	LII	0.00	0.06	LII	0.11	0.02	LII	0.23	0.13	LII
RY Cas	0.61	0.40	LII	LII	0.35	0.41	LII	0.40	0.31	LII	0.53	0.43	LII
SU Cas	0.26	0.05	LII	0.22	-0.07	LII	-0.05	0.01	LII	0.14	0.05	LII	0.09	-0.01	LII
SW Cas	0.31	0.10	LII	0.30	0.01	LII	-0.12	-0.06	LII	0.16	0.07	LII	0.15	0.05	LII
SY Cas	0.11	-0.10	LII	0.42	0.13	LII	0.01	0.07	LII	0.14	0.05	LII	0.10	0.00	LII
SZ Cas	0.15	-0.00	LIII	0.46	0.15	LIII	0.30	0.13	LIII	0.31	0.16	LIII	0.28	0.17	LIII
TU Cas	0.17	-0.04	LII	0.24	-0.05	LII	-0.05	0.01	LII	0.08	-0.01	LII	0.11	0.01	LII
UZ Cas	0.06	-0.09	LIII	0.15	-0.16	LIII	0.15	-0.02	LIII	0.19	0.04	LIII	0.03	-0.08	LIII
V1017 Cas	-0.15	-0.30	LIII	0.06	-0.25	LIII	-0.02	-0.19	LIII	0.00	-0.15	LIII	0.02	-0.09	LIII
V1019 Cas	0.18	0.03	LIII	0.51	0.20	LIII	0.18	0.01	LIII	0.22	0.07	LIII	0.36	0.25	LIII
V1020 Cas	0.30	0.15	LIII	0.53	0.22	LIII	0.37	0.20	LIII	0.23	0.08	LIII	0.19	0.08	LIII
V1100 Cas	-0.06	-0.21	LIII	0.30	-0.01	LIII	0.05	-0.12	LIII	0.08	-0.07	LIII	0.10	-0.01	LIII
V1154 Cas	-0.25	-0.40	LIII	0.28	-0.03	LIII	-0.08	-0.25	LIII	-0.08	-0.23	LIII	-0.33	-0.44	LIII
V1206 Cas	0.18	0.03	LIII	0.38	0.07	LIII	0.19	0.02	LIII	0.27	0.12	LIII	0.12	0.01	LIII
V342 Cas	0.11	-0.04	LIII	0.16	-0.15	LIII	0.13	-0.04	LIII	0.19	0.04	LIII	0.03	-0.08	LIII
V379 Cas	0.16	-0.05	LII	0.30	0.01	LII	-0.06	-0.00	LII	0.12	0.03	LII	0.12	0.02	LII
V395 Cas	0.07	-0.08	LIII	0.30	-0.01	LIII	0.09	-0.08	LIII	0.11	-0.04	LIII	0.26	0.15	LIII
V407 Cas	0.08	-0.07	LIII	0.19	-0.12	LIII	0.05	-0.12	LIII	0.17	0.02	LIII	0.25	0.14	LIII
V556 Cas	0.10	-0.05	LIII	0.25	-0.06	LIII	0.19	0.02	LIII	0.19	0.04	LIII	-0.12	-0.23	LIII
V636 Cas	0.18	-0.03	LII	0.14	-0.15	LII	-0.15	-0.09	LII	0.11	0.02	LII	0.02	-0.08	LII

continued on next page

Table 7. continued.

Name	[Y/H] _{lit}	[Y/H]	Ref.	[La/H] _{lit}	[La/H]	Ref.	[Ce/H] _{lit}	[Ce/H]	Ref.	[Nd/H] _{lit}	[Nd/H]	Ref.	[Eu/H] _{lit}	[Eu/H]	Ref.
VV Cas	0.06	-0.09	LIII	0.14	-0.17	LIII	0.24	0.07	LIII	0.21	0.06	LIII	0.21	0.10	LIII
VW Cas	0.30	0.15	LIII	0.34	0.03	LIII	0.41	0.24	LIII	0.38	0.23	LIII	0.28	0.17	LIII
XY Cas	0.18	0.03	LIII	0.35	0.04	LIII	0.07	-0.10	LIII	0.13	-0.02	LIII	0.29	0.18	LIII
AY Cen	0.17	0.02	LIII	0.21	-0.10	LIII	0.12	-0.05	LIII	0.15	0.00	LIII	0.12	0.01	LIII
AZ Cen	0.23	0.08	LIII	0.27	-0.04	LIII	0.14	-0.03	LIII	0.17	0.02	LIII	0.06	-0.05	LIII
BB Cen	0.34	0.19	LIII	0.35	0.04	LIII	0.20	0.03	LIII	0.26	0.11	LIII	0.46	0.35	LIII
KK Cen	0.31	0.16	LIII	0.35	0.04	LIII	0.25	0.08	LIII	0.27	0.12	LIII	0.29	0.18	LIII
KN Cen	0.23	0.23	TS	0.04	0.04	TS	-0.02	-0.02	TS	0.05	0.05	TS	0.07	0.07	TS
MZ Cen	-0.08	-0.08	TS	-0.22	-0.22	TS	0.16	-0.01	LIII	0.27	0.27	TS	-0.05	-0.05	TS
OO Cen	0.14	0.14	TS	0.01	0.01	TS	-0.04	-0.04	TS	0.05	0.05	TS
QY Cen	0.28	0.13	LIII	0.51	0.20	LIII	0.12	-0.05	LIII	0.23	0.08	LIII	0.60	0.49	LIII
TX Cen	0.17	0.17	TS	0.01	0.01	TS	0.07	0.07	TS	-0.05	-0.05	TS	0.07	0.07	TS
V Cen	0.15	-0.00	LIII	0.31	0.00	LIII	0.08	-0.09	LIII	0.14	-0.01	LIII	0.17	0.06	LIII
V339 Cen	-0.09	-0.09	TS	-0.25	-0.25	TS	-0.21	-0.21	TS	-0.28	-0.28	TS	-0.10	-0.10	TS
V378 Cen	0.23	0.08	LIII	0.28	-0.03	LIII	0.12	-0.05	LIII	0.22	0.07	LIII	0.44	0.33	LIII
V381 Cen	0.11	-0.04	TS	0.20	-0.11	LIII	0.03	-0.14	LIII	0.01	-0.14	LIII	-0.06	-0.17	LIII
V419 Cen	0.25	0.10	LIII	0.50	0.19	LIII	0.24	0.07	LIII	0.28	0.13	LIII	0.18	0.07	LIII
V496 Cen	0.20	0.05	LIII	0.28	-0.03	LIII	0.16	-0.01	LIII	0.15	0.00	LIII	0.13	0.02	LIII
V659 Cen	0.20	0.05	LIII	0.34	0.03	LIII	0.14	-0.03	LIII	0.17	0.02	LIII	0.10	-0.01	LIII
V737 Cen	0.20	0.05	LIII	0.21	-0.10	LIII	0.12	-0.05	LIII	0.16	0.01	LIII	0.15	0.04	LIII
VW Cen	0.07	0.07	TS	-0.14	-0.14	TS	-0.19	-0.19	TS	0.23	0.23	TS	-0.05	-0.05	TS
XX Cen	0.28	0.13	LIII	0.28	-0.03	LIII	0.17	-0.00	LIII	0.25	0.10	LIII	0.02	-0.09	LIII
AK Cep	0.16	0.01	LIII	0.31	0.00	LIII	0.13	-0.04	LIII	0.17	0.02	LIII	-0.19	-0.30	LIII
CN Cep	0.12	-0.03	TS	0.19	-0.12	LIII	0.05	-0.12	LIII	0.23	0.08	LIII	0.24	0.13	LIII
CP Cep	0.05	-0.16	LII	0.12	-0.17	LII	-0.12	-0.06	LII	0.03	-0.06	LII	0.00	-0.10	LII
CR Cep	0.05	-0.16	LII	0.14	-0.15	LII	-0.20	-0.14	LII	0.00	-0.09	LII	-0.11	-0.21	LII
DR Cep	-0.11	-0.26	LIII	0.43	0.12	LIII	-0.31	-0.48	LIII	0.07	-0.08	LIII	0.07	-0.04	LIII
IR Cep	0.13	-0.08	LII	0.16	-0.13	LII	0.02	0.08	LII	0.09	0.00	LII	0.12	0.02	LII
IY Cep	-0.05	-0.20	LIII	0.29	-0.02	LIII	-0.08	-0.25	LIII	0.02	-0.13	LIII	0.35	0.24	LIII
MU Cep	0.23	0.08	LIII	0.70	0.39	LIII	0.27	0.10	LIII	0.27	0.12	LIII	0.43	0.32	LIII
V901 Cep	0.10	-0.05	LIII	0.32	0.01	LIII	0.08	-0.09	LIII	0.21	0.06	LIII
V911 Cep	0.10	-0.05	LIII	0.34	0.03	LIII	0.34	0.17	LIII	0.20	0.05	LIII	0.45	0.34	LIII
δ Cep	0.22	0.07	LIII	0.43	0.12	LIII	0.16	-0.01	LIII	0.24	0.09	LIII	0.14	0.03	LIII
AV Cir	0.32	0.17	LIII	0.32	0.01	LIII	0.21	0.04	LIII	0.24	0.09	LIII	0.13	0.02	LIII
AX Cir	0.05	-0.10	LIII	0.26	-0.05	LIII	0.06	-0.11	LIII	0.09	-0.06	LIII	0.06	-0.05	LIII
BPCir	0.14	-0.01	LIII	0.22	-0.09	LIII	0.03	-0.14	LIII	0.03	-0.12	LIII	-0.15	-0.26	LIII
AD Cru	0.16	0.01	LIII	0.26	-0.05	LIII	0.14	-0.03	LIII	0.19	0.04	LIII	0.40	0.29	LIII
AG Cru	0.16	0.01	LIII	0.26	-0.05	LIII	0.01	-0.16	LIII	0.08	-0.07	LIII	-0.03	-0.14	LIII
BG Cru	0.10	-0.05	LIII	0.47	0.16	LIII	0.09	-0.08	LIII	0.28	0.13	LIII	0.23	0.13	LII
R Cru	0.24	0.09	LIII	0.24	-0.07	LIII	0.13	-0.04	LIII	0.18	0.03	LIII	0.26	0.15	LIII
S Cru	0.20	0.05	LIII	0.32	0.01	LIII	0.11	-0.06	LIII	0.11	-0.04	LIII	-0.05	-0.16	LIII
T Cru	0.18	0.03	LIII	0.29	-0.02	LIII	0.10	-0.07	LIII	0.15	0.00	LIII	0.01	-0.10	LIII
VW Cru	0.26	0.11	LIII	0.31	0.00	LIII	0.18	0.01	LIII	0.25	0.10	LIII	0.38	0.27	LIII
X Cru	0.16	0.01	LIII	0.29	-0.02	LIII	0.14	-0.03	LIII	0.16	0.01	LIII	0.00	-0.11	LIII
BZ Cyg	0.17	-0.04	LII	0.31	0.02	LII	-0.07	-0.01	LII	0.15	0.06	LII	0.12	0.02	LII
CD Cyg	0.23	0.08	LIII	0.40	0.09	LIII	0.17	-0.00	LIII	0.23	0.08	LIII	0.39	0.28	LIII
DT Cyg	0.31	0.10	LII	0.22	-0.07	LII	-0.03	0.03	LII	0.19	0.10	LII	0.18	0.08	LII
EPCyg	-0.09	-0.24	LIII	0.08	-0.23	LIII	-0.08	-0.25	LIII	0.07	-0.08	LIII	-0.09	-0.20	LIII
EU Cyg	-0.22	-0.37	LIII	0.12	-0.19	LIII	0.02	-0.15	LIII	0.03	-0.12	LIII	-0.03	-0.14	LIII
EX Cyg	0.28	0.13	LIII	0.35	0.04	LIII	0.23	0.06	LIII	0.38	0.23	LIII	0.48	0.37	LIII
EZ Cyg	0.35	0.20	LIII	0.38	0.07	LIII	0.55	0.38	LIII	0.30	0.15	LIII	0.25	0.14	LIII
GH Cyg	0.32	0.17	LIII	0.32	0.01	LIII	0.20	0.03	LIII	0.27	0.12	LIII	0.36	0.25	LIII
GI Cyg	0.23	0.08	LIII	0.46	0.15	LIII	0.38	0.21	LIII	0.34	0.19	LIII	0.26	0.15	LIII
GL Cyg	0.10	-0.05	LIII	0.22	-0.09	LIII	0.16	-0.01	LIII	0.16	0.01	LIII	0.20	0.09	LIII
IY Cyg	0.05	-0.10	LIII	0.33	0.02	LIII	0.07	-0.10	LIII	0.18	0.03	LIII	-0.28	-0.39	LIII
KX Cyg	0.29	0.14	LIII	0.51	0.20	LIII	0.20	0.03	LIII	0.33	0.18	LIII	0.23	0.12	LIII
MW Cyg	0.24	0.03	LII	0.15	-0.14	LII	0.04	0.10	LII	0.13	0.04	LII	0.06	-0.04	LII
SU Cyg	0.15	-0.06	LII	0.24	-0.05	LII	-0.11	-0.05	LII	0.15	0.06	LII	0.08	-0.02	LII
SZ Cyg	0.22	0.01	LII	0.21	-0.08	LII	0.00	0.06	LII	0.03	-0.06	LII	0.15	0.05	LII
TX Cyg	0.45	0.24	LII	0.44	0.15	LII	0.23	0.29	LII	0.30	0.21	LII	0.13	0.03	LII
V1020 Cyg	0.46	0.31	LIII	0.55	0.24	LIII	0.58	0.41	LIII	0.40	0.25	LIII
V1025 Cyg	0.24	0.09	LIII	0.24	-0.07	LIII	0.15	-0.02	LIII	0.22	0.07	LIII	0.33	0.22	LIII
V1033 Cyg	0.23	0.08	LIII	0.34	0.03	LIII	0.20	0.03	LIII	0.25	0.10	LIII	0.06	-0.05	LIII
V1046 Cyg	0.34	0.19	LIII	0.43	0.12	LIII	0.28	0.11	LIII	0.38	0.23	LIII	0.33	0.22	LIII
V1154 Cyg	0.08	-0.13	LII	0.18	-0.11	LII	-0.10	-0.04	LII	0.05	-0.04	LII	-0.06	-0.16	LII
V1334 Cyg	0.18	-0.03	LII	0.27	-0.02	LII	-0.09	-0.03	LII	0.16	0.07	LII	0.17	0.07	LII
V1364 Cyg	0.26	0.11	LIII	0.32	0.01	LIII	0.32	0.15	LIII	0.25	0.10	LIII	0.15	0.04	LIII
V1397 Cyg	0.07	-0.08	LIII	0.23	-0.08	LIII	0.14	-0.03	LIII	0.16	0.01	LIII	0.02	-0.09	LIII
V1726 Cyg	0.14	-0.07	LII	LII	LII	0.24	0.15	LII	0.31	0.21	LII
V347 Cyg	0.33	0.18	LIII	0.36	0.05	LIII	0.29	0.12	LIII	0.36	0.21	LIII	0.16	0.05	LIII
V356 Cyg	0.24	0.09	LIII	0.34	0.03	LIII	0.28	0.11	LIII	0.20	0.05	LIII	0.29	0.18	LIII
V386 Cyg	0.35	0.14	LII	0.41	0.12	LII	0.10	0.16	LII	0.42	0.33	LII	0.41	0.31	LII
V396 Cyg	0.00	-0.15	LII	0.19	-0.12	LII	0.01	-0.16	LII	0.05	-0.10	LII	0.00	-0.11	LII
V402 Cyg	0.15	-0.06	LII	0.16	-0.13	LII	0.03	0.09	LII	0.01	-0.08	LII	0.01	-0.09	LII
V438 Cyg	0.05	-0.10	LIII	0.19	-0.12	LIII	-0.01	-0.18	LIII	0.12	-0.03	LIII	-0.03	-0.14	LIII

Table 7. continued.

Name	[Y/H] _{lit}	[Y/H]	Ref.	[La/H] _{lit}	[La/H]	Ref.	[Ce/H] _{lit}	[Ce/H]	Ref.	[Nd/H] _{lit}	[Nd/H]	Ref.	[Eu/H] _{lit}	[Eu/H]	Ref.
V459 Cyg	0.40	0.25	LIII	0.44	0.13	LIII	0.28	0.11	LIII	0.35	0.20	LIII	0.24	0.13	LIII
V492 Cyg	0.24	0.09	LIII	0.38	0.07	LIII	0.25	0.08	LIII	0.26	0.11	LIII	0.19	0.08	LIII
V495 Cyg	0.23	0.08	LIII	0.14	-0.17	LIII	0.22	0.05	LIII	0.26	0.11	LIII	0.24	0.13	LIII
V514 Cyg	0.25	0.10	LIII	0.35	0.04	LIII	0.22	0.05	LIII	0.29	0.14	LIII	0.35	0.24	LIII
V520 Cyg	0.11	-0.04	LIII	0.12	-0.19	LIII	0.23	0.06	LIII	0.18	0.03	LIII	0.13	0.02	LIII
V532 Cyg	0.12	-0.09	LII	0.09	-0.20	LII	0.00	0.06	LII	-0.05	-0.14	LII	-0.03	-0.13	LII
V538 Cyg	0.08	-0.07	LIII	0.12	-0.19	LIII	0.20	0.03	LIII	0.18	0.03	LIII	0.10	-0.01	LIII
V547 Cyg	0.24	0.09	LIII	0.26	-0.05	LIII	0.24	0.07	LIII	0.24	0.09	LIII	0.18	0.07	LIII
V609 Cyg	0.36	0.21	LIII	0.50	0.19	LIII	0.37	0.20	LIII	0.38	0.23	LIII	0.53	0.42	LIII
V621 Cyg	0.07	-0.08	LIII	0.47	0.16	LIII	0.17	-0.00	LIII	0.12	-0.03	LIII	0.41	0.30	LIII
V924 Cyg	-0.18	-0.39	LII	LII	0.04	-0.05	LII
VX Cyg	0.14	-0.07	LII	0.16	-0.13	LII	-0.01	0.05	LII	0.01	-0.08	LII	0.17	0.07	LII
VY Cyg	0.17	-0.04	LII	0.21	-0.08	LII	0.01	0.07	LII	0.09	0.00	LII	0.01	-0.09	LII
VZ Cyg	0.17	-0.04	LII	0.14	-0.15	LII	0.01	0.07	LII	0.08	-0.01	LII	0.11	0.01	LII
X Cyg	0.28	0.07	LII	0.23	-0.06	LII	-0.07	-0.01	LII	0.12	0.03	LII	0.11	0.01	LII
EK Del	-1.40	-1.55	LIII	-1.28	-1.59	LIII	-1.35	-1.52	LIII	-1.39	-1.54	LIII	-0.68	-0.79	LIII
β Dor	0.02	-0.19	LII	0.18	-0.11	LII	0.05	0.11	LII	-0.05	-0.14	LII	0.04	-0.06	LII
AA Gem	-0.18	-0.18	TS	-0.16	-0.16	TS	0.34	0.34	TS	0.02	0.02	TS	0.08	0.08	TS
AD Gem	-0.31	-0.31	TS	-0.17	-0.17	TS	0.26	0.11	LEM	-0.16	-0.16	TS	-0.25	-0.25	TS
BB Gem	-0.08	-0.23	LIII	0.23	-0.08	LIII	0.05	-0.12	LIII	0.03	-0.12	LIII	0.01	-0.10	LIII
BW Gem	-0.36	-0.36	TS	-0.18	-0.18	TS	-0.06	-0.23	LIII	-0.09	-0.09	TS	-0.08	-0.08	TS
DX Gem	-0.09	-0.09	TS	0.00	0.00	TS	0.08	-0.09	LIII	0.07	0.07	TS	-0.03	-0.03	TS
RZ Gem	-0.15	-0.15	TS	-0.27	-0.50	LEM	-0.02	-0.17	LEM	-0.19	-0.36	LEM	-0.27	-0.46	LEM
W Gem	-0.05	-0.20	LIII	0.12	-0.19	LIII	0.02	-0.15	LIII	0.01	-0.14	LIII	-0.04	-0.15	LIII
ζ Gem	0.20	0.05	LIII	0.33	0.02	LIII	0.24	0.07	LIII	0.22	0.07	LIII	0.04	-0.07	LIII
BB Her	0.29	0.14	LIII	0.26	-0.05	LIII	0.14	-0.03	LIII	0.20	0.05	LIII	0.27	0.16	LIII
BG Lac	0.07	-0.08	LIII	0.25	-0.06	LIII	0.09	-0.08	LIII	0.16	0.01	LIII	-0.03	-0.14	LIII
DF Lac	0.15	-0.00	LIII	0.24	-0.07	LIII	0.14	-0.03	LIII	0.14	-0.01	LIII	0.12	0.01	LIII
FQ Lac	-0.74	-0.89	LIII	0.08	-0.09	LIII	0.08	-0.07	LIII
RR Lac	0.13	-0.02	LIII	0.26	-0.05	LIII	0.08	-0.09	LIII	0.15	0.00	LIII	-0.01	-0.12	LIII
V Lac	0.22	0.07	LIII	0.33	0.02	LIII	0.15	-0.02	LIII	0.25	0.10	LIII	0.33	0.22	LIII
V411 Lac	0.18	0.03	LIII	0.48	0.17	LIII	0.16	-0.01	LIII	0.24	0.09	LIII	0.20	0.09	LIII
X Lac	0.12	-0.03	LIII	0.25	-0.06	LIII	0.17	-0.00	LIII	0.20	0.05	LIII	-0.10	-0.21	LIII
Y Lac	0.16	0.01	LIII	0.46	0.15	LIII	0.11	-0.06	LIII	0.14	-0.01	LIII	0.03	-0.08	LIII
Z Lac	0.18	0.03	LIII	0.43	0.12	LIII	0.28	0.11	LIII	0.34	0.19	LIII	0.03	-0.08	LIII
GH Lup	0.13	-0.02	LIII	0.23	-0.08	LIII	0.10	-0.07	LIII	0.16	0.01	LIII	0.02	-0.09	LIII
V473 Lyr	0.05	-0.10	LIII	0.14	-0.17	LIII	0.04	-0.13	LIII	0.05	-0.10	LIII	-0.02	-0.13	LIII
AA Mon	0.09	-0.06	LIII	0.40	0.09	LIII	0.03	-0.14	LIII	0.09	-0.06	LIII	0.16	0.05	LIII
AC Mon	0.07	-0.08	LIII	0.21	-0.10	LIII	0.17	-0.00	LIII	0.17	0.02	LIII	0.14	0.03	LIII
BE Mon	0.04	0.04	TS	0.02	0.02	TS	0.11	-0.04	LEM	0.07	0.07	TS	0.11	0.11	TS
BV Mon	-0.12	-0.24	LEM	0.24	0.01	LEM	-0.02	-0.19	LIII	-0.07	-0.22	LIII	0.27	0.08	LEM
CS Mon	0.02	-0.13	LIII	0.34	0.03	LIII	0.12	-0.05	LIII	0.13	-0.02	LIII	0.25	0.14	LIII
CU Mon	-0.14	-0.29	LIII	0.22	-0.09	LIII	0.11	-0.06	LIII	0.08	-0.07	LIII	0.00	-0.11	LIII
CV Mon	-0.07	-0.07	TS	-0.16	-0.16	TS	-0.02	-0.02	TS	-0.07	-0.07	TS	-0.12	-0.12	TS
EE Mon	-0.58	-0.73	LIII	-0.02	-0.33	LIII	-0.58	-0.75	LIII	-0.60	-0.75	LIII
EK Mon	-0.19	-0.31	LEM	-0.05	-0.28	LEM	0.18	0.03	LEM	0.16	-0.01	LEM	0.01	-0.18	LEM
FG Mon	-0.08	-0.23	LIII	0.12	-0.19	LIII	-0.12	-0.29	LIII	0.07	-0.08	LIII	-0.21	-0.32	LIII
FI Mon	0.05	-0.10	LIII	0.58	0.27	LIII	-0.03	-0.20	LIII	0.04	-0.11	LIII	0.11	0.01	LII
FT Mon	-0.34	-0.34	TS	-0.17	-0.17	TS	0.09	0.09	TS	0.14	0.14	TS	-0.02	-0.02	TS
SV Mon	-0.06	-0.06	TS	-0.14	-0.14	TS	0.02	0.02	TS	0.10	0.10	TS	-0.07	-0.07	TS
T Mon	0.30	0.15	LIII	0.54	0.23	LIII	0.16	-0.01	LIII	0.35	0.20	LIII	0.36	0.25	LIII
TW Mon	-0.12	-0.12	TS	0.03	0.03	TS	0.00	-0.17	LIII	0.09	0.09	TS	0.01	0.01	TS
TX Mon	0.13	0.13	TS	0.26	0.26	TS	0.20	0.20	TS	0.23	0.23	TS	0.14	0.14	TS
TY Mon	-0.09	-0.09	TS	-0.01	-0.01	TS	0.02	-0.13	LEM	0.06	0.06	TS	-0.11	-0.11	TS
TZ Mon	0.00	0.00	TS	0.06	0.06	TS	0.08	0.08	TS	0.04	0.04	TS	0.07	0.07	TS
UY Mon	-0.35	-0.47	LEM	-0.12	-0.35	LEM	-0.04	-0.19	LEM	0.01	-0.16	LEM	-0.11	-0.30	LEM
V446 Mon	-0.34	-0.49	LIII	-0.06	-0.37	LIII	-0.04	-0.21	LIII	-0.10	-0.25	LIII
V447 Mon	-0.33	-0.48	LIII	-0.58	-0.89	LIII	-0.14	-0.31	LIII	-0.11	-0.26	LIII	0.03	-0.08	LIII
V465 Mon	-0.14	-0.14	TS	0.06	0.06	TS	0.22	0.05	LIII	0.23	0.23	TS	0.05	0.05	TS
V484 Mon	0.15	-0.00	LIII	0.48	0.17	LIII	0.38	0.21	LIII	0.21	0.06	LIII	0.21	0.10	LIII
V495 Mon	-0.26	-0.26	TS	-0.06	-0.06	TS	-0.03	-0.03	TS	-0.04	-0.04	TS	-0.04	-0.04	TS
V504 Mon	0.22	0.07	LIII	0.41	0.10	LIII	0.25	0.08	LIII	0.35	0.20	LIII	-0.15	-0.25	LII
V508 Mon	-0.15	-0.15	TS	0.03	0.03	TS	0.13	-0.02	LEM	0.07	0.07	TS	-0.06	-0.06	TS
V510 Mon	-0.23	-0.23	TS	-0.14	-0.14	TS	-0.07	-0.07	TS	-0.11	-0.11	TS	-0.04	-0.04	TS
V526 Mon	-0.04	-0.19	LIII	0.10	-0.21	LIII	0.03	-0.14	LIII	0.05	-0.10	LIII	0.06	-0.05	LIII
V911 Mon	0.13	-0.02	LIII	0.35	0.04	LIII	0.37	0.20	LIII	0.39	0.24	LIII	0.28	0.17	LIII
VZ Mon	0.05	-0.10	LIII	0.13	-0.18	LIII	0.20	0.03	LIII	0.04	-0.11	LIII
WW Mon	-0.26	-0.38	LEM	-0.23	-0.46	LEM	-0.21	-0.36	LEM	-0.14	-0.31	LEM	-0.02	-0.21	LEM
XX Mon	-0.07	-0.07	TS	-0.11	-0.11	TS	0.11	0.11	TS	0.44	0.44	TS	0.08	0.08	TS
YY Mon	-0.51	-0.66	LIII	-0.24	-0.55	LIII	-0.65	-0.82	LIII	-0.27	-0.42	LIII	-0.76	-0.87	LIII
R Mus	0.24	0.09	LIII	0.29	-0.02	LIII	0.15	-0.02	LIII	0.20	0.05	LIII	0.31	0.20	LIII
RT Mus	0.23	0.08	LIII	0.24	-0.07	LIII	0.14	-0.03	LIII	0.19	0.04	LIII	-0.09	-0.20	LIII
S Mus	0.15	-0.00	LIII	0.23	-0.08	LIII	0.11	-0.06	LIII	0.18	0.03	LIII	0.14	0.03	LIII
TZ Mus	0.18	0.03	LIII	0.53	0.22	LIII	0.09	-0.08	LIII	0.08	-0.07	LIII	0.17	0.06	LIII
UU Mus	0.34	0.19	LIII	0.48	0.17	LIII	0.24	0.07	LIII	0.27	0.12	LIII	0.50	0.39	LIII

continued on next page

Table 7. continued.

Name	[Y/H] _{lit}	[Y/H]	Ref.	[La/H] _{lit}	[La/H]	Ref.	[Ce/H] _{lit}	[Ce/H]	Ref.	[Nd/H] _{lit}	[Nd/H]	Ref.	[Eu/H] _{lit}	[Eu/H]	Ref.
GU Nor	-0.08	-0.08	TS	-0.08	-0.08	TS	0.18	0.01	LIII	-0.23	-0.23	TS	-0.07	-0.07	TS
IQ Nor	-0.06	-0.06	TS	-0.15	-0.15	TS	-0.06	-0.06	TS	-0.05	-0.05	TS
QZ Nor	0.25	0.25	TS	-0.07	-0.07	TS	0.03	0.03	TS	0.12	0.12	TS	0.16	0.16	TS
RS Nor	0.15	0.15	TS	0.01	0.01	TS	0.01	0.01	TS	0.17	0.17	TS
S Nor	0.21	0.06	LIII	0.27	-0.04	LIII	0.11	-0.06	LIII	0.19	0.04	LIII	0.08	-0.03	LIII
SY Nor	0.06	0.06	TS	-0.10	-0.10	TS	0.08	0.08	TS	-0.04	-0.04	TS	0.08	0.08	TS
TW Nor	-0.10	-0.10	TS	-0.19	-0.19	TS	-0.11	-0.11	TS	-0.15	-0.15	TS	0.08	0.08	TS
U Nor	0.23	0.08	LIII	0.24	-0.07	LIII	0.15	-0.02	LIII	0.25	0.10	LIII	0.15	0.04	LIII
V340 Nor	-0.31	-0.31	TS	-0.13	-0.13	TS	0.06	-0.11	LIII	-0.15	-0.15	TS	-0.18	-0.18	TS
BF Oph	0.24	0.09	LIII	0.25	-0.06	LIII	0.14	-0.03	LIII	0.18	0.03	LIII	-0.02	-0.13	LIII
Y Oph	0.31	0.10	LII	0.24	-0.05	LII	-0.07	-0.01	LII	0.17	0.08	LII	0.13	0.03	LII
CR Ori	-0.13	-0.28	LIII	0.17	-0.14	LIII	0.06	-0.11	LIII	0.01	-0.14	LIII	0.02	-0.09	LIII
CS Ori	-0.27	-0.27	TS	0.21	-0.08	LII	0.14	-0.01	LEM	-0.21	-0.21	TS	-0.25	-0.25	TS
DF Ori	-0.17	-0.32	LIII	-0.02	-0.33	LIII	-0.16	-0.33	LIII	-0.05	-0.20	LIII	-0.39	-0.50	LIII
GQ Ori	0.32	0.11	LII	0.30	0.01	LII	0.04	0.10	LII	0.05	-0.04	LII	0.16	0.06	LII
RS Ori	0.15	0.15	TS	0.12	0.12	TS	0.37	0.37	TS	0.25	0.25	TS	0.21	0.21	TS
AS Per	0.18	0.03	LIII	0.32	0.01	LIII	0.07	-0.10	LIII	0.10	-0.05	LIII	0.10	0.00	LII
AW Per	0.21	0.06	LIII	0.46	0.15	LIII	0.20	0.03	LIII	0.23	0.08	LIII	0.00	-0.11	LIII
BM Per	0.31	0.16	LIII	0.54	0.23	LIII	0.27	0.10	LIII	0.39	0.24	LIII	0.36	0.25	LIII
CI Per	-0.32	-0.47	LIII	-0.32	-0.63	LIII	-0.45	-0.62	LIII	-0.26	-0.41	LIII	-0.55	-0.66	LIII
DW Per	-0.05	-0.20	LIII	0.20	-0.11	LIII	0.02	-0.15	LIII	0.10	-0.05	LIII	0.28	0.17	LIII
GP Per	-1.03	-1.18	LIII	-0.72	-1.03	LIII	-0.79	-0.96	LIII	-0.79	-0.94	LIII	-0.45	-0.56	LIII
HQ Per	-0.35	-0.50	LIII	-0.11	-0.42	LIII	-0.20	-0.37	LIII	-0.14	-0.29	LIII	-0.18	-0.29	LIII
HZ Per	-0.20	-0.35	LIII	0.26	-0.05	LIII	-0.02	-0.19	LIII	0.04	-0.11	LIII	0.20	0.09	LIII
MM Per	0.05	-0.10	LIII	0.18	-0.13	LIII	0.11	-0.06	LIII	0.17	0.02	LIII	-0.01	-0.12	LIII
OT Per	-0.05	-0.20	LIII	0.55	0.24	LIII	0.12	-0.05	LIII	0.16	0.01	LIII	0.46	0.35	LIII
SV Per	0.19	0.04	LIII	0.45	0.14	LIII	0.21	0.04	LIII	0.24	0.09	LIII	0.16	0.05	LIII
SX Per	0.05	-0.10	LIII	0.28	-0.03	LIII	0.13	-0.04	LIII	0.19	0.04	LIII	0.15	0.04	LIII
UX Per	0.02	-0.13	LIII	0.20	-0.11	LIII	0.08	-0.09	LIII	0.07	-0.08	LIII	-0.11	-0.22	LIII
UY Per	0.23	0.08	LIII	0.38	0.07	LIII	0.29	0.12	LIII	0.29	0.14	LIII	0.28	0.17	LIII
V440 Per	0.27	0.06	LII	0.31	0.02	LII	-0.07	-0.01	LII	0.18	0.09	LII	0.15	0.05	LII
V891 Per	0.09	-0.06	LIII	0.30	-0.01	LIII	0.19	0.02	LIII	0.22	0.07	LIII	0.27	0.16	LIII
VX Per	0.09	-0.06	LIII	0.45	0.14	LIII	0.15	-0.02	LIII	0.19	0.04	LIII	-0.01	-0.12	LIII
VY Per	0.13	-0.02	LIII	0.29	-0.02	LIII	0.19	0.02	LIII	0.18	0.03	LIII	0.05	-0.06	LIII
AD Pup	0.23	0.11	LEM	0.42	0.19	LEM	0.31	0.16	LEM	0.50	0.33	LEM	0.17	-0.02	LEM
AP Pup	0.11	-0.01	LEM	0.30	0.07	LEM	0.35	0.20	LEM	0.33	0.16	LEM	0.32	0.13	LEM
AQ Pup	0.48	0.48	TS	0.05	0.05	TS	-0.13	-0.13	TS	0.03	0.03	TS	0.12	0.12	TS
AT Pup	-0.19	-0.31	LEM	-0.11	-0.34	LEM	0.06	-0.09	LEM	0.06	-0.11	LEM	-0.21	-0.40	LEM
BC Pup	-0.35	-0.35	TS	-0.15	-0.15	TS	0.07	0.07	TS	0.37	0.37	TS	0.02	0.02	TS
BM Pup	-0.05	-0.05	TS	-0.11	-0.11	TS	0.19	0.19	TS	0.06	0.06	TS	0.04	0.04	TS
BN Pup	0.30	0.30	TS	0.09	0.09	TS	0.12	0.12	TS	0.07	0.07	TS	0.16	0.16	TS
CE Pup	0.08	-0.07	LIII	0.25	-0.06	LIII	0.11	-0.06	LIII	0.21	0.06	LIII	0.15	0.04	LIII
CK Pup	-0.13	-0.13	TS	-0.09	-0.09	TS	0.04	0.04	TS	-0.00	-0.00	TS	0.04	0.04	TS
HW Pup	-0.16	-0.16	TS	-0.18	-0.18	TS	-0.10	-0.10	TS	-0.15	-0.15	TS	-0.07	-0.07	TS
LS Pup	-0.11	-0.11	TS	-0.01	-0.01	TS	-0.04	-0.04	TS	0.03	0.03	TS	0.01	0.01	TS
MY Pup	0.01	-0.11	LEM	0.17	-0.06	LEM	0.25	0.10	LEM	0.16	-0.01	LEM	0.16	-0.03	LEM
NT Pup	0.03	-0.12	LIII	0.21	-0.10	LIII	0.09	-0.08	LIII	0.19	0.04	LIII	0.14	0.03	LIII
RS Pup	0.30	0.18	LEM	0.24	0.01	LEM	0.19	0.04	LEM	0.39	0.22	LEM	0.37	0.18	LEM
V335 Pup	0.26	0.11	LIII	0.25	-0.06	LIII	0.33	0.16	LIII	0.29	0.14	LIII	0.24	0.13	LIII
VW Pup	-0.35	-0.35	TS	-0.38	-0.38	TS	0.08	0.14	LII	-0.46	-0.46	TS	-0.18	-0.18	TS
VX Pup	0.04	-0.08	LEM	0.32	0.09	LEM	0.35	0.20	LEM	0.26	0.09	LEM	0.23	0.04	LEM
VZ Pup	-0.01	-0.01	TS	0.09	0.09	TS	0.14	-0.01	LEM	0.18	0.18	TS	0.06	0.06	TS
WW Pup	-0.30	-0.30	TS	-0.23	-0.23	TS	0.00	0.06	LII	-0.44	-0.44	TS	-0.07	-0.07	TS
WX Pup	-0.01	-0.13	LEM	0.13	-0.10	LEM	0.18	0.03	LEM	0.24	0.07	LEM	-0.05	-0.24	LEM
WY Pup	-0.43	-0.43	TS	-0.18	-0.18	TS	0.13	0.13	TS	-0.03	-0.03	TS
WZ Pup	-0.16	-0.16	TS	-0.09	-0.09	TS	0.01	0.01	TS	-0.09	-0.09	TS	-0.04	-0.04	TS
X Pup	-0.15	-0.15	TS	-0.02	-0.02	TS	-0.13	-0.13	TS	0.03	0.03	TS	-0.26	-0.26	TS
KQ Sco	0.03	0.03	TS	-0.08	-0.08	TS	-0.02	-0.02	TS	-0.24	-0.24	TS	-0.02	-0.02	TS
RV Sco	0.13	-0.02	LIII	0.26	-0.05	LIII	0.10	-0.07	LIII	0.10	-0.05	LIII	0.27	0.16	LIII
RY Sco	-0.02	-0.02	TS	-0.01	-0.01	TS	0.09	0.09	TS	0.06	0.06	TS	0.09	0.09	TS
V470 Sco	0.11	0.11	TS	-0.07	-0.07	TS	-0.12	-0.12	TS	0.03	0.03	TS	0.16	0.16	TS
V482 Sco	0.27	0.12	LIII	0.32	0.01	LIII	0.20	0.03	LIII	0.25	0.10	LIII	0.35	0.24	LIII
V500 Sco	-0.19	-0.19	TS	-0.13	-0.13	TS	0.00	0.00	TS	-0.01	-0.01	TS	-0.05	-0.05	TS
V636 Sco	0.14	-0.01	LIII	0.28	-0.03	LIII	0.14	-0.03	LIII	0.08	-0.07	LIII	0.02	-0.09	LIII
V950 Sco	0.33	0.18	LIII	0.35	0.04	LIII	0.20	0.03	LIII	0.26	0.11	LIII	0.42	0.31	LIII
BX Sct	0.32	0.17	LIII	0.36	0.05	LIII	0.24	0.07	LIII	0.39	0.24	LIII	0.53	0.42	LIII
CK Sct	0.27	0.12	LIII	0.37	0.06	LIII	0.23	0.06	LIII	0.26	0.11	LIII	0.23	0.12	LIII
CM Sct	0.21	0.06	LIII	0.17	-0.14	LIII	0.06	-0.11	LIII	0.13	-0.02	LIII
CN Sct	0.30	0.15	LIII	0.19	-0.12	LIII	0.13	-0.04	LIII	0.22	0.07	LIII	0.05	-0.06	LIII
EV Sct	0.01	0.01	TS	0.07	0.07	TS	0.23	0.06	LIII	0.15	0.15	TS	0.20	0.20	TS
EW Sct	0.22	0.01	LII	0.29	0.00	LII	-0.07	-0.01	LII	0.17	0.08	LII	0.06	-0.04	LII
RU Sct	0.18	0.18	TS	-0.09	-0.09	TS	-0.11	-0.11	TS	-0.07	-0.07	TS	0.00	0.00	TS
SS Sct	0.16	0.01	LIII	0.48	0.17	LIII	0.15	-0.02	LIII	0.20	0.05	LIII	-0.06	-0.17	LIII
TY Sct	0.38	0.23	LIII	0.31	0.00	LIII	0.16	-0.01	LIII	0.29	0.14	LIII	0.14	0.03	LIII
UZ Sct	0.19	0.19	TS	-0.01	-0.01	TS	0.16	0.16	TS	0.05	0.05	TS	0.17	0.17	TS

continued on next page

Table 7. continued.

Name	[Y/H] _{lit}	[Y/H]	Ref.	[La/H] _{lit}	[La/H]	Ref.	[Ce/H] _{lit}	[Ce/H]	Ref.	[Nd/H] _{lit}	[Nd/H]	Ref.	[Eu/H] _{lit}	[Eu/H]	Ref.
V367 Sct	-0.12	-0.12	TS	-0.14	-0.14	TS	0.23	0.23	TS	0.12	0.12	TS	-0.01	-0.01	TS
X Sct	0.04	0.04	TS	-0.07	-0.07	TS	0.03	0.03	TS	0.08	0.08	TS
Y Sct	0.30	0.15	LIII	0.32	0.01	LIII	0.20	0.03	LIII	0.30	0.15	LIII	0.14	0.03	LIII
Z Sct	-0.26	-0.26	TS	-0.31	-0.31	TS	0.03	0.03	TS	-0.04	-0.04	TS	-0.06	-0.06	TS
AA Ser	0.39	0.39	TS	0.09	0.09	TS	0.04	0.04	TS	0.15	0.15	TS	0.30	0.30	TS
BQ Ser	0.13	-0.08	LII	0.13	-0.16	LII	-0.09	-0.03	LII	0.22	0.13	LII	0.07	-0.03	LII
CR Ser	0.05	0.05	TS	-0.15	-0.15	TS	0.06	0.06	TS	0.08	0.08	TS	0.15	0.15	TS
DV Ser	0.39	0.24	LIII	0.43	0.12	LIII	0.23	0.06	LIII	0.27	0.12	LIII	0.34	0.23	LIII
DG Sge	0.21	0.06	LIII	0.23	-0.08	LIII	0.02	-0.15	LIII	0.14	-0.01	LIII	0.12	0.01	LIII
GX Sge	0.37	0.22	LIII	0.43	0.12	LIII	0.28	0.11	LIII	0.34	0.19	LIII	0.33	0.22	LIII
GY Sge	0.48	0.33	LIII	0.56	0.25	LIII	0.15	-0.02	LIII	0.40	0.25	LIII	0.37	0.26	LIII
S Sge	0.26	0.05	LII	0.23	-0.06	LII	-0.08	-0.02	LII	0.15	0.06	LII	0.07	-0.03	LII
AP Sgr	0.28	0.07	LII	0.02	-0.27	LII	0.05	0.11	LII	0.14	0.04	LII
AV Sgr	0.11	0.11	TS	-0.04	-0.04	TS	0.04	0.04	TS	-0.04	-0.04	TS	0.24	0.24	TS
AY Sgr	0.07	0.07	TS	-0.05	-0.05	TS	-0.04	-0.04	TS	0.09	0.09	TS	0.08	0.08	TS
BB Sgr	0.18	-0.03	LII	0.22	-0.07	LII	-0.09	-0.03	LII	-0.03	-0.12	LII	0.04	-0.06	LII
U Sgr	0.19	-0.02	LII	0.18	-0.11	LII	-0.03	0.03	LII	0.09	0.00	LII	0.07	-0.03	LII
V1954 Sgr	0.07	0.07	TS	-0.11	-0.11	TS	-0.07	-0.07	TS	0.04	0.04	TS
V350 Sgr	0.33	0.12	LII	0.26	-0.03	LII	0.05	0.11	LII	0.16	0.07	LII	0.15	0.05	LII
V773 Sgr	-0.07	-0.07	TS	-0.04	-0.04	TS	-0.09	-0.09	TS	-0.06	-0.06	TS
VY Sgr	-0.01	-0.01	TS	-0.11	-0.11	TS	-0.04	-0.04	TS	-0.02	-0.02	TS	0.09	0.09	TS
W Sgr	0.20	-0.01	LII	0.23	-0.06	LII	-0.04	0.02	LII	0.10	0.01	LII	0.03	-0.07	LII
WZ Sgr	0.07	0.07	TS	-0.03	-0.03	TS	0.05	0.05	TS	0.05	0.05	TS	0.04	0.04	TS
XX Sgr	-0.09	-0.09	TS	-0.10	-0.10	TS	0.10	0.10	TS	0.04	0.04	TS	-0.03	-0.03	TS
Y Sgr	0.23	0.02	LII	0.15	-0.14	LII	-0.18	-0.12	LII	0.08	-0.01	LII	0.01	-0.09	LII
YZ Sgr	0.30	0.09	LII	0.19	-0.10	LII	-0.10	-0.04	LII	0.09	0.00	LII	0.07	-0.03	LII
AE Tau	-0.10	-0.25	LIII	0.04	-0.27	LIII	0.00	-0.17	LIII	-0.02	-0.17	LIII	-0.12	-0.23	LIII
AV Tau	-0.08	-0.20	LEM	0.08	-0.15	LEM	0.11	-0.06	LEM	0.28	0.11	LEM	0.16	-0.03	LEM
EF Tau	-0.67	-0.88	LII	-0.80	-1.09	LII	-0.68	-0.62	LII	-0.33	-0.42	LII	-0.55	-0.65	LII
EU Tau	0.07	-0.14	LII	0.16	-0.13	LII	-0.18	-0.12	LII	-0.02	-0.11	LII	0.01	-0.09	LII
ST Tau	-0.01	-0.13	LEM	0.09	-0.14	LEM	0.37	0.22	LEM	0.19	0.02	LEM	0.12	-0.07	LEM
SZ Tau	0.21	-0.00	LII	0.25	-0.04	LII	-0.03	0.03	LII	0.11	0.02	LII	0.14	0.04	LII
LR TrA	0.35	0.20	LIII	0.56	0.25	LIII	0.16	-0.01	LIII	0.27	0.12	LIII	0.30	0.19	LIII
R TrA	0.29	0.14	LIII	0.51	0.20	LIII	0.29	0.12	LIII	0.32	0.17	LIII	0.47	0.36	LIII
S TrA	0.28	0.13	LIII	0.35	0.04	LIII	0.17	-0.00	LIII	0.21	0.06	LIII	0.30	0.19	LIII
AE Vel	0.13	-0.02	LIII	0.31	0.00	LIII	0.14	-0.03	LIII	0.20	0.05	LIII	0.26	0.15	LIII
AH Vel	0.11	-0.01	LEM	0.26	0.03	LEM	0.33	0.18	LEM	0.30	0.13	LEM	0.30	0.11	LEM
AX Vel	0.02	-0.10	LEM	0.28	0.05	LEM	0.44	0.29	LEM	0.16	-0.01	LEM	0.14	-0.05	LEM
BG Vel	0.08	-0.04	LEM	0.24	0.01	LEM	0.35	0.20	LEM	0.27	0.10	LEM	0.21	0.02	LEM
CS Vel	0.21	0.06	LIII	0.38	0.07	LIII	0.20	0.03	LIII	0.27	0.12	LIII	0.08	-0.03	LIII
CX Vel	0.18	0.03	LIII	0.21	-0.10	LIII	0.07	-0.10	LIII	0.16	0.01	LIII	0.05	-0.05	LII
DK Vel	0.30	0.15	LIII	0.39	0.08	LIII	0.19	0.02	LIII	0.27	0.12	LIII	0.22	0.11	LIII
DR Vel	0.13	0.01	LEM	0.14	-0.09	LEM	0.29	0.14	LEM	0.17	-0.00	LEM	-0.04	-0.23	LEM
EX Vel	0.14	-0.01	LIII	0.28	-0.03	LIII	0.13	-0.04	LIII	0.21	0.06	LIII	0.23	0.12	LIII
EZ Vel	-0.02	-0.02	TS	-0.01	-0.01	TS	0.13	0.13	TS	-0.08	-0.08	TS	0.04	0.04	TS
FG Vel	0.05	-0.10	LIII	0.27	-0.04	LIII	0.02	-0.15	LIII	0.14	-0.01	LIII	0.05	-0.06	LIII
FN Vel	0.11	-0.04	LIII	0.27	-0.04	LIII	0.11	-0.06	LIII	0.17	0.02	LIII	0.27	0.16	LIII
RY Vel	0.19	0.07	LEM	0.07	-0.16	LEM	0.15	-0.00	LEM	0.17	-0.00	LEM	0.50	0.31	LEM
RZ Vel	0.34	0.22	LEM	0.27	0.04	LEM	0.25	0.10	LEM	0.54	0.37	LEM	0.37	0.18	LEM
ST Vel	-0.04	-0.16	LEM	0.12	-0.11	LEM	0.17	0.02	LEM	0.16	-0.01	LEM	0.20	0.01	LEM
SV Vel	0.20	0.05	LIII	0.27	-0.04	LIII	0.13	-0.04	LIII	0.19	0.04	LIII	0.17	0.06	LIII
SW Vel	-0.03	-0.15	LEM	0.10	-0.13	LEM	0.04	-0.11	LEM	-0.02	-0.19	LEM	0.08	-0.11	LEM
SX Vel	0.01	-0.11	LEM	0.15	-0.08	LEM	0.19	0.04	LEM	0.05	-0.12	LEM	0.19	-0.00	LEM
T Vel	0.30	0.18	LEM	0.49	0.26	LEM	0.63	0.48	LEM	0.39	0.22	LEM	0.45	0.26	LEM
V Vel	-0.13	-0.25	LEM	0.07	-0.16	LEM	0.24	0.09	LEM	0.19	0.02	LEM	-0.04	-0.23	LEM
XX Vel	0.27	0.12	LIII	0.30	-0.01	LIII	0.20	0.03	LIII	0.27	0.12	LIII	0.48	0.37	LIII
AS Vul	0.27	0.12	LIII	0.34	0.03	LIII	0.20	0.03	LIII	0.39	0.24	LIII	0.26	0.15	LIII
DG Vul	0.26	0.11	LIII	0.21	-0.10	LIII	0.13	-0.04	LIII	0.24	0.09	LIII	0.35	0.24	LIII
S Vul	0.23	0.08	LIII	0.35	0.04	LIII	0.08	-0.09	LIII	0.21	0.06	LIII	0.23	0.12	LIII
SV Vul	0.24	0.03	LII	0.20	-0.09	LII	-0.13	-0.07	LII	0.06	-0.03	LII	0.04	-0.06	LII
T Vul	0.15	-0.06	LII	0.24	-0.05	LII	-0.08	-0.02	LII	0.14	0.05	LII	0.08	-0.02	LII
U Vul	0.35	0.20	LIII	0.39	0.08	LIII	0.29	0.12	LIII	0.32	0.17	LIII	0.21	0.10	LIII
X Vul	0.20	-0.01	LII	0.15	-0.14	LII	-0.06	-0.00	LII	0.13	0.04	LII	0.07	-0.03	LII